Calibration of pressure-velocity probes and measurement of sound power and ear canal conductance

dott. Giorgio Sacchi

10th March 2011

Acknowledgments

This thesis work has been made possible thanks to an official agreement between the Physics Department of the University of Ferrara and the Imamoter Institute of the Italian National Research Council (CNR), which also actively collaborated for sound power measurements in terms of human and material resources.

Contents

Introduction

The appearance in the last decade of a new generation of p-u sound intensity probes, allowing the direct measurement of the air particle velocity using MEMS-designed anemometric sensors, represented a great chance to advance a domain of acoustics not entirely studied yet.

This domain is usually termed "sound intensimetry" and is concerned with the measurement and analysis of sound intensity fields, the acoustic power of sound sources and sound energy absorption phenomena. Such a wide area of knowledge can be anyway better systematized under the term *Sound Energetics*, including the study of sound energy generation, propagation and absorption as well as the study of the structure of the energy field of sound.

It is then clear that the development of new acoustic sensors able to capture both the pressure and velocity signals is of fundamental importance for Sound Energetics: in fact, mathematical objects studied by Sound Energetics are all those quadratic (i.e. non-linear) combinations of pressure p and the three components of air particle velocity u_i, solutions of d'Alembert wave equation, which form together what it can be called *sound event*. This term is borrowed from special relativity, and any sound event is identified by a four-vector $\left(pc^{-1}, \rho_0 u_x, \rho_0 u_y, \rho_0 u_z\right)$, where c is speed of sound and ρ_0 is the unperturbed medium density.

Possible applications of Sound Energetics are manifold: from traditional ones, as the measurement of acoustic power emitted by any source [1, 2], to the monitoring of sound fields generated by musical instruments [3, 4]. But also more advanced applications, as for instance the development of active control algorithms [5] or multi-channel audio recording and reproduction processes [6] can benefit from the design and production of new acoustic sensors .

At present, most of intensimetric data are collected using standard intensimetric probes, which are formed by a couple of phase-matched pressure microphones (p-p probes). Such probes, quite expensive because the microphones have to be accurately selected and coupled according to their phase responses during the production phase, have some drawbacks. These are mainly due to the finite difference approximation algorithm, inevitably used for the indirect measurement of the air particle velocity data from pressure

gradient. This is not the case for p-u probe recently developed by Microflown Technologies®, which by performing a direct measure of particle velocity signals can be properly used for innovative applications of Sound Energetics as the one that will be presented in chapter 4 of this work. This new kind of probes, based on the anemometric transduction principle of double heated wires, are however still far from being a reference instrument in sound intensimetry. In particular, calibration is nowadays still an open issue, even if some studies are already presented in literature [7, 8]. Therefore the author's main research activity has been just focused on a new approach of calibration of p-u probes using a progressive plane wave field as reference field for calibration.

This work is organized in 4 chapters, whose main topics are here below summarized.

1. In first chapter acoustical motion equation are obtained from the more general fluid dynamical ones using mass, momentum, energy conservation laws and small perturbation approximation. Then, after a brief introduction of relativistic four-dimensional formalism transposed from special relativity, main laws of linear acoustics are rewritten in this terms, showing that this point of view fits perfectly and allows an elegant and very effective description of the topic: conservation laws come out from differential properties of 4-dimensional vectors and tensors, and quantities such as radiation pressure are naturally defined. Finally, energetic average properties of general sound fields for stationary events are studied in an innovative way, which leads to the definition of new quantities of sound conductance and susceptance.

2. Second chapter is intended a collection and a bit of explanation of all those signal processing instruments which will be needed in further experimental analysis: moreover, the primary aim is to show that such algorithms are not just useful tools but have a precise physical meaning. It is then illustrated how this demonstration allows a reformulation of quantities defined in previous chapter in frequency domain, thanks to correlation functions.

3. Third chapter represents the core of both this work and of the research activity of PhD itself: the development of a new method for p-u probe calibration. After a brief but necessary introduction of instrumentation for the study of Sound Energetics, particular attention is payed to anemometric p-u probes: its features and working principles, as well as a describing model, are reported, as well as an overview of possible approaches to its calibration. Then main part is dedicated to a formal theorisation of the calibration process, followed by the specific case of progressive plane wave field. Experimental apparatus is described in detail, then calibration results for a test axial p-u probe are reported

and discussed, accordingly to producing company working model of the probe itself. Finally necessary considerations about uncertainties of the method here introduced are given.

4. Fourth and last chapter illustrates some experimental applications of Sound Energetics using the calibrated p-u probe. As a benchmark for this instrument, a classical measurement of sound power emitted from a source was chosen: both a p-p and a p-u probe are used, so that a direct comparison is possible. Results for both instruments are reported and their consistency is discussed. An original application is then given, the calculus of sound conductance and susceptance defined in chapter 1: such measurements were first carried out both in a very controlled environment and in a more realistic case. Firstly, a one-dimensional wave guide which simulated different environments changing absorption properties at one end was considered, whose average properties were studied both in time and along trajectory of propagating energy. Then, focusing on sound conductance, the original case of human ear canal was considered: frequency dependent functions are studied and compared with literature and a substantial agreement was found.

Chapter 1

Linear acoustics and Sound Energetics

1.1 Derivation of wave equation from fluid dynamics

1.1.1 Fluid motion equation

Acoustics can be defined as that particular branch of fluid dynamics which studies small perturbations of physical quantities describing the status of a certain medium over time. Its equations, as it is well known, are the consequence of fundamental conservation laws of mass, momentum, energy and thermodynamical properties of the medium itself.

Fluid dynamical phenomena, in particular acoustical ones, have a macroscopic nature: the fluid can therefore be treated as a continuum and described by scalar physical quantities as density $\rho(\mathbf{x}, t)$ instead of mass of air molecules and pressure $p(\mathbf{x}, t)$ instead of single forces. Together with the vector quantity fluid velocity $\mathbf{u}(\mathbf{x}, t)$, these fields represent the unknowns to be solved in the physical problem, in order to fully describe a physical event. Equations derived from conservation laws allow to do so.

Mass conservation law

Conservation of mass simply states that in a fluid mass cannot vanish or be created if no "mass source" is present. In other words, if mass changes in a given volume V_0, mass flux crossing the surface S_0 enclosing the volume must be non-zero: the rate of increase/decrease of the mass in that volume is equal to the net flux over the surface

$$\frac{d}{dt}\left(\int_{V_0} \rho dV\right) = \int_{\partial V_0} \rho \mathbf{u} \cdot \hat{\mathbf{n}} dS$$

where $\hat{\mathbf{n}}$ is the vector locally normal to the surface.

Table 1.1: Thermodynamical parameters of dry air in normal conditions.

	$\rho_0\,{}^{\mathrm{kg}}/_{\mathrm{m}^3}$	$p_0\,\mathrm{Pa}$	$u_0\,{}^{\mathrm{m}}/_{\mathrm{s}}$	$T\,\mathrm{K}$	$\eta\,{}^{\mathrm{kg}}/_{\mathrm{mol}}$	γ
Air	1.2928	101325	485	273.15	0.0290	1.4018

This relation, known as the integral form of mass conservation, can be expressed locally thanks to Gauss´ theorem (differential form of the same equation):

$$\frac{\partial \rho}{\partial t} = -\nabla \cdot (\rho \mathbf{u}) \tag{1.1.1}$$

Momentum conservation law

This equation, also known as Navier-Stokes´ relation, connects momentum variation to pressure p, viscosity (internal friction) and the net external force $\mathbf{F}$ per unit volume applied to the fluid (body force). Acoustics is interested in particular in the study of Newtonian fluids, whose internal friction can be expressed in terms of shear viscosity coefficient, constant over the direction of motion.

Momentum conservation equation for Newtonian, incompressible fluids such the ones studied in acoustics, can be written then as:

$$\rho \frac{D\mathbf{u}}{Dt} = -\nabla p + \eta \left(\nabla^2 \mathbf{u} + \frac{1}{3} \nabla (\nabla \cdot \mathbf{u}) \right) + \mathbf{F} \tag{1.1.2}$$

where

$$\frac{D(\cdot)}{Dt} = \frac{\partial}{\partial t} + \mathbf{u} \cdot \nabla (\cdot) \tag{1.1.3}$$

is the total or Lagrangian derivative with respect to time.

In case the viscous friction is negligible and no net force per unit volume is applied, i.e. $\eta = 0$, $\mathbf{F} = 0$, relation (1.1.2) is called *Euler's equation*, from the mathematician who first obtained it in 1755.

$$\rho \frac{\partial \mathbf{u}}{\partial t} + \mathbf{u} \cdot \nabla \mathbf{u} + \nabla p = 0 \tag{1.1.4}$$

Apart from sound absorption due to internal friction at high frequencies, in acoustics usually the viscous term can be neglected because the coefficient is quite small: in table 1.1 values of the main thermodynamical quantities for dry air at normal conditions ($T = 0\,^{\circ}\mathrm{C}$ and $p = 1\,\mathrm{atm}$) are reported.

Energy conservation law and entropy continuity equation

When energy dissipation for internal friction and heat transfer between its different parts are negligible effects in a fluid, then it is called ideal. In this case, equations of motion are Euler's ones and the thermodynamical transformations which every particle of the fluid undergoes are adiabatic by

definition, because fluid particles may be considered as thermally isolated one from another. Under these conditions, entropy is conserved.

In acoustics the oscillatory motions of the medium particles usually respect such constrains: their *specific entropy*, defined as $s = {}^{S}/_{N}$ where S is the whole system entropy and N is the number of particles, is then conserved during the motion. In other words, its total derivative defined in equation (1.1.3) must be null:

$$\frac{Ds}{Dt} = 0 \tag{1.1.5}$$

If during the motion the entropy does not change, pressure p and volume of the particle V are related by the very well known relation $pV^{\gamma} = constant$ or, in terms of pressure and density, which is inversely proportional to the volume,

$$p = constant \times \rho^{\gamma}$$

where γ is the adiabatic index, the ratio between the heat capacities. In case of dry air its value is $\gamma = 1.403$, as reported in table 1.1.

1.1.2 Linear acoustics: wave equation

Acoustic condition

The intensity of a sound or acoustic event is generally described by the mean value of pressure perturbation over time $p_{RMS} = \sqrt{\langle p^2 \rangle}$, where RMS stands for Root Mean Square ans the symbol $\langle \cdot \rangle$ indicates the time average. The value of these perturbations have variations of several orders of magnitude between what people perceive as a faint sound and a deafening one: added to the fact that the human hearing perception is sensitive to ratios, both in pitch and intensity, it is somehow natural to describe logarithmically such quantities. Sound pressure level SPL, or sound level L_p, is thus defined in decibel scale as:

$$L_p = 10 \times \log\left(\frac{p_{RMS}^2}{p_0^2}\right) = 20 \log\left(\frac{p_{RMS}}{p_0}\right) \text{ dB} \tag{1.1.6}$$

where p_0 represents a reference given by the limit of sound level detectable by human hear, set at $20\,\mu$Pa (RMS) at a frequency of 1000 Hz. An ideal excitation whose pressure were of magnitude of the same order of atmospheric one ($p_{atm} \approx 10^5$ Pa) would lead to a level about equal to 194 dB, although such a "sound" would hardly be studied within linear acoustics! Typically a sound level pressure of 120 dB is considered painful and is able to cause damage to hearing apparatus. Such a level corresponds to a p_{RMS} equal to

$$p_{120} = p_0 \cdot 10^{\left(\frac{L_p}{20}\right)} = 20 \text{ Pa} \tag{1.1.7}$$

about four order of magnitude smaller than atmospheric (static) pressure. What turns out then is that even strong and painful sounds or noises are

just small perturbation of pressure around its equilibrium value p_{atm}. This consideration is the basis of linear acoustics.

An upper bound of this domain can be set for a pressure corresponding to a level of about 160 dB SPL, since $p_{160}/p_{atm} \simeq 0.02$, a ratio which starts to be too big to be treated pertubatively. In fact, in Euler's equation (1.1.4) the non linear term $\mathbf{u} \cdot \nabla \mathbf{u}$ is not so small to be neglected, making the linear approximation not good to describe this situation.

Linear acoustics is considered as the study of wave phenomena whose pressure amplitudes are then included between $p_0 = 2 \cdot 10^{-5}$ Pa and $p_{160} = 2 \cdot 10^3$ Pa in air, corresponding to a RMS value of acoustic particle vibration velocity of $v_0 = 4.8 \cdot 10^{-8}$ m/s and $v_{160} = 4.8$ m/s[1].

These subjective consideration are very important because are a way to define the *acoustic range* where the d'Alembert wave equation is obtainable, as the following section will explain.

Wave equation

The starting point of the linearization process are, of course, the laws of conservation for air particle defined above (Eqs. (1.1.1), (1.1.4) and (1.1.5)). The solutions of these equation completely identify the motion of a fluid particle along its trajectory (Lagrangian interpretation). Alternatively, the same solutions can be seen as scalar and vector fields, characterizing this way the behaviour of the whole fluid at given spatial points $\mathbf{x}$ and time instants t (Eulerian interpretation).

Within the range $[0, 160]$ dB defined in the previous subsection, the oscillatory variation of physical quantities around their equilibrium value can be considered small: this is true for velocity in particular, which means that second-order term (i.e. non linear ones) of Euler's equation $(\mathbf{u} \cdot \nabla)\mathbf{u}$ can be neglected.

The same method can be used for other fields: in general, it is always possible to write pressure p and density ρ as the sum of equilibrium value (p_0, ρ_0), given in table 1.1, and perturbations (p', ρ'):

$$p = p_0 + p'$$
$$\rho = \rho_0 + \rho'$$

Perturbation theory can be applied when the following conditions are

[1] Similarly to what was done for pressure, it is possible to express velocity in dB units with respect to a reference value, naturally defined by $v_0 = 5 \cdot 10^{-8}$ m/s. This way the Acoustic Velocity Level (AVL) is given by

$$AVL = 20 \log \left(\frac{v_{RMS}}{v_0} \right) \text{ dB}$$

true:

$$p' \ll p_0$$
$$\rho' \ll \rho_0$$
$$\mathbf{u} \ll \mathbf{u}_0$$

where, since equilibrium value for velocity is 0, last condition is given in term of mean thermal agitation velocity $|\mathbf{u_0}| = \sqrt{\frac{3kT}{\mu}} \simeq 15.9\,\mathrm{ms}^{-1}$.

Keeping only first-order terms, laws of conservation can be rewritten as

$$\begin{cases} \frac{\partial \rho'}{\partial t} - \rho_0 \nabla \cdot (\mathbf{u}) = 0 \\ \rho_0 \frac{\partial \mathbf{u}}{\partial t} + \nabla p' = 0 \\ p' = \rho' \left(\frac{\partial p}{\partial \rho}\right)_s \end{cases} \tag{1.1.8}$$

With proper substitutions it is possible to "decouple" the equations into second order partial hyperbolic differential equations for each field, each of the same form: wave equations.

Third equation of system (1.1.8) simply states that p and ρ are linearly related. Proportionality factor is constant in first-order approximation and is the square of the speed at which a sound wave travels in the medium: speed of sound is then given by equilibrium values:

$$c = \sqrt{\left(\frac{\partial p}{\partial \rho}\right)_s} = \sqrt{\gamma \frac{p_0}{\rho_0}}$$

thus it depends on the gas composition (γ), static pressure (p_0) and unperturbed density (ρ_0). Using this relation one obtains two other equations, for pressure and velocity, formally identical[2]

$$\begin{cases} \frac{1}{c^2} \frac{\partial^2 \mathbf{u}}{\partial t^2} - \Delta \mathbf{u} = 0 \\ \frac{1}{c^2} \frac{\partial^2 p'}{\partial t^2} - \Delta p' = 0 \\ p' = \rho' c^2 \end{cases} \tag{1.1.9}$$

The physical meaning of such equations is that all the perturbations of the given fields propagate as concatenated waves travelling at the same speed, equal to c.

A step further can finally be done if the velocity field is separated in the sum of one irrotational and one solenoidal field, an operation mathematically always possible:

$$\mathbf{u} = \mathbf{u}_{irr} + \mathbf{u}_{sol}; \quad \nabla \cdot \mathbf{u}_{sol} = 0; \quad \nabla \wedge \mathbf{u}_{irr} = 0$$

Just $\mathbf{u}_{irr}$ can be solution of the wave equation, which means that $\mathbf{u}_{sol}$ must be a constant; moreover, it can be demonstrated that $\mathbf{u}_{sol} \equiv 0$ if it has to be limited $\forall t$.

[2] The operator $\left(\frac{1}{c^2}\frac{\partial^2}{\partial t^2} - \Delta\right)$ is usually synthesized by d'Alembertian symbol $\Box_c$

The main consequence of this constraint of the velocity field is that only *longitudinal* acoustic waves are allowed to be excited in gases: as a direct consequence, $\mathbf{u}$ can be expressed as the gradient of a scalar function, called *velocity potential* ϕ; from linearized Euler's equation (second equation of system (1.1.8)), also p can be rewritten in terms of ϕ:

$$\begin{aligned} \mathbf{u} &= \nabla\phi \\ p &= -\rho_0 \frac{\partial\phi}{\partial t} \end{aligned} \tag{1.1.10}$$

It is easily demonstrable that velocity potential is a solution of wave equation as well, using the gauge freedom[3] in an appropriate way ($\Box_c\phi = 0$).

1.2 Four-dimensional formalism for acoustics

1.2.1 Geometry of acoustic space-time

In analogy with relativistic field theory, it is possible to apply the four-dimensional formalism, born with special relativity, to the description of acoustic phenomena [9]. This will lead not only to a more elegant mathematical structure, but also to a original and somewhat simpler introduction of energetic properties of acoustic fields. Before the necessary mathematical instruments are introduced, however, appropriate distinctions have to be done.

Even if it is possible to describe acoustic phenomena within the relativistic framework treated in standard textbooks simply by replacing the speed of light with the speed of sound, the acoustic case presents only a formal analogy with relativity, since the Lorentz transformations obtained in this way still form an invariance group of the wave equation, but do not connect inertial reference frames. The physical meaning of such transformations is related to the study of the radiation from a point source, moving with constant speed ([10], Sect. 11.2). From another point of view, acoustic Lorentz transformations connect all space-time coordinates, which describe sound propagation with the same speed and therefore leave invariant the wave equation. Since the common notation of relativistic field theory is not usual in acoustics, a short account of it is given in the present and in the following subsections.

Any vector $\mathbf{x}$ in $\mathbb{R}^3$ can be represented in terms of any set of three linearly independent vectors $\{\mathbf{v}_i\}_{i=1,2,3}$ and components x^i as

$$\mathbf{x} = \sum_{i=1}^{3} x^i \mathbf{v}_i =: x^i \mathbf{v}_i$$

[3] pressure and velocity fields are obtainable by an infinite number of different velocity potentials: adding a constant term to ϕ does not change p and $\mathbf{u}$. This concept is very well known and studied in electromagnetism.

where in the last passage the summation convention is introduced, meaning that a pair of equal upper and lower Latin indices denotes summation over all the values from 1 to 3. The euclidean metric is defined in terms of the ordinary scalar product

$$\mathbf{x} \cdot \mathbf{y} = x^i \mathbf{v}_i \cdot y^j \mathbf{v}_j = v_{ij} x^i y^j \tag{1.2.1}$$

and the distance d as

$$d(\mathbf{x}, \mathbf{y}) = \sqrt{(\mathbf{x} - \mathbf{y}) \cdot (\mathbf{x} - \mathbf{y})} = |\mathbf{x} - \mathbf{y}| \tag{1.2.2}$$

where v_{ij} are the components of the (never singular) metric tensor

$$v' = v_{ij} \mathbf{v}^i \otimes \mathbf{v}^j \tag{1.2.3}$$

$\left\{\mathbf{v}^i\right\}_{i=1,2,3}$ is the dual basis of $\{\mathbf{v}_i\}$, defined by

$$\left(\mathbf{v}_i, \mathbf{v}^j\right) = \delta_i^j = \begin{cases} 1, \, i = j \\ 0, \, i \neq j \end{cases}$$

and $\otimes$ denotes the tensor (or dyadic) product.

Whereas the necessary and sufficient condition for a group of vector $\{\mathbf{v}_i\}_{i=1,2,3}$ to be a basis of the space $\mathbb{R}^3$ is the linear independence, it is usually more useful, and generally done, to choose an *orthonormal basis*[4] $\{\mathbf{e}_i\}_{i=1,2,3}$, which has the additional property that the metric tensor is given by the identity matrix

$$\mathrm{e} = \{e_{ij}\} = \mathbb{I} = \begin{pmatrix} 1 & 0 & 0 \\ 0 & 1 & 0 \\ 0 & 0 & 1 \end{pmatrix}$$

which belongs to the space $E_3 \otimes E_3$. Vectors $\mathbf{x}'$ of the dual space are represented by

$$\mathbf{x}' = x_i \mathbf{e}^i$$

where the components x_i are connected to x^i by metric tensor: $x_i = e_{ij} x^j$, so that in Cartesian coordinates $x_i = x^i$. The components x_i change under linear transformations according to the same law as the basis vectors $\mathbf{e}_i$ and, therefore, are called covariant components, to distinguish them from the contravariant components x^i, which transform in an opposite way compared with $\mathbf{e}_i$. From contravariant components and covariant space basis, invariant vector $\mathbf{x} = x^i \mathbf{e}_i$ is obtained.

To describe an event which happens at a point $\mathbf{x}$ and at time t, it is convenient to introduce a fourth dimension, labelled by 0, and set $x^0 = ct$, where c is the speed of sound. Coordinate x^0 represents the distance covered

[4] In $\mathbb{R}^3$ this basis is normally referred as Cartesian coordinates

by sound in time . The 4-dimensional real space $\mathbb{R}^4$, whose vectors have components x^0, x^1, x^2, x^3, is called acoustic space-time. Also in this case a basis vectors $\{g_\lambda\}_{\lambda=0,1,2,3}$ [5] can be introduced, so that

$$x = \sum_{\lambda=0}^{3} x^\lambda g_\lambda =: x^\lambda g_\lambda$$

Here, summation convention in the acoustic space-time is denoted by a pair of equal upper and lower Greek indices and denotes summation on all values from 0 to 3. In order to leave the wave equation invariant under acoustic Lorentz transformations

$$x' = Ax = \begin{pmatrix} \gamma & -\gamma\beta_x & -\gamma\beta_y & -\gamma\beta_z \\ -\gamma\beta_x & 1+(\gamma-1)\frac{\beta_x^2}{\beta^2} & (\gamma-1)\frac{\beta_x\beta_y}{\beta^2} & (\gamma-1)\frac{\beta_x\beta_z}{\beta^2} \\ -\gamma\beta_y & (\gamma-1)\frac{\beta_y\beta_x}{\beta^2} & 1+(\gamma-1)\frac{\beta_y^2}{\beta^2} & (\gamma-1)\frac{\beta_y\beta_z}{\beta^2} \\ -\gamma\beta_z & (\gamma-1)\frac{\beta_z\beta_x}{\beta^2} & (\gamma-1)\frac{\beta_z\beta_y}{\beta^2} & 1+(\gamma-1)\frac{\beta_z^2}{\beta^2} \end{pmatrix} \begin{pmatrix} x^0 \\ x^1 \\ x^2 \\ x^3 \end{pmatrix}$$

where $\gamma = 1/\sqrt{1-\beta^2}$, $\beta_i = u_i/c$, $\beta = |\mathbf{u}|/c$, a *pseudo-euclidean metric* has to be introduced in $\mathbb{R}^4$. Under these conditions it is possible to define the *acoustic Minkowski space* $M_4 = \left(\mathbb{R}^4, m\right)$. The pseudo-euclidean metric is defined by means of the non-positive definite scalar product

$$x \odot y = x^0 y^0 - \left(x^1 y^1 + x^2 y^2 + x^3 y^3\right) = x^\lambda g_\lambda \odot y^\lambda g_\lambda = g_{\lambda\mu} x^\lambda y^\mu$$

as

$$[m\,(x,y)]^2 = (x-y) \odot (x-y) = g_{\lambda\mu}\left(x^\lambda - y^\lambda\right)(x^\mu - y^\mu) \qquad (1.2.4)$$

where $g_{\lambda\mu} =: g_\lambda \odot g_\mu$ are the components of pseudoeuclidean metric tensor.

The physical meaning of such a formalism is quite straightforward: what is conserved is the "distance" $|x| = m\,(x,x) = \sqrt{(ct)^2 - |\mathbf{x}|^2}$. The set of all vectors of vanishing length ($|x| = 0$) is the four dimensional cone of equation $c^2t^2 = |\mathbf{x}|$, analogous to the light-cone of the relativistic theory, with axis in the direction of x^0-axis and vertex in $x = 0$: this is a characteristic surface of the wave equation. Transformations leaving invariant the scalar product given in equation (1.2.4) and the characteristic surfaces of the wave equation are just the acoustic Lorentz transformations. The cone, which in this case should be called *sound-cone*, is related to the causality principle: only all points inside the future sound-cone, i.e. satisfying the relation $c^2t^2 - |\mathbf{x}|^2 \geqslant 0$ ($\forall t \geqslant 0$) can be the support of an acoustic field (effect), produced by a source (cause) placed at the point and switched on at time $t = 0$.

[5] From this point on Greek letters will be used for indices referred to $\mathbb{R}^4$ (from 0 to 3), while Latin letters for indices in $\mathbb{R}^3$(from 1 to 3).

As for the three dimensional case, a dual basis can be defined whose vectors g^λ have the same relation written above with g_λ:

$$(g_\lambda, g^\mu) = \delta_\lambda^\mu = \begin{cases} 1, \lambda = \mu \\ 0, \lambda \neq \mu \end{cases}$$

In Minkowski space is not possible to choose a basis in which the metric tensor is equal to $\mathbb{I}\,(4 \times 4)$, since the scalar product is not positive definite, but *pseudo-Cartesian* coordinates can be introduced so that metric tensor has the following form:

$$\mathrm{g} = \{g_{\lambda\mu}\} = \begin{pmatrix} 1 & 0 & 0 & 0 \\ 0 & -1 & 0 & 0 \\ 0 & 0 & -1 & 0 \\ 0 & 0 & 0 & -1 \end{pmatrix} = \begin{pmatrix} 1 & \mathbf{0} \\ \mathbf{0} & -e_{ij} \end{pmatrix}$$

Of course, the matrix is still non-singular, but not positive definite anymore. The components of the inverse metric tensor $g^{\lambda\mu}$ are defined by

$$g^{\lambda\mu} g_{\mu\nu} = \delta_\nu^\lambda$$

x', the dual vector of x, is expressed by $x' = x_\lambda g^\lambda$ and its components are given by

$$x_\lambda = g_{\lambda\mu} x^\mu \quad x^0 = x_0 \quad x^i = -x_i$$

Finally, differentiation operators with respect to coordinates of spaces E_3 and M_4 are denoted by

$$\partial_\mu =: \frac{\partial}{\partial x^\mu} \quad \partial_0 = \tfrac{1}{c}\tfrac{\partial}{\partial t} \quad \nabla = \mathbf{e}^k \partial_k \tag{1.2.5}$$

1.2.2 Wave equation in four-dimensional form

Pressure and velocity perturbations in this new frame are rewritten as:

$$\begin{aligned} p' &= -z\partial_0 \phi \\ \mathbf{u}' &= u_k \mathbf{e}^k = (\partial_k \phi)\, \mathbf{e}^k = \nabla \phi \end{aligned}$$

from now on the primes on the acoustic quantities will be omitted for simplicity, since the context is now clearly that of linear acoustics. Moreover, according to the formalism of tensor algebra used up to now, covariant differentiation with respect to a particular index will be denoted by a comma:

$$\partial_\lambda \phi =: \phi_{,\lambda} \tag{1.2.6}$$

.

Kinetic, potential and total energy densities, K, U, W of an acoustic field in the lowest order approximation are given by the second order quantities

$$K = \frac{1}{2}\rho_0 \left|\nabla\phi\right|^2 = \frac{1}{2}\rho_0 e^{ij}\phi_{,i}\phi_{,j}$$

$$U = \frac{1}{2}\rho_0 \frac{1}{c^2}\left(\frac{\partial\phi}{\partial t}\right)^2 = \frac{1}{2}\rho_0 \left(\phi_{,0}\right)^2$$

$$W = K + U = \frac{1}{2}\rho_0 \left[e^{ij}\phi_{,i}\phi_{,j} + \left(\phi_{,0}\right)^2\right] \tag{1.2.7}$$

With the above definitions, Lagrangian density $\mathcal{L} = K - U$ can be written as an expression which is invariant under acoustic Lorentz transformations:

$$\mathcal{L} = -\frac{1}{2}\rho_0 g^{\lambda\mu}\phi_{,\lambda}\phi_{,\mu} \tag{1.2.8}$$

The wave equation may be obtained from the Lagrangian density by means of either the minimal action or the variational principle ([11], pg. 32): in both case the result is Euler-Lagrange equation

$$\frac{\partial\mathcal{L}}{\partial\phi} - \left[\frac{\partial\mathcal{L}}{\partial\phi_{,\mu}}\right]_{,\mu} = 0 \tag{1.2.9}$$

which in linear acoustics takes the form of the above-mentioned d'Alembert equation

$$\Box\phi = 0 \quad \left(\Box =: g^{\lambda\mu}\partial_\lambda\partial_\mu = \tfrac{1}{c^2}\tfrac{\partial^2}{\partial t^2} - \nabla^2\right) \tag{1.2.10}$$

Second term of equation (1.2.9) is called generalized momentum in field theory, a vector $P \in M_4$ and its components are defined as

$$P^\mu = \frac{\partial\mathcal{L}}{\partial\phi_{,\mu}} = -\rho_0 g^{\lambda\mu}\phi_{,\lambda} = -\rho_0\phi^{,\mu}$$

P^0 is equal to the acoustic pressure divided by c, while the other components are equal to the momentum density of the gas:

$$\begin{aligned} P^0 &= -\rho_0 g^{00}\phi_{,0} = -\tfrac{\rho_0}{c}\tfrac{\partial\phi}{\partial t} = \tfrac{p}{c} \\ P^i &= -\rho_0 g^{i\nu}\phi_{,\nu} = \rho_0\phi^{,i} = \rho_0\tfrac{\partial\phi}{\partial x_i} = \rho_0 v^i \end{aligned}$$

It is then easy to see that the wave equation (1.2.10) coincides with the condition of null divergence of the generalized momentum in M_4:

$$\partial_\mu P^\mu = P^\mu_{,\mu} = 0 \tag{1.2.11}$$

1.2.3 Four-dimensional energy-momentum tensor and conservation laws

A well known result of field theory is the following: if the Lagrangian density is invariant under coordinate or field transformations of a certain group, a conserved quantity exists, whose conservation law is expressed as the vanishing of the divergence of a certain tensor (Emmy Nöther's theorem). The Lagrangian of equation (1.2.8) and the wave equation (1.2.10) are invariant under both acoustic Lorentz transformations and translations in M_4:

$$\hat{x}^\mu = Ax^\mu + a^\mu$$

Invariance property under Lorentz transformations A lead to angular momentum conservation, but it will not be treated here because it is not one of the subjects of present work. Conserved quantities corresponding, to the second invariance property, are the acoustic energy and momentum: the tensor, whose vanishing divergence represents the related conservation laws, is generally called *energy-momentum tensor*

$$T^{\lambda\mu} := \left[\rho_0 \phi^{,\lambda}\phi^{,\mu} + g^{\lambda\mu}\mathcal{L}\right] \tag{1.2.12}$$

Component T^{00} is equal to the acoustic energy density :

$$T^{00} = \rho_0 \phi^{,0}\phi^{,0} + g^{00}\mathcal{L} = \rho_0 \phi^{,0}\phi^{,0} + \frac{1}{2}\rho_0 \sum_{\nu=0}^{3} (\phi^{,\nu})^2 = W$$

Spatial components are

$$\begin{aligned} T^{0i} = T^{i0} &= \rho_0 \phi^{,0}\phi^{,i} = \frac{p}{c}\phi^{,i} = \frac{pv^i}{c} = \frac{j^i}{c} \\ T^{ik} = T^{ki} &= \rho_0 \phi^{,i}\phi^{,k} + g^{ik}\mathcal{L} = \\ &= \rho_0 v^i v^k + \frac{1}{2}\rho_0 \left(\frac{p^2}{z^2} - |\mathbf{v}|^2\right) e^{ik} \end{aligned}$$

where the E_3-vector

$$\mathbf{j} := cT^{0k}\mathbf{e}_k = p\mathbf{v} = c^2\mathbf{q} \tag{1.2.13}$$

is the acoustic energy-flux density (instantaneous acoustic intensity), while the E_3-vector $\mathbf{q}$ is the acoustic momentum density. Tensor T can then be represented by the matrix

$$T = \begin{pmatrix} W & \mathbf{t} \\ \mathbf{t} & \mathrm{T} \end{pmatrix}$$

where $\mathbf{t} = \mathbf{j}/c = c\mathbf{q} \in E_3$; T is the tensor of space $E_3 \otimes E_3$, represented by[6]

$$\mathrm{T} = \rho_0 \mathbf{v}\otimes\mathbf{v} - \mathcal{L}\mathrm{e} = \rho\left[\mathbf{v}\otimes\mathbf{v} + \frac{1}{2}\left(\frac{p^2}{z^2} - |\mathbf{v}|^2\right)\mathrm{e}\right]$$

Tensor T has some properties worth to be outlined.

[6] In [10] the tensor T is denoted by W and called *wave-stress tensor*

1. Its trace is equal to twice the Lagrangian density:

$$\mathrm{Tr}\,(T) := T^{\mu}_{\mu} = \rho_0 \phi^{,\mu}\phi_{,\mu} + g^{\mu}_{\mu}\mathcal{L} = -2\mathcal{L} + 4\mathcal{L} = 2\mathcal{L}$$

2. As expected, the divergence of T identically vanishes:

$$\begin{aligned} T^{\lambda\mu}_{\ \ ,\mu} &= \rho_0 \left(\phi^{,\lambda}\phi^{,\mu}\right)_{,\mu} + g^{\lambda\mu}\mathcal{L}_{,\mu} \\ &= \rho_0 \left(\phi^{,\lambda}_{\ ,\mu}\phi^{,\mu} + \phi^{,\lambda}\phi^{,\mu}_{\ ,\mu}\right) - \frac{1}{2}\rho_0 \left(\phi^{,\mu\lambda}\phi_{,\mu} + \phi^{,\mu}\phi^{,\lambda}_{\ ,\mu}\right) \\ &= \frac{1}{2}\rho_0 \underbrace{\left(\phi^{,\lambda}_{\ ,\mu}\phi^{,\mu} - \phi^{,\mu\lambda}\phi_{,\mu}\right)}_{=0} + \phi^{,\lambda}\underbrace{P^{\mu}_{\ ,\mu}}_{=0} \equiv 0 \end{aligned} \tag{1.2.14}$$

3. The component 0 of equation (1.2.14) can be written in the form

$$\begin{aligned} T^{00}_{\ \ ,0} + T^{0i}_{\ \ ,i} &= 0 \\ \frac{1}{c}\left(\frac{\partial W}{\partial t} + \nabla\cdot\mathbf{j}\right) &= 0 \end{aligned} \tag{1.2.15}$$

   and therefore represents the conservation law of acoustic energy.

4. The components i of equation (1.2.14) can be written in vector form as

$$\tfrac{\partial \mathbf{q}}{\partial t} + \nabla\cdot\mathrm{T} = 0, \quad \nabla\cdot\mathrm{T} = \mathbf{e}_i \mathrm{T}^{ij}_{\ \ ,j} \tag{1.2.16}$$

   which represents the acoustic momentum conservation law, if the vector $-\nabla\cdot\mathrm{T}$ is interpreted as a force density.

Another form of equation (1.2.16) can be found integrating equation (1.2.16) on any fixed volume V:

$$\int_V \left[\frac{\partial \mathbf{q}}{\partial t} + \nabla\cdot\mathrm{T}\right] d^3\mathbf{x} = 0 \tag{1.2.17}$$

Calling S the surface enclosing V and $\hat{\mathbf{n}}$ its normal unit vector (pointing outwards), equation (1.2.17) can be rewritten in either form

$$\begin{aligned} \frac{d}{dt}\int_V \mathbf{q}(\mathbf{x},t) d^3\mathbf{x} &= \int_V \mathbf{f}(\mathbf{x},t) d^3\mathbf{x} \\ \frac{d}{dt}\int_V \mathbf{q}(\mathbf{x},t) d^3\mathbf{x} &= \int_S \mathbf{s}(\mathbf{x},t) d^2\mathbf{x} \end{aligned} \tag{1.2.18}$$

where $\mathbf{f} = -\nabla\cdot\mathrm{T}$, $\mathbf{s} = -\mathrm{T}\cdot\hat{\mathbf{n}}$ and divergence theorem for second equation is used. If left-hand sides of Eqs. (1.2.18) are the time derivative of the momentum produced by the acoustic wave in the volume, right-hand sides represent the force of the radiation field, expressed either in terms of a volume force (first case) or a surface force (second one). Thus, vectors $\mathbf{f}$ and $\mathbf{s}$ are respectively volume force density and surface force density of the acoustic field, the latter representing the instantaneous *acoustic radiation pressure*. It is worth to note that the time average value of $\mathbf{s}$ integrated over a surface of finite area has been called radiation force by Beissner [12].

1.3 Energy average behaviour

The main subject of the present work is the study of the average behaviour of acoustic energetic quantities. Defining stationary average operator as [13]:

$$\langle \cdot \rangle =: \lim_{T \to +\infty} \frac{1}{2T} \int_{-T}^{T} (\cdot) \mathrm{d}t$$

as far as concerns the energy density, average values of the kinetic and potential components are proportional to mean square pressure and mean square velocity respectively: in fact, averaging T^{00} component of energy-momentum tensor one obtains

$$\begin{aligned} \left\langle T^{00} \right\rangle &= \left\langle \phi^{,0} \phi^{,0} - \frac{1}{2} \rho_0 g^{00} \phi_{,\mu} \phi^{,\mu} \right\rangle \\ &= \left\langle \frac{1}{2} \rho_0 \sum_{\mu=0}^{4} \left(\phi^{,\mu} \right)^2 \right\rangle \\ &= \left\langle \frac{1}{2} \rho_0 \left(-\frac{p}{\rho_0 c} \right)^2 + \frac{1}{2} \rho_0 \mathbf{v}^2 \right\rangle \\ &= \frac{\left\langle p^2 \right\rangle}{2 \rho_0 c^2} + \frac{1}{2} \rho_0 \left\langle \mathbf{v}^2 \right\rangle =: W_p + W_k \end{aligned}$$

1.3.1 Hilbert-orthogonal decomposition of air particle velocity; radiant and oscillating intensity

Monochromatic fields

In case of monochromatic, expressions for average sound intensity and energy densities can be given analytically just in terms of pressure field and its derivative over time: this approach played a fundamental role because instruments for intensity measurements were almost exclusively based on pressure gradient technique up to the 90's. A detailed overview of the theory can be found in [1].

Recalling Euler's linearized equation (1.1.4), velocity can be derived from pressure:

$$\mathbf{u}(t) = \frac{1}{\rho_0} \int_{-\infty}^{t} \left(-\nabla p(\tau) \right) \mathrm{d}\tau$$

where $p = p_m e^{i\omega t}$, $p_m = P e^{i\phi_p}$and spatial dependence of P, ϕ_pwere omitted for clarity. Velocity is thus given by the expression:

$$\mathbf{u}(t) = -\frac{1}{i\omega\rho_0} \nabla p = \frac{1}{\omega \rho_0} \left[-P \nabla \phi_p + i \nabla P \right] e^{i(\omega t + \phi)}$$

which shows that velocity has two distinct components: one in phase with pressure, proportional to gradient of its phase, and one in quadrature, proportional to the gradient of pressure magnitude. This reflects into instantaneous intensity $\mathbf{j} = p\mathbf{u}$, which can be separated as well into an *active part* $\mathbf{i}$ and a *reactive* one $\mathbf{q}$:

$$\mathbf{j}(t) = \underbrace{-\frac{1}{\omega\rho_0} P\nabla\phi_p \cos^2(\omega t + \phi_p)}_{\mathbf{i}} + \underbrace{\frac{\nabla P}{\omega\rho_0} \sin 2(\omega t + \phi_p)}_{\mathbf{q}}$$

Introducing the time average operator $\langle\cdot\rangle_T =: T^{-1}\int_0^T \cdot dt$ over a period $T = 2\pi\omega^{-1}$, where ω is the circular frequency of the monochromatic wave, it is clear from properties of trigonometric functions that

$$\begin{aligned} \langle\mathbf{j}\rangle_T &= \langle\mathbf{i}\rangle_T = \frac{P\nabla\phi_p}{2\omega\rho_0} \\ \langle\mathbf{q}\rangle_T &= 0 \end{aligned} \tag{1.3.1}$$

that is, reactive intensity has no role in mean energy propagation.

Another very sharp description of the radiative and oscillating behaviour of the sound energy transported by plane monochromatic waves resulting by superposition of progressive and regressive waves in opposite spatial directions can be found in ref. [14]. There, it is clearly stated that the purely reactive (imaginary) character of the complex specific acoustic impedance defined as the ratio

$$\mathbf{z} = \frac{p}{\mathbf{u}}$$

is associated with the absence of net energy transport, so obtaining a picture of standing waves where energy is confined into isolated cells between the nodes of pressure and velocity, with a back-and-forth movement. The purely resistive (real) character of impedance is instead associated with sound energy that travels through each point in space (i.e. with no discontinuities along the energy path) in a series of pulses rather than a steady flow. The steady character of sound energy flow per unit area (i.e. intensity) comes out from the averaging operation. In fact, the application of the time average operator to the well known exact general expression of the instantaneous intensity $\mathbf{j}(\mathbf{x}, t) = p\mathbf{u}$ yields, in the monochromatic case studied by Towne, the following expression holding at any field point x:

$$\langle\mathbf{j}\rangle_T = (p_{rms}u_{rms}\cos\Delta\phi)\,\hat{\mathbf{k}} \tag{1.3.2}$$

where $p_{rms} = |p_m|/\sqrt{2}$ and $u_{rms} = |u_m|/\sqrt{2}$ stand respectively for the root-mean-square values of the pressure and air velocity signals $p(x,t) = p_m e^{i\omega t}$, $u(x,t) = u_m e^{i\omega t}$ along the path determined by the wave number versor $\hat{\mathbf{k}}$. Here p_m and u_m are the "complex amplitudes" of pressure and velocity allowing to synchronize the phases ϕ_p and ϕ_u of p and u to the same clock

$e^{i\omega t}$ in such a way that the "power factor" $\cos\Delta\phi$, depending only upon the phase difference $\Delta\phi = \phi_p - \phi_v$, is locked to the complex specific impedance defined as $Z =: p/u = |Z|e^{i\Delta\phi}$. Eq. (1.3.2) then states an algebraic analogy with the electrical power calculation in AC-circuits, where p corresponds to the potential difference and u to the current.

General fields

To generalize the mathematical formalism which will lead to an equation similar to equation (1.3.2) for non-monochromatic and/or non-plane wave fields, it is worth here to stress a remarkable property of the time averaged intensity $\langle\mathbf{j}\rangle_T(x)$ for monochromatic waves: wave versor $\hat{\mathbf{k}}(x)$ is given by the ratio $\langle\mathbf{j}\rangle(x)/|\langle\mathbf{j}\rangle(x)|$, determining – at each point x – a tangent vector to a spatial curve (energy streamline) always locally orthogonal to the zero phase planes of any "carrier-wave". Such a carrier-wave always transports radiative energy apart from the extreme case when the power factor is zero, which corresponds to the stationary storing of energy oscillating into isolated cells of some standing waves structure. Clearly, neither purely radiative nor pure oscillating energy is encountered in the real physical world, but energy always shows both these behaviour, due to a superposition of carrier-waves with standing interference waves (room modes). These prototypical dual behaviours of sound energy can be mathematically worked out also in general fields: using the extension of the time-averaging operator for handling general signals, radiative and oscillating properties of sound energy can be modeled through the following decomposition of the air particle velocity $\mathbf{u}$

$$\mathbf{u}(x,t) = \mathbf{u}_p + \mathbf{u}_q \tag{1.3.3}$$

already introduced in [13, 15]. Component $\mathbf{u}_p$, in phase with pressure, has the remarkable spatial property of being constrained by definition upon the same direction $\hat{\mathbf{t}}(x) =: \langle\mathbf{j}\rangle(x)/|\langle\mathbf{j}\rangle(x)|$ of the carrier-wave and the temporal property of reproducing in modulus the same time history of the pressure signal rescaled by the factor $|\langle\mathbf{j}\rangle|/\langle p^2\rangle$. Component in quadrature with pressure $\mathbf{u}_q$ is instead defined by subtraction, i.e. $\mathbf{u}_q = \mathbf{u} - \mathbf{u}_p$, so that orthogonality condition with respect time average operator is always true: $\langle\mathbf{u}_p\mathbf{u}_q\rangle \equiv 0$. In the last relation stationary time averaging procedure $\langle\cdot\rangle$ is considered as a scalar product, with which a norm and a Hilbert space can be then defined.

From this point of view, both pressure p and velocity components $(u_i)_{i=1,3}$ are considered as vectors in the Hilbert space defined above, and $\mathbf{u}_p$ and $\mathbf{u}_q$ are the projection of velocity Hilbert vector on the direction of pressure Hilbert vector and its Hilbert-orthogonal one[7]. From the above imposed properties, following explicit definitions are derived:

[7] Hilbert orthogonality does not absolutely involve spatial one. Therefore, in general velocity component $\mathbf{u}_q$ is not orthogonal to component $\mathbf{u}_p$ in the usual three dimensional space.

$$\mathbf{u}_p = \frac{\langle p\mathbf{u}\rangle}{\langle p^2\rangle} p \tag{1.3.4}$$

$$\mathbf{u}_q = \frac{\langle p^2\rangle \mathbf{u} - \langle p\mathbf{u}\rangle p}{\langle p^2\rangle} \tag{1.3.5}$$

which can be used to generalize equation (1.3.2). In fact, velocity decomposition applied to the instantaneous intensity $\mathbf{j}(x,t) = p\mathbf{u}$ leads to $\mathbf{j} = p\mathbf{u}_p + p\mathbf{u}_q =: \mathbf{i} + \mathbf{q}$. Applying time average operator, one has

$$\begin{aligned}
\langle p\mathbf{u}_p\rangle &= \left\langle p\frac{\langle p\mathbf{u}\rangle}{\langle p^2\rangle} p \right\rangle = \\
&= \frac{\langle p^2\rangle}{\langle p^2\rangle} \langle p\mathbf{u}\rangle \\
&= \langle p\mathbf{u}\rangle \\
\langle p\mathbf{u}_q\rangle &= \left\langle p\frac{\langle p^2\rangle \mathbf{u} - \langle p\mathbf{u}\rangle p}{\langle p^2\rangle} \right\rangle = \\
&= \left\langle \frac{\langle p^2\rangle p\mathbf{u} - \langle p\mathbf{u}\rangle p^2}{\langle p^2\rangle} \right\rangle = \\
&= \frac{\langle p^2\rangle \langle p\mathbf{u}\rangle - \langle p\mathbf{u}\rangle \langle p^2\rangle}{\langle p^2\rangle} \\
&= 0
\end{aligned}$$

so proving as always true the following identities:

$$\langle p\mathbf{u}_p\rangle \equiv \langle p\mathbf{u}\rangle\,;\ \langle p\mathbf{u}_q\rangle \equiv 0.$$

These identities confirm respectively that at every spatial point x of any general sound field the radiative power $\mathbf{i} = p\mathbf{u}_p$ is transported in the direction $\hat{\mathbf{t}}$ with intensity $I = |\langle\mathbf{i}\rangle|$, while the same point x can be interpreted as the "running" origin ($\langle p\mathbf{u}_q\rangle \equiv 0$) of an intensity space where reactive power $\mathbf{q} = p\mathbf{u}_q$ is stored. Clearly, from the same origin also active intensity vector $\mathbf{I} = I\hat{\mathbf{t}}$ is stuck out. This picture is in perfect agreement with the monochromatic case modeled by equation (1.3.2), which states a strict upper and lower bound for I corresponding to $\Delta\phi = [0, \pi]$, and $\Delta\phi = [\pm\pi/2]$; i.e.

$$0 \leq I \leq p_{rms} u_{rms}. \tag{1.3.6}$$

Bounding condition given in equation (1.3.6) can be proved to hold true also for general fields: squaring and averaging the definition of $\mathbf{u}_p$ (Eq. (1.3.5)), one obtains

$$I^2 = \langle p^2\rangle \langle \mathbf{u}_p^2\rangle \tag{1.3.7}$$

Substituting now $\mathbf{u}_p = \mathbf{u} - \mathbf{u}_q$ and taking into account the Hilbert-orthogonality condition $\langle \mathbf{u}_p \mathbf{u}_q \rangle \equiv 0$,

$$I^2 = \langle p^2 \rangle \left[\langle \mathbf{u}^2 \rangle - \langle \mathbf{u}_q^2 \rangle \right] \tag{1.3.8}$$

from which it is clear that I^2 has strict upper and lower bounds $0 \leq I^2 \leq \langle p^2 \rangle \langle \mathbf{u}^2 \rangle$, or

$$0 \leq I \leq \sqrt{\langle p^2 \rangle \langle \mathbf{u}^2 \rangle} = p_{rms} u_{rms}. \tag{1.3.9}$$

This relationship is then the sought generalization of (1.3.6), and its derivation in terms of $\mathbf{u}_p$ and $\mathbf{u}_q$ will ease the understanding of the physical meaning of power factor $\cos \Delta\phi$ for general sound fields. If the scalar quantity

$$Q = \sqrt{\langle p^2 \rangle \langle \mathbf{u}_q^2 \rangle} \tag{1.3.10}$$

is defined as the magnitude of the "reactive" intensity[8], equation (1.3.8) can then be rewritten as

$$I^2 + Q^2 = \langle p^2 \rangle \langle \mathbf{u}^2 \rangle$$

establishing the Pythagorean relationship with $p_{rms} u_{rms}$ which the explicit expression for power factor in general fields can be derived from:

$$\xi = \frac{I}{\sqrt{I^2 + Q^2}}, \; -\frac{\pi}{2} \leq \Delta\phi \leq \frac{\pi}{2} \tag{1.3.11}$$

Power factor is then the ratio of active intensity to time-averaged total intensity calculated at the same point. This parameter, already indicated as ξ in [15], refers to magnitudes of intensities and does not give any information about the nature of the mathematical objects, which these magnitudes come from. This aspect is evident in case of active intensity: in fact, using power factor as defined in equation (1.3.11) and versor $\hat{\mathbf{t}}(x) =: \langle \mathbf{j} \rangle(x) / |\langle \mathbf{j} \rangle(x)|$, equation (1.3.2) can be easily generalized and explicit expression of the active intensity vector field are obtained:

$$\mathbf{I}(x) = (p_{rms} u_{rms} \cos \Delta\phi)\, \hat{\mathbf{t}}. \tag{1.3.12}$$

For what it is here concerned, the definition of the magnitude Q given in equation (1.3.10) is completely self-consistent, and relation (1.3.11) suggests – in perfect analogy with the electric theory of AC circuits – that it could be derived as the imaginary part of a complex quantity $\bar{S}$, from now on called "complex intensity", whose real part is I:

$$\bar{S} = I + iQ$$

[8] Differently from Ref. [15], the term "reactive" is here used in strict connection with the elecro-acoustic analogy coming from the physical meaning of the power factor.

where i is the imaginary unit. This quantity is then a phase vector of magnitude $\sqrt{I^2+Q^2}$ and phase angle $\Delta\phi = \arccos(\xi)$, telling that at each point x of a general distributed acoustic network:

- real power is given by active intensity magnitude I;
- reactive power is the reactive intensity magnitude Q;
- apparent power is $S = \left|\bar{S}\right| = p_{rms}u_{rms}$;

all these quantities have the physical dimensions of a power per area unit.

1.3.2 Trajectories of sound energy, sound conductance and susceptance

A detailed exam of quantities just defined and the introduction of a powerful instrument to have an overall overview of average energetic features of a stationary phenomenon, called energy compass, are given in [16]. Here only a little part will be treated.

The concept of energy trajectories, based on the analogy between fluid motion and sound energy motion, has been definitively stated in acoustics in [17], where in particular connection with absorption of boundary elements was studied. In particular, mass conservation and energy conservation laws are formally the same if compared. This analogy can then be used to define the energy instantaneous velocity:

$$\begin{array}{ccc} \dfrac{\partial \rho}{\partial t} = -\nabla\cdot(\mathfrak{q}) & \leftrightarrow & \dfrac{\partial w}{\partial t} = -\nabla\cdot(\mathbf{j}) \\ \downarrow & & \downarrow \\ \mathbf{u} = \dfrac{\mathfrak{q}}{\rho} & \leftrightarrow & \bar{\mathbf{u}} = \dfrac{\mathbf{j}}{w} \end{array}$$

where $\mathfrak{q} = \rho\mathbf{u}$ is the fluid momentum density defined in (1.2.13). Also for this quantity, it is interesting to study its average behaviour in stationary conditions. Average energy velocity $\mathbf{U}$ is considered every point in space, then it forms a vector field which univocally identifies the trajectories of energy in stationary condition:

$$\frac{d\mathbf{s}(\mathbf{x}_0,t)}{dt} = \mathbf{U}(\mathbf{s})\ \mathbf{s}(\mathbf{x}_0,0) = \mathbf{x}_0 \tag{1.3.13}$$

This may however be accomplished in different ways, depending on how the average of $\bar{\mathbf{u}}$ is defined. This issue is treated in [18, 15] and what was found is that rather than consider $\mathbf{U} = \langle\bar{\mathbf{u}}\rangle = \langle\mathbf{j}/w\rangle$, it is more convenient to define the mean energy velocity as the ratio of average quantities:

$$\mathbf{U} = \frac{\langle\mathbf{j}\rangle}{\langle w\rangle} = \frac{\mathbf{I}}{W} \tag{1.3.14}$$

Among various advantages, one of the biggest is that velocity defined in equation (1.3.14) has always the same direction of the mean intensity vector $\mathbf{I}$, which identifies flux streamlines, while it is not usually the case for the other one. Moreover, energy velocity normalized to its maximum, speed of sound c, gives information on which fraction of total available energy in a neighbourhood of a point x is being radiated. This parameter, called η in already cited and given by

$$\eta = \frac{I}{cW} \tag{1.3.15}$$

satisfies the relations $0 \leq \eta \leq 1$, the extremes occurring when no energy (stationary field) or all energy (progressive field) radiates through space.

As it will be demonstrated in the following, indicator η is strictly related to a newly defined quantity, called *sound wave conductance* or *acoustic conductance*. The physical meaning of acoustic conductance is easily understood as a generalization of the concept of impedance, in terms of sound power element per unit area and mass (see [17], pp. 940-942), which can be written as:

$$z(\mathbf{x}, t, \hat{\mathbf{n}}) = \frac{1}{u^2}\frac{\mathbf{d}\Pi}{\mathbf{d}\Sigma} = \frac{\hat{\mathbf{n}} \cdot \mathbf{j}}{u^2} = \frac{p}{|\mathbf{u}|}. \tag{1.3.16}$$

where $\hat{\mathbf{n}}$ is the (adimensional) unit vector normal to the area element. Looking now at equation (1.3.16), one can reason out that there is no physical reason why only the kinetic part of the sound energy density, proportional to u^2, has to appear in the denominator. In fact, considering that the total energy density $w = w_p + w_k$ is a never vanishing quantity in any sound field, w/ρ_0 can be safely substituted in the denominator, so obtaining a quantity which has the same physical dimensions of acoustic impedance but is much more regular, since it does not have any singularity point. Its time average is then defined as

$$G(\mathbf{x}, \hat{\mathbf{n}}) = \frac{\rho_0}{\langle w \rangle}\frac{\mathbf{d}\Pi}{\mathbf{d}\Sigma} = \rho_0 \frac{\hat{\mathbf{n}} \cdot \langle \mathbf{j} \rangle}{\langle w_k + w_p \rangle} = \frac{2\hat{\mathbf{n}} \cdot \langle \mathbf{j} \rangle}{\left\langle v^2 + \left(\frac{p}{z_0}\right)^2 \right\rangle} \tag{1.3.17}$$

where $w_k = \frac{1}{2}\rho_0 v^2$ is the kinetic energy density and $w_p = \frac{p^2}{2\rho_0 c^2}$ is the potential energy density.

G and η are closely related: in fact, looking at equations (1.3.17) and (1.3.15) it is very easy to find the relations that links these quantities, if the surface considered is directed along direction of mean intensity, i.e. $\hat{\mathbf{n}} \parallel \hat{\mathbf{t}}$:

$$G(\mathbf{x}) = z_0 \eta \tag{1.3.18}$$

It is fairly easy to demonstrate that, in the case of a progressive plane wave, acoustic impedance and acoustic conductance have the same value,

equal to air characteristic impedance $z_0 = \rho_0 c$: in fact, under these conditions there is a perfect equipartition of total energy between kinetic and potential components and thus it is the same to consider either total energy density or twice only the kinetic one. Differently from impedance, this value represents an upper limit for conductance, which is limited in the range $[0, z_0]$.

Another interesting quantity characterising the whole energy transport along any trajectory is the path integral of the sound conductance $z_0\eta$ over the energy path. In fact, suppose to follow the energy particle $W(x)$ along its trajectory $\mathbf{x} = \mathbf{s}(\mathbf{x}_0, t)$ defined by equation (1.3.13), then the η-path integral can be defined as

$$\mathring{\eta}(\mathbf{x}) = \frac{\int_{\mathbf{x}_0}^{\mathbf{x}} \eta(\mathbf{s})\mathrm{d}\mathbf{s}}{\int_{\mathbf{x}_0}^{\mathbf{x}} \mathrm{d}\mathbf{s}} \tag{1.3.19}$$

and characterises the energy transport along the distance from x_0 to the running point x along the path s as a whole process. Above defined quantities in real physical situations will be studied in chapter 4 for non-monochromatic sound fields with different absorbing boundaries.

To complete the electro-acoustic-electric analogy, it is then natural to introduce here the concept of acoustic susceptance, extending to the reactive intensity the concept of acoustic conductance $G = \eta\rho_0 c$ already introduced above. In fact, defining the reactivity index as

$$\mu = \frac{Q}{cW} \tag{1.3.20}$$

the apparent power per unit area $\sqrt{I^2 + Q^2}$ can be assimilated to the total power of a circuit with normalized admittance

$$\bar{\sigma} = \frac{\bar{S}}{cW} =: \eta + i\mu \tag{1.3.21}$$

If $G = z_0\Re(\sigma) = z_0\eta$ is the acoustic conductance, then $B = z_0\Im(\sigma) = z_0\mu$ is the acoustic susceptance. These quantities and their relation are easily representable in complex plane (Fig. 1.3.1).

Finally, it is worthwhile to note here that the magnitude of the z_0-normalized admittance $\sigma = |\bar{\sigma}|$, plays the role of kinetic-potential energy partition index: it becomes evident if relations are made explicit:

$$\begin{aligned}
\sigma &= \frac{\sqrt{I^2 + Q^2}}{cW} = \frac{\sqrt{\langle p^2 \rangle \langle \mathbf{u}^2 \rangle}}{c\,(W_p + W_k)} = \\
&= \frac{\sqrt{\left(2\rho_0 c^2 W_p\right)\left(2\rho_0^{-1} W_k\right)}}{c\,(W_p + W_k)} = \\
&= \frac{\sqrt{W_p W_k}}{\frac{1}{2}\,(W_p + W_k)}
\end{aligned}$$

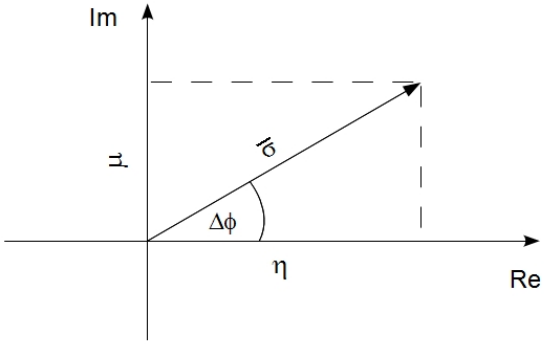

Figure 1.3.1: Graphical synthesis of sound wave conductance η and susceptance μ, normalized admittance $\bar{\sigma}$ and phase angle $\Delta\phi$.

Partition index σ, i.e. the ratio of the geometric to arithmetic means of potential and kinetic parts of energy density, describes the relative magnitude of these quantities, assuming values between 0, when energy density is either totally potential or totally kinetic, and 1, when perfect equipartition occurs.

Chapter 2

DSP techniques in Sound Energetics

Since the birth of digital systems, it is almost impossible to separate acoustic measurements from Digital Signal Processing and this work is no exception: what will be here studied does not refer to "traditional" signal processing such as octave band filtering and similar methods, therefore a brief introduction and contextualisation of algorithms used for measurements reported in Chapter 4 is certainly useful.

After an introduction which presents the known topics and relations that will be used to obtained operative expressions of the parameters given in Section 1.3, a new expression for these quantities will be given, more useful from an experimental point of view, and demonstrated. What will be written about DSP is taken from [1, 19, 20], while the original concept that will be here treated more in detail is given in [13].

2.1 Correlation and Power Spectral Density

As explained in previous chapter, second-order quantities such as intensity and energy densities are rapidly-changing variables, whose instantaneous values are sometimes not very interesting for the description of energetic properties of sound field. This is always true, but assumes particular importance for stationary phenomena, where average quantities are quite easy to achieve experimentally.

Stationary average of a function of time $f(t)$ is given by the limit of the standard time average operator:

$$\langle f \rangle = \lim_{T \to \infty} \frac{1}{2T} \int_{-T}^{T} f(t) \mathrm{d}t \tag{2.1.1}$$

Obviously it is impossible to measure the *exact* stationary value of an acoustic field, since by definition it would require an infinite time. Equation (2.1.1)

simply means that a sufficiently long measurement time has to be considered, so that the acoustic field is in equilibrium with the environment. This time range greatly depends on the environment itself: sometimes a good approximation of an infinite time measure may be even less than one second, in other cases longer time ranges are required. If the stationary average of the pressure or the velocity field is calculated, usually it vanishes since they have an oscillatory behaviour: therefore, to obtain an estimation of the mean amplitude signals, what is averaged is instead the squared value of the field: this is the definition of *root mean square value*, normally used to define pressure (or also velocity) levels.

$$p_{RMS} = \sqrt{\langle p^2 \rangle}$$

Quadratic quantities do not share this problem, so average values of intensity and total energy density are straightly defined:

$$\begin{aligned} \langle \mathbf{j} \rangle &= \langle p\mathbf{u} \rangle \\ \langle w \rangle &= \frac{1}{2}\rho_0 \left(\langle \mathbf{v}^2 \rangle + \frac{\langle p^2 \rangle}{z_0^2} \right) \end{aligned}$$

The concept of stationary average for second-order quantities can be generalized introducing the cross-correlation operator:

$$R_{xy}(\tau) =: \lim_{T\to\infty} \frac{1}{2T} \int_{-T}^{T} x(t)y(t+\tau)\mathrm{d}t \tag{2.1.2}$$

for real function such as acoustic fields in time domain[1]. Cross correlation expresses time-averaged relationship between two signals with respect to a time delay τ: when the function has a maximum, the biggest similarity occurs. A particular case is given by *autocorrelation* $R_{xx}(\tau)$, when correlation between a function and itself is calculated. Obviously, in this case the maximum value is always given for $\tau = 0$. Stationarity hypothesis can be used to determine properties of correlation functions:

$$\begin{aligned} R_{xx}(-\tau) &= R_{xx}(\tau) \\ R_{xy}(-\tau) &= R_{yx}(\tau) \end{aligned} \tag{2.1.3}$$

First relation is almost trivial: stationarity in fact involves invariance under time translations, then the same result is obtained if $t + \tau$ is considered instead of t in integral (2.1.3). Considering explicitly the second equation, if

[1] The most general definition of cross-correlation is $R_{xy}(\tau) =: \lim_{T\to\infty} \frac{1}{T} \int_0^T x^*(t)y(t+\tau)\mathrm{d}t$, where * denotes complex conjugation.

variables are directly substituted one obtains

$$\begin{aligned} R_{xy}(-\tau) &= \lim_{T\to\infty}\frac{1}{2T}\int_{-T}^{T} x(t)y(t-\tau)\mathrm{d}t \\ &= \lim_{T\to\infty}\frac{1}{2T}\int_{-(T+\tau)}^{T+\tau} x(t+\tau)y(t+\tau-\tau)\mathrm{d}(t+\tau) \\ &= \lim_{T\to\infty}\frac{1}{2T}\int_{-(T+\tau)}^{T+\tau} x(t+\tau)y(t)\mathrm{d}t \\ &= R_{yx}(\tau) \end{aligned}$$

where in the limit the finite quantity τ has been neglected. Another important relation is the *cross-correlation inequality*

$$|R_{xy}(\tau)|^2 \leq R_{xx}(0)R_{yy}(0)$$

which somewhat recalls, in time domain, coherence relation in frequency one, a function which will play a fundamental role in p-u probe calibration process described in chapter 3.

A relation similar to convolution theorem links cross-correlation of two functions and their Fourier transforms: it can be calculated from convolution theorem itself. In fact, defining convolution between two functions $x(t), y(t)$ as

$$(x * y)(\tau) =: \int_{-\infty}^{\infty} x(t)y(\tau - t)\mathrm{d}t$$

it is easily demonstrable that

$$\begin{aligned} R_{xy}(\tau) &= \int_{-\infty}^{\infty} x(t)y(t+\tau)\mathrm{d}t \\ &= \int_{-\infty}^{\infty} x(-t)y(-t+\tau)\mathrm{d}t \\ &= x(-\tau) * y(\tau) \end{aligned}$$

In frequency domain, calling with capital letters $X(\omega), Y(\omega)$ the corresponding Fourier transform of $x(t), y(t)$[2], one obtains:

$$\begin{aligned} S_{xy}(\omega) = \mathcal{F}\left(R_{xy}(\tau)\right) &= \mathcal{F}\left(x(-\tau)\right)\cdot\mathcal{F}\left(y(\tau)\right) \\ &= \overline{X}(\omega)\cdot Y(\omega) \end{aligned} \tag{2.1.4}$$

where convolution theorem itself was used to obtain last expression.

$S_{xy}(\omega)$ is called cross power spectral density and is a complex quantity whose magnitude is given by the product of magnitudes of function X, Y while phase is given by difference of phase angles. In case of auto-correlation,

[2] In this thesis the following convention for Fourier transform is assumed: $\mathcal{F}(\cdot) = \frac{1}{\sqrt{2\pi}}\int_{-\infty}^{+\infty}(\cdot)e^{-i\omega t}\mathrm{d}t$

$S_{xx}(\omega)$ is simply called power spectral density and is given by the real function $|X(\omega)|^2$: this follows both from relation (2.1.4) and from the fact that auto-correlation is an even function (Eq. (2.1.3)).

Inverse equations of (2.1.4) for cross correlation and auto-correlation are called Wiener-Khinchine relations after the two mathematicians who independently proved them in the early 1930s:

$$\begin{aligned} R_{xx}(\tau) &= \frac{1}{\sqrt{2\pi}} \int_{-\infty}^{+\infty} S_{xx}(\omega) e^{i\omega\tau} \mathrm{d}\omega \\ R_{yy}(\tau) &= \frac{1}{\sqrt{2\pi}} \int_{-\infty}^{+\infty} S_{yy}(\omega) e^{i\omega\tau} \mathrm{d}\omega \\ R_{xy}(\tau) &= \frac{1}{\sqrt{2\pi}} \int_{-\infty}^{+\infty} S_{xy}(\omega) e^{i\omega\tau} \mathrm{d}\omega \end{aligned} \tag{2.1.5}$$

These relation are of particular interest because they are the key to link stationary average of a given second-order quantity to its (cross) power spectral density: recalling that

$$\begin{aligned} \langle x^2 \rangle &= \int_{-\infty}^{\infty} x^2(t) \mathrm{d}t = R_{xx}(0) \\ \langle xy \rangle &= \int_{-\infty}^{\infty} x(t) y(t) \mathrm{d}t = R_{xy}(0) \end{aligned}$$

simply substituting expressions of correlation with their formulation in frequency domain, one obtains:

$$\begin{aligned} \langle x^2 \rangle &= \frac{1}{\sqrt{2\pi}} \int_{-\infty}^{+\infty} S_{xx}(\omega) \mathrm{d}\omega \\ \langle xy \rangle &= \frac{1}{\sqrt{2\pi}} \int_{-\infty}^{+\infty} S_{xy}(\omega) \mathrm{d}\omega \end{aligned} \tag{2.1.6}$$

where, in particular, right hand of equation (2.1.6) is real: in fact, being $S_{xy}(\omega)$ the Fourier transform of a real function, its real part is even while its imaginary one is odd. Then, in the integration over the whole frequency range, contribute from $\Im(S_{xy}(\omega))$ is vanishing.

Instead of the whole frequency range, only the positive ones can be considered to define spectral densities: both autospectral and cross-spectral densities are in fact uniquely determined by only positive frequencies. This leads to definition to *one-sided* power spectral densities and cross-power spectral densities:

$$G_{xy}(\omega) = \begin{cases} 2S_{xy}(\omega) & \omega > 0 \\ S_{xy}(\omega) & \omega = 0 \\ 0 & \omega < 0 \end{cases} \tag{2.1.7}$$

Whereas autospectral densities are not affected by this reformulation, excluded an obvious change of integration extremes, relation (2.1.6) has to be rewritten in the following form:

$$\langle xy \rangle = \frac{1}{\sqrt{2\pi}} \int_{-\infty}^{+\infty} \Re \left(G_{xy}(\omega) \right) \mathrm{d}\omega$$

because imaginary part contribution does not vanish anymore. This be an advantage however: both *coincident spectral density function (co-spectrum)* $C_{xy}(\omega)$ and *quadrature spectral density function (quad-spectrum)* $Q_{xy}(\omega)$, defined as real and imaginary parts of one-sided cross power spectral density:

$$G_{xy}(\omega) = C_{xy}(\omega) + iQ_{xy}(\omega)$$

A physical meaning can be associated to these function, as will be explained in the following subsection.

2.2 Correlative quantities

Using the formalism presented in [13], *correlative intensity* and *correlative energy density* can be defined as

$$\begin{aligned} \mathcal{J}(\tau) &= R_{pu}(\tau) \\ \mathcal{W}(\tau) &= \frac{1}{2}\rho_0 \left(R_{uu}(\tau) + \frac{R_{pp}(\tau)}{z_0^2} \right) \end{aligned}$$

As a special case, standard stationary values are obtained for $\tau = 0$. Their Fourier transform are the frequency distribution of such quantities: in particular, correlative energy density in the frequency domain will be a real, even function, while correlative intensity will transform into a complex function whose real part will be even and imaginary one odd, as explained in previous subsection. These properties, in particular intensity ones, have a precise physical interpretation: if stationary averages of energetic quantities are written, one obtains

$$\begin{aligned} \langle w_p \rangle &= \frac{1}{2\rho_0 c^2} \int_{-\infty}^{+\infty} S_{pp}(\omega) \mathrm{d}\omega \\ \langle w_k \rangle &= \frac{1}{2}\rho_0 \int_{-\infty}^{+\infty} S_{uu}(\omega) \mathrm{d}\omega \\ \langle \mathbf{j} \rangle &= \int_{-\infty}^{+\infty} \mathbf{S}_{p\mathbf{u}}(\omega) \mathrm{d}\omega \end{aligned}$$

Real part of $\mathbf{S}_{p\mathbf{u}}$ is commonly called *active intensity* and is responsible of the propagation of energy over its trajectories, as explained in 1.3; on the other hand, imaginary part of $\mathbf{S}_{p\mathbf{u}}$ is called *reactive intensity* and gives the

amount of energy that oscillates back and forth around a point in space. For its own definition, it is clear that the average value of reactive intensity *must* be null, since no net transport happens in a symmetric oscillation, which is exactly reflected by vanishing integral of $\Im(\mathbf{S}_{p\mathbf{u}})$. If one-sided quantities G are considered instead of two sided ones S, which is always possible because the symmetry properties of the latter ones makes relations univocal, then definitions of mean quantities $\mathbf{I}, \mathbf{Q}$ given in equations (1.3.7) and (1.3.10) as integrals over frequency are possible. It can be demonstrated that

$$\mathbf{I} = \int_0^{+\infty} \mathbf{C}_{p\mathbf{u}}(\omega)\mathrm{d}\omega \tag{2.2.1}$$

$$\mathbf{Q} = \int_0^{+\infty} \mathbf{Q}_{p\mathbf{u}}(\omega)\mathrm{d}\omega \tag{2.2.2}$$

where modulus come out from definition of $\mathbf{I}$ and $\mathbf{Q}$. Together with one-sided definition of autospectral pressure and velocity density, they form the complete set to determine sound conductance and susceptance, the quantities defined in subsection 1.3.2.

Such quantities describe how each monochromatic sound wave, grouped by energetic transport ([1], pp. 93-96) along the trajectory defined by (1.3.13) with energy velocity $\mathbf{U}(\mathbf{x}(t))$ contributes to sound admittance. As showed in previous section, this task can be accomplished by correlative analysis of pressure and velocity signals, having care to consider the cross and auto spectral densities for a zero delay time. As an extension of this approach, D'Spain [21] performed a complete analysis of the conductive part of the admittance (1.3.21) in order to characterise the acoustic energy propagation in deep ocean. Following the notation introduced in that work, frequency distribution of the above defined z_0-normalized conductance and susceptance can be written – for the 1-D case – as follows:

$$\check{\eta}(x,\omega) = \frac{2z_0 C_{pu}(x,\omega)}{G_{pp}(x,\omega)+G_{uu}(x,\omega)} =: \frac{N_\eta}{D} \tag{2.2.3}$$

$$\check{\mu}(x,\omega) = \frac{2z_0 Q_{pu}(x,\omega)}{G_{pp}(x,\omega)+G_{uu}(x,\omega)} =: \frac{N_\mu}{D} \tag{2.2.4}$$

where C_{pu} and Q_{pu} are respectively the coincident and quadrature spectrum. It is essential to note here that the time-averaged values $\eta(x)$ and $\mu(x)$ appearing in equations (1.3.15),(1.3.20) are obtained by a separate integration of the numerator N and the denominator D of respectively $\check{\eta}(x,\omega)$ and $\check{\mu}(x,\omega)$ over the common frequency range $\Delta\omega$ characterising the phenomenon under

investigation, i.e. explicitly

$$\eta(x) = \frac{2z_0 \left| \int_{\Delta\omega} C_{pu}(x,\omega) \mathrm{d}\omega \right|}{\int_{\Delta\omega} \left[G_{pp}(x,f) + z_0^2 G_{uu}(x,\omega) \right] \mathrm{d}\omega} \tag{2.2.5}$$

$$\mu(x) = \frac{2z_0 \left| \int_{\Delta\omega} Q_{pu}(x,\omega) \mathrm{d}\omega \right|}{\int_{\Delta\omega} \left[G_{pp}(x,f) + z_0^2 G_{uu}(x,\omega) \right] \mathrm{d}\omega} \tag{2.2.6}$$

$$\begin{aligned} \bar{\sigma}(x) &= \eta(x) + i\mu(x) \\ &= \frac{\left| \int_{\Delta\omega} \left(N_\eta(x,\omega) + i N_\mu(x,\omega) \right) \mathrm{d}\omega \right|}{\int_{\Delta\omega} D(x,\omega) \mathrm{d}\omega} \end{aligned} \tag{2.2.7}$$

But for particular studies, among which an example is given in section 4.2 where the frequency range of interest was fixed in the range f = [85, 580] Hz due to the cut-off frequency of the tube bounding the sound field, in general the overall frequency range of measurements should coincide with the acoustic band of the sound source.

Chapter 3

Calibration of p-u probes

3.1 Intensimetric probes: an overview

The experimental study of air particle velocity started many years later than the acoustic pressure one, mainly because of the lacking of a proper sensor that could measure it. It was in fact only in the late seventies that first intensimetric probes were developed by assembling two phase-matched pressure microphones, able to indirectly measure particle velocity with pressure gradient technique. Later, other sensors based on different transduction principles were born, but nearly none of them proved to be efficient enough for a wide scale employment, leaving p-p probe (as it is usually called) the only reliable instrument for intensimetric measurements . Among former p-u probes, called in this way because they directly measure particle velocity, some were based on ultrasound beams that determined velocity through Doppler effect (Fig. 3.1.1), while others used in the same way two laser beams [22]. Instruments just mentioned, and traditional p-p probe as well, have however some disadvantages, one of which is represented by sizeable magnitudes, at least compared to wavelength of high frequencies sound fields. Even if it is completely negligible in a lot of situations, this limitation may become critical in others, for example if pressure and velocity have to be measured very near to a source or to a boundary element, or when measurements in small cavities or ducts are required[1].

A new generation p-u probes started to be developed and commercially distributed around mid-nineties [23] (Fig. 3.1.2). Particle velocity MEMS sensor of this instrument is based on hot wire anemometry, a measurement principle already well known, but adapted for linear acoustics by the coupling of two thin wires. "Wind" caused by oscillatory motion of air particle under the effect of sound wave alters the temperature of both wires, causing a measurable variation in electrical resistance whose difference is proportional to velocity. This way, information about direction as well as magnitude is

[1] One example will be given also in this work, in section 4.2

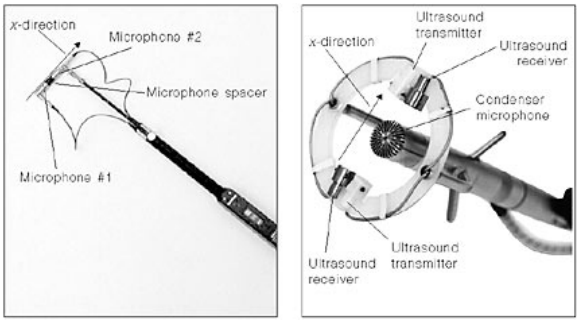

Figure 3.1.1: Examples of p-p and p-u "ultrasonic" 1D probes.

Figure 3.1.2: p-u probe: the new generation

available and sensitivity is enhanced, since differential measurements tend to be more precise and less affected by thermal self noise.

P-p and last generation p-u functioning principles pros and cons will be the topic of this section.

3.1.1 p-p intensity probes

This kind of intensity probe consists of a pair of phase-matched pressure microphones (see figure 3.1.3) which measure pressure in two distinct points and determine air particle velocity component, along instrument axis, by finite difference approximation. Starting from early 1980s, face-to-face configuration was favoured, because it was experimentally demonstrated that it increased the working bandwidth [24], and nowadays such instruments are the only ones officially recognised for intensity measurements. Vector probes are composed by three microphone pairs oriented orthogonally and represent the most evolute instrument of this kind for intensimetric measurements.

As was written above, p-p probe allows to perform the indirect measure-

Figure 3.1.3: Example of axial p-p intensity probe: microphones are in face-to face configuration

ment of the particle velocity. Named for simplicity a and b two points where the microphones are placed, pressure is obtained with a simple spatial mean $p(\mathbf{x},t) = 1/2\,(p(\mathbf{x}_a,t) + p(\mathbf{x}_b,t))$, while it is possible to estimate velocity in the middle point using finite approximation of Euler's relation (1.1.4)

$$\begin{aligned} \rho_0 \frac{\partial \mathbf{u}}{\partial t} &= -\nabla p \\ u_i(\mathbf{x},t) &= -\frac{1}{\rho_0}\int_{-\infty}^{t} \frac{\partial p(\mathbf{x},\tau)}{\partial x_i}\mathrm{d}\tau \\ &\simeq -\frac{1}{\rho_0 \left|\mathbf{x}_b - \mathbf{x}_a\right|_i}\int_{-\infty}^{t} \left(p(\mathbf{x}_b,\tau) - p(\mathbf{x}_a,\tau)\right)\mathrm{d}\tau \end{aligned} \qquad (3.1.1)$$

Usual intensity measurements in a given direction $\hat{\mathbf{n}}$ are obtained then by pressure signals from theoretical formula by substitution:

$$I_n(t) = pu_n = \frac{p_b(t) + p_a(t)}{2\rho_0 d}\int_{-\infty}^{t} \left(p_b(\tau) - p_a(\tau)\right)\mathrm{d}\tau$$

where spatial dependency was omitted for simplicity and $d = \left|\mathbf{x}_b - \mathbf{x}_a\right|_n$was introduced. Generally, however mean value of intensity is more interesting than instantaneous one:

$$\langle I_n \rangle_t = \langle pu_n \rangle_t = \frac{1}{2\rho_0 d}\lim_{T\to\infty}\frac{1}{2T}\int_{-T}^{T}\left[\left(p_b(t) + p_a(t)\right)\int_{-\infty}^{t}\left(p_b(\tau) - p_a(\tau)\right)\mathrm{d}\tau\right]\mathrm{d}t. \qquad (3.1.2)$$

Remembering that $\langle p_a \rangle_t = \langle p_b \rangle_t = 0$, and so also their time integration, equation (3.1.2) can be simplified in the following expression ([1], pg. 92):

$$\langle I_n \rangle_t = -\frac{1}{\rho_0 d}\lim_{T\to\infty}\frac{1}{2T}\int_{-T}^{T}\left[p_a(t)\int_{-\infty}^{t} p_b(\tau)\mathrm{d}\tau\right]\mathrm{d}t$$

In frequency domain integration over time is substituted by $1/i\omega$: velocity assumes the following expression

$$u_n(\mathbf{x},\omega) = \frac{p(\mathbf{x}_b,\omega) - p(\mathbf{x}_a,\omega)}{i\omega\rho_0 d}$$

and mean intensity is given by integration over frequency of cross-spectrum, as explained in section 2.2:

$$\langle I_n \rangle = \int_{-\infty}^{\infty} S_{pu}(f)\mathrm{d}f = \int_{-\infty}^{\infty} \Re\left[S_{pu}(f)\right]\mathrm{d}f$$

since cross-spectrum is the Fourier's transform of cross-correlation function ($S_{pu}(f) = \mathcal{F}\left(R_{pu}(\tau)\right)$), a real function, integration over frequency of its imaginary part gives a null contribution. For harmonic signals, it can be written in terms of pressure signals Fourier transforms thanks to analytic relation given in equation (1.3.1):

$$\langle I_n \rangle = \frac{P_1 P_2(\phi_1 - \phi_2)}{2\rho_0\omega d}$$

provided, of course that finite difference approximation holds true, that is $\phi_1 - \phi_2 \ll 1$. Here P_1, ϕ_1, P_2, ϕ_2 are magnitude and phase of pressure signals transforms, measured by the two microphones.

Since finite approximation of spatial differentiation plays a crucial role in the calculation of the particle velocity with this instrument, distance between microphones must be wisely chosen: an increase in the frequency means shorter wavelengths, so typical distances of $12 \sim 25\,\mathrm{mm}$ are good for low or mid frequencies. For λ comparable with d, i.e. $f \approx 10\,\mathrm{kHz}$, a great portion of wavelength is included between the microphones, so the approximation is no longer valid for geometric reason. This cutoff would happen even earlier, about an octave lower, but diffraction and scattering phenomena for face-to-face configuration tend to counterbalance the error of finite distance, as it was experimentally demonstrated [25]. For frequencies lower than about 80 Hz, another problem occurs, which is quite the opposite of the one exposed above, as expectable. In this case the wavelength is so much longer than the distance d that differences between measured signals p_a, p_b are at the same order of instrument noise, losing therefore their physical meaning. The only option for low-frequencies measurements is then to increase the distance between sensors: generally, for standard probes, 50 mm is a good value.

Another most important feature of p-p probes is the microphones phase responses: theory in fact takes for granted that microphones are ideally equal, an hypothesis that can be translated in the constraint that pressure responses must be as similar in magnitude and phase as possible, for every frequency. Magnitude is usually not big deal, preamplifiers or microphones themselves can be "tuned" to obtain the desired result, but phase is a more painful

issue. Unless the signals are corrected, phase match has to be as good as possible, which means that microphones for intensity probes must be chosen *a priori* with a phase response as similar as possible: state of the art sound intensity microphones are matched to a maximum phase response difference of 0.05° below 250 Hz and a phase difference proportional to the frequency above 250 Hz say, 0.2° at 1 kHz. The proportionality to the frequency is a consequence of the fact that phase mismatch in this frequency range is caused by differences between the resonance frequencies and the damping of the two microphones.

Error in velocity, or more generally in energetic measurements, depend not only on the physical features of the probe, such as sensitivity differences of the two microphones or their phase mismatch, but also on the very acoustic field measured, which can make "physical" errors either totally negligible or very important. Since in the last chapter a sound power measurement where p-p probe was used will be reported and apart from that application this kind probe was never used, this issue won't be considered here. Just to mention, usually an estimation of the probe systematic error is given by Pressure-Intensity index $\delta_{p\mathbf{I}} =: L_p - L_{|\mathbf{I}|}\,\mathrm{dB}$.

3.1.2 p-u intensity probes

Contrary to p-p ones, p-u probes combine two totally independent sensors for pressure and air velocity measurements: among different kinds available, just mentioned at the beginning of this section, this work is focused on the one invented, created and commercialised by Microflown Technologies, which couples to a canonical pressure microphone one or more velocity sensors. The Microflown is an acoustic sensor measuring particle velocity instead of sound pressure across two tiny: in fluid dynamics, the motion of gas or liquid particles is called a flow, hence the name Microflown, which is sensitive to the movement of air rather than pressure. The Microflown was invented in 1994 at the University of Twente, the Netherlands [23, 26]. All information about the sensor which will be here reported are taken from scientific documentation distributed by producing company[27].

Working principle, qualitative model

The transducer resembles a micro machined hot wire anemometer, but it is based on two heated extremely thin strips. A typical sensor is about 1 mm wide, 2 mm long and 300 μm thick (see Fig. 3.1.4). The two ultra thin platinum wires resistors that act as temperature sensors (see Fig. 3.1.4) are 200 nm thin and 10 μm wide, which means the instrument belongs to MEMS technologies, and are powered by an electrical current causing them to heat up. If no particle velocity is present, both sensors will have a typical operational temperature of about 200°C to 400°C and all the heat is transferred

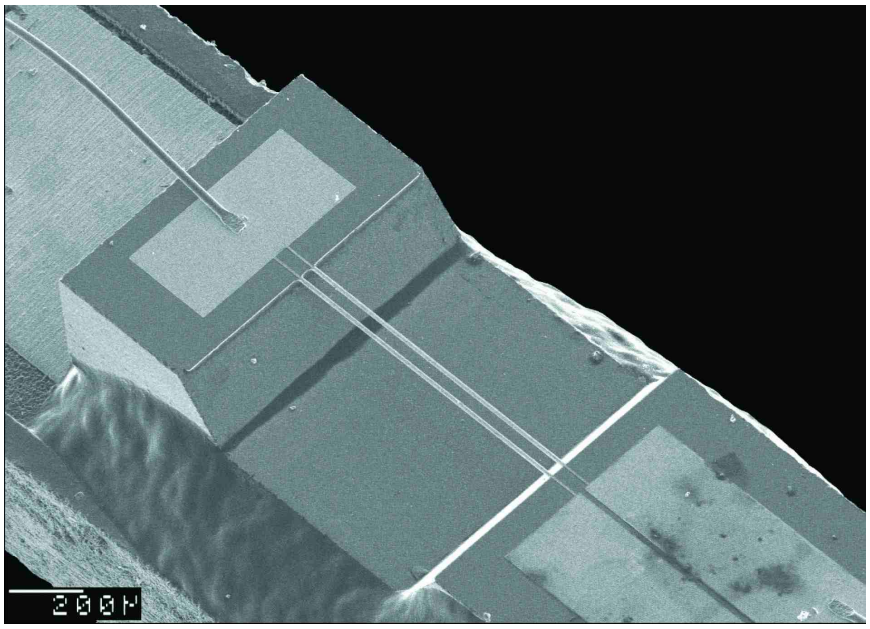

Figure 3.1.4: Picture of Microflown sensor with electron microscope

in the surrounding air. When particle velocity (sound) propagates orthogonally across the wires, it asymmetrically alters the temperature distribution around the resistors: since an increase of the temperature of the sensors leads to an increase of the resistance and vice versa, the resulting resistance difference provides a broad band (0 Hz up to at least 20 kHz, according to the company) linear and with a typical "figure of eight" directionality that is proportional to the particle velocity up to sound levels of 135 dB. The lower (noise) detectable level is in the order of . $20 \cdot 10^{-9}$ m/s $= 20$ nm/s RMS for 1 Hz bandwidth around 1 kHz, while the maximum one is about1 m/s RMS. Low Frequency Sensitivity (LFS) is the sensitivity determined at 250 Hz and represents the most practical value because at lower frequencies ($f < 100$ Hz) and higher frequencies ($f > 1$ kHz) the sensitivity decreases, as it will be explained below.

When sound wave crosses the Microflown sensor, a first order approximation shows no cooling down of the sensors: particle velocity causes the temperature distribution of both wires to alter and the total temperature distribution, because it is a linear system, is simply the sum of the temperature distribution of the two single wires. Due to the convective heat transfer however, the upstream sensor is heated less by the downstream sensor and vice versa (Fig. 3.1.5): thanks to this operation principle, the Microflown can also distinguish between positive and negative velocity direction.

Two forms of heat transport play a role: heat diffusion and convection (radiation is negligible). For large wires spacing, the heat transfer due to

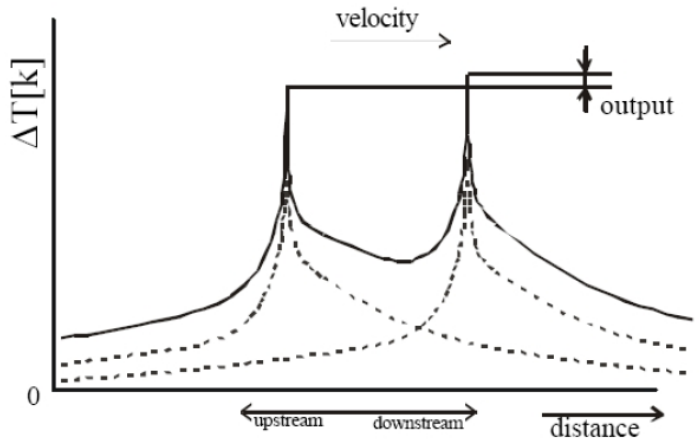

Figure 3.1.5: Temperature profile near the wires perturbed by a sound wave.

convection does not influence the sensor and because of this the temperature of the wires will be diminished in the same way, causing no output signal. On the other hand, if the wires are brought very close to each other, almost no temperature differences are possible, because a temperature difference would result in a relatively large diffusion heat transfer in the opposite direction.

At low frequencies the sensitivity of this particle velocity transducer increases 6 dB per octave; between 100 Hz and 1 kHz the frequency response is relatively flat; at higher frequencies the sensitivity of the Microflown is decreasing. This high-frequency roll-off is caused by diffusion effects (to which the time it takes for heat to travel from one wire to the other is related). The effect can be estimated by a first order low pass frequency response that has a (diffusion) corner frequency in the order of 1 kHz. The second high frequency roll-off is caused by the finite heat capacity (thermal mass) and shows an exact first order low pass behaviour that has a heat capacity corner frequency, usually in the order of 8 kHz to 20 kHz. In 2000 Svetovoy and Winter developed a mathematical model of the operation principle of the Microflown that predicted two high frequency corner frequencies [28]. This mathematical model was based on two boundary layers, i.e. the practical device as it is used now. On the other hand, low frequency sensitivity increase was first measured from later calibration, around 2004, so this behaviour has not been physically modelled yet, although it is believed to be referable to the thermal boundary layer on the wires.

The frequency response of a Microflown can be then approximated by :

$$out(f) = \frac{LFS}{\sqrt{1+\frac{f_{c1}^2}{f^2}}\sqrt{1+\frac{f^2}{f_{c2}^2}}\sqrt{1+\frac{f^2}{f_{c3}^2}}} \tag{3.1.3}$$

where LFS is the Low Frequency Sensitivity, determined at 250Hz.

A model involving electric network and based to the same physical behaviours provided also a phase response, which is given by:

$$phase(f) = \arctan\frac{C_1}{f} - \arctan\frac{f}{C_2} - \arctan\frac{f}{C_3} \tag{3.1.4}$$

where the constants C_1, C_2, C_3 are in first approximation the same as the corner frequencies f_{c1}, f_{c2}, f_{c3}.

3.2 General methodology of p-u probe calibration

3.2.1 Formalization of the problem

As known from textbooks on measurement processes [29, 30], the link between a physical quantity under measurement g and its measured value $\mathrm{g} \in \mathbb{R}^2$ in a certain system of units is given by the adimensional ratios

$$\mathrm{g} = \frac{g}{[g]} \tag{3.2.1}$$

where $[g]$ is a "sample" – i.e. a physical quantity having the same physical nature of g – adopted by international standards to serve as the measurement unit of g. This very fundamental and universal physical model is the basis for any calibration methodology and will now be considered from the point of view of the more refined theory of measurement processes based on the convolution operation $*$ as sketched for instance in [13]. A complete and detailed treatment of the theory of distributions with applications can be found in [31].

When any physical quantity g is measured by a certain instrument M yielding a measured signal g_m, and the link between g and g_m is linear, continuous, and invariant under time translations, then the measurement process can be represented, from a mathematical point of view, with a distribution m characterizing M:

$$g_m(t) = (m*g)(t) =: \int_{-\infty}^{+\infty} m(\tau)g(t-\tau)\mathrm{d}\tau. \tag{3.2.2}$$

Combining this statement with Eq. 3.2.1, a careful normalization of the measurement process $(m*g)(t)$ has to be done, by considering $\int_{-\infty}^{+\infty} m(\tau)\mathrm{d}\tau$ as an adimensional quantity and then choosing the normalization constant as $N = [g]\int_{-\infty}^{+\infty} m(\tau)\mathrm{d}\tau$, a quantity that possesses the same physical dimensions of the quantity under measurement and takes into account the

[2] From now on physical quantities will be written in italics, while roman letters refer to the associated numerical values and will always be followed by the relative unit of measurement, if they refer to a particular physical quantity.

non-transparency of the instrument itself. This way, in fact, any measured quantity g(t) can be written in terms of the normalized convolution as

$$\mathrm{g}(t) = \frac{1}{N}(m*g)(t) \equiv \frac{\int_{-\infty}^{+\infty} m(\tau)g(t-\tau)\mathrm{d}\tau)}{[g]\int_{-\infty}^{+\infty} m(\tau)\mathrm{d}\tau} \tag{3.2.3}$$

The most intuitive case is the ideal measurement process, when the convolution kernel $m(\tau)$ coincides with the Dirac's distribution: $m(\tau) \equiv \delta(\tau)$. Applying the fundamental properties of Dirac's delta distribution to Eq. 3.2.2, relation given by Eq. 3.2.1 is re-obtained. However, generally $m(\tau) \neq \delta(\tau)$: kernel m has then to be experimentally determined. Theoretically, it can be achieved by feeding the instrument with a unit impulse of the physical quantity under measurement and registering its impulse response.

In most cases response of the measuring device does not always have the same physical nature of the input signal, so a different normalization process is required in order to perform the correct measurement process[3]. When sound pressure $p(t)$ is measured by a microphone, Eq. 3.2.2 gives

$$\tilde{p}(t) = (m*p)(t) = \int_{-\infty}^{+\infty} m(\tau)p(t-\tau)\mathrm{d}\tau \tag{3.2.4}$$

where $\tilde{p}(t) = \tilde{\mathrm{p}}(t)\,\mathrm{V}$ is the "analogue" quantity of $p(t) = \mathrm{p}(t)\,\mathrm{Pa}$. This time the quantity $\int_{-\infty}^{+\infty} m(\tau)\mathrm{d}\tau$ has physical dimension given by the ratio $\tilde{p}(t)/p(t)$, in the considered case V/Pa. As with the homogeneous case, normalization constant S can be obtained measuring a pressure impulse.

$$\mathrm{S} = \int_{-\infty}^{+\infty} m(t)\mathrm{d}t\,\frac{\mathrm{V}}{\mathrm{Pa}}. \tag{3.2.5}$$

Constant S is usually called *sensitivity* of the microphone and allows to rescale the output signal from the microphone to the same gauge of the input quantity measured in Pa , or in formulas:

$$\mathrm{p}(t)Pa = \left[\mathrm{S}^{-1}\,\frac{\mathrm{Pa}}{\mathrm{V}}\right][\tilde{\mathrm{p}}(t)\,\mathrm{V}] \quad \Leftrightarrow \quad p(t) = S^{-1}\tilde{p}(t). \tag{3.2.6}$$

The general problem of the calibration of any sensor just consists in the experimental determination of S. The rigorous experimental determination of S is called the absolute or primary calibration of the sensor and is usually done by the reciprocity technique. Alternatively, S can be determined by simply comparing the readings of the instrument under calibration with those given by an already calibrated one through a trial and error measurement process in equal reference conditions [32]. This process is known as

[3] Acoustic measurements behave so: measured acoustical quantities, obtained with acousto-electrical transducers like microphones, are electric signals given in Volts

comparison calibration and is the usual one adopted in practice for microphones.

In the case of different sensors, such as p-u sound intensity probes – i.e. an assemblage of two different and non-homogeneous sensors – this strategy can be adopted only for the built-in pressure microphone: the calibration of acoustic particle velocity sensors is in fact nowadays still difficult due to the lack of standardized sensors to compare with. Despite this, as it will be explained in the next subsection, calibration by comparison can be still carried out, though indirectly, imposing the right relationship between the output reading from the velocity sensor and the pressure one when the probe is exposed to a reference sound field of known impedance (relative calibration). However, this relative calibration process requires in general the accomplishment of two preliminary steps:

1. a linearity check between output signals of the pressure (PT) and velocity (VT) probe transducers, in a reference field, in order to establish the working acoustic bandwidth of the sound intensity probe;

2. the calibration of the built-in pressure microphone by comparison with a one, having a certified flat frequency responseover the working frequency range, in order to cancel out the sensitivity deviations of the PT .

These two steps will be detailed respectively in subsection 3.3.3 and subsection 3.4.1 using a progressive plane wave as a reference field, while the general methodology for relative calibration of p-u sound intensity probes will now follow.

3.2.2 Identification and relative calibration of an axial p-u probe in a known impedance wave field

Any p-u axial intensimetric probe is a complex sensor, built-up by assembling on a single support a pressure and an air particle velocity transducer, each one having of course its own sensitivity with respect to the corresponding input signal. Calling $S_p = \tilde{p}/p$ the sensitivity of the sound pressure transducer (PT) and $S_v = \tilde{u}/u$ the one of the air particle velocity transducer (VT). If both PT and VT were ideal sensors, their sensitivities would be constant over the frequency range considered and the calibration process would be quite easy. After having defined the working frequency range and the pressure sensitivity S_p by direct comparison with a reference microphone (step 1 and two given ad the end of the previous subsection), S_v could be found from the theoretically known $Z(\omega)$ and the experimentally measured $\tilde{Z}(\omega)$ specific impedances:

$$Z(\omega) = \frac{P(\omega)}{U(\omega)} = \frac{S_p^{-1}\tilde{P}(\omega)}{S_u^{-1}\tilde{U}(\omega)} = \frac{S_u}{S_p}\tilde{Z}(\omega)$$

where $P(\omega) = \mathcal{F}(p(\omega))$ and $U(\omega) = \mathcal{F}(u(t))$. S_v is given simply inverting the first-order relation above:

$$S_v = S_p \left(\frac{Z(\omega)}{\tilde{Z}(\omega)} \right) = \left[\mathrm{S}_p \, \frac{\mathrm{V}}{\mathrm{Pa}} \right] \cdot [\mathrm{C\,rayl}]$$

where $C = {}^{Z(\omega)}/_{\tilde{Z}(\omega)}$ is a real constant and $1\,\mathrm{rayl} = 1\,{}^{Pa \cdot s}/_{\mathrm{m}}$. In fact, if PT and VT are really ideal, no variation in amplitude (apart from a constant factor) or phase will be introduced passing from acoustic quantities p, u to relative measured signals $\tilde{p}, \widetilde{u}$, so the ratio ${}^{Z}/_{\tilde{z}}$ is constant and does not depend on frequency. This ratio can therefore be measured for a single frequency, using a pure tone excitation as happens with microphone calibration with pistonphone or other calibrators.

Unfortunately, neither PTs nor VTs are ideal sensors, being their sensitivity dependent from frequency. Thus, a more general process is needed in order to get S_v, called here *relative calibration*, taking into account both PT and VT transfer functions. This process consists of two logical steps which are not necessarily sequential in time. The first is the comparison calibration of the PT with a reference pressure microphone. Differently to the common practice using a single-frequency comparison, this step has now to be extended to the whole calibration acoustic bandwidth of the probe under test so to allow the amplitude realignment of the PT frequency response over the flat response of the reference microphone. The second step is the relative adjustment of the VT transfer function (magnitude and phase) over the calibrated PT one. This adjustment can be quantified in terms of a frequency dependent complex function, called here *correction function,* and indicated with $\Gamma(\omega)$. Given the relative nature of the correction function Γ (see Eq. (3.2.13)), its determination can be calculated whether the comparison calibration process of the PT probe has been already executed or not. This is possible because the output of the PT calibration only operates on the $p(t)$ amplitude spectrum, without affecting its phase properties, and the amplitude realignment is automatically accounted for when VT sensitivity $S_v(\omega)$ is determined. In fact, it turns out that this latter quantity is obtained simply dividing $S_p(\omega)$ with the magnitude of the correction function $\Gamma(\omega)$, i.e.

$$S_u(\omega) = \frac{\mathrm{S}_p(\omega)}{|\Gamma(\omega)|} \, \frac{\mathrm{V}}{\mathrm{ms}^{-1}} \tag{3.2.7}$$

This formula, defining the magnitude of the p-u calibration filter, will be derived in detail in subsection 3.4.2 and its calculation ends the relative calibration process. The physical meaning of Eq. 3.2.7 may be understood considering that $S_u(\omega)$ is the conversion factor that for each single angular frequency ω associates the voltage value to a velocity field using the same voltage scale of pressure transducer PT, scaled of course by a factor $1/\rho_0 c$. An example is perhaps more plain: if S_p associates at a certain frequency a

1 V signal to a pressure value of 1 Pa, S_v at the same frequency will transform a measured 1 V signal to a velocity value of $^1/_{\rho_0 c}\,^{\mathrm{Pa}}/_{\mathrm{rayl}} \approx 2.4{\times}10^{-3}\,^{\mathrm{m}}/_{\mathrm{s}}$ at 15 °C.

Let's now outline the model of the relative calibration algorithm: called p_m and u_m respectively the measurements of true acoustic pressure p and air particle velocity u; moreover, whenever a quantity or its associated measure is taken in a reference field it will have 0 as a superscript. For instance, true signals from pressure and velocity waveforms under measurement in any reference model field will be indicated with $p^0(t)$ and $u^0(t)$, while $p_m^0(t)$ and $u_m^0(t)$ will be the measured signals in the same field. Then, following this notation, links between measured and true signals are given by the convolutions defined in equation (3.2.2)

$$p_m^0(t) = (m_p * p^0)(t),\ u_m^0(t) = (m_u * u)(t), \tag{3.2.8}$$

In circular frequency ω domain, convolutions become algebraic products of complex distributions:

$$P_m^0(\omega) = M_p(\omega)P^0(\omega),\ U_m^0(\omega) = M_u(\omega)U^0(\omega), \tag{3.2.9}$$

where each couple of small and capital letters in Eq. 3.2.8 and Eq. 3.2.9 corresponds to quantities related by a Fourier transform. From Eq. 3.2.9 transfer functions of pressure and velocity sensors can be easily found as:

$$M_p(\omega) = \left(\frac{P_m^0}{P^0}\right)(\omega),\ M_u = \left(\frac{U_m^0}{U^0}\right) \tag{3.2.10}$$

Now, since $M_p(\omega)$ and $M_u(\omega)$ only depend on the sensor internal features and not on the characteristics of the particular acoustic field under measurement, Eq. 3.2.9 can be extended to every general sound field, obtaining:

$$P_m(\omega) = M_p(\omega)P(\omega),\ V_m(\omega) = M_u(\omega)V(\omega).$$

Thus, if the probe, identified with the couple of transfer functions (M_p, M_u) defined by Eq. 3.2.10, is used to measure pressure and velocity in any point $\mathbf{x}$ of any unknown sound field, the link between true values under measurement and measured ones is given by:

$$P_m(\omega) = \left(\frac{P_m^0}{P^0}\right)P(\omega),\ U_m(\omega) = \left(\frac{U_m^0}{U^0}\right)U(\omega), \tag{3.2.11}$$

where the dependence on frequency has been dropped for simplifying the notation. However, the two equations in (3.2.11) are not independent one from another and can be always packed into a single equation: pressure and velocity wave fields are in fact linearly related by the acoustic Euler's equation. The ratio of the two equations (3.2.11) is then

$$Z(\mathbf{x},\omega) = \frac{Z^0}{Z_m^0} Z_m(\mathbf{x},\omega) \tag{3.2.12}$$

where $\mathbf{x}$ is the measurement point in a general field. This important relationship states that the ratio between true and measured specific impedances is independent from the particular sound field and thus can be used to identify any p-u probe. Equation (3.2.12) prescribes also the general experimental procedure for the relative calibration of any axial intensimetric probe. True impedance operator Z in any general sound field can be obtained by the non-calibrated measure of it Z_m times a correction function

$$\Gamma(\omega) = \frac{Z^0}{Z_m^0} \tag{3.2.13}$$

calculated from experimental data collected in the reference field. As formula (3.2.13) states, relative correction function is obtained once the specific impedance is measured at a given point of the reference field, where its true value is known, usually from theory. It is also worth noting that correction function $\Gamma(\omega)$ is independent from the choice of the reference field. This degree of freedom can be conveniently exploited to implement the calibration facility.

Relative calibration process ends dividing true pressure signal $P(\mathbf{x},\omega)$ by corrected specific impedance $Z(\mathbf{x},\omega) = \Gamma(\omega) Z_m(\mathbf{x},\omega)$ calculated from Eq. (3.2.13) and Eq. (3.2.12), getting the true velocity signal, which in the frequency domain looks like

$$V(\mathbf{x},\omega) = \frac{P(\mathbf{x},\omega)}{Z(\mathbf{x},\omega)}. \tag{3.2.14}$$

Here $P(\mathbf{x},\omega) = S_p^{-1}(\omega)\,|P_m(\omega)|\,e^{i\Phi_p}$. The real function $S_p(\omega)$ is the frequency dependent PT sensitivity which can be determined comparing directly the PT signal output with one given by a reference microphone of flat response in a wide band calibration field. This means that the relative calibration process of any p-u probe is always affected by a systematic error depending on the precision of the PT comparison calibration. We are finally in the position of calculating $S_p(\omega)$ according to Eq. (3.2.7). This will be done explicitly in subsection 3.4.2.

3.2.3 P-U probes calibration: state of the art

p-u intensity probes calibration is a still interesting and open issue: some works and possible solutions appeared in the last years, following in general the methodology explained in the previous section, even if exceptions are present in literature [33]. The method is simple only in theory, since there are very few cases where acoustic impedance can be considered known, corresponding mainly to ideal cases. The procedures presented up to now consist

in experimentally recreate either free field conditions, in anechoic chambers as well as in common rooms, or a standing wave field in wave guides.

Free field calibration

If a point source produce a sound in a free field, specific sound admittance will be given by the relation

$$Y = \frac{1}{\rho_0 c}\left(1 + \frac{1}{ikr}\right) \tag{3.2.15}$$

where k is the wave number and r is the distance of the probe from the source. Of course, this expression is true if the sound source can be considered an emitting monopole at all frequencies, which means big distance between loudspeaker and probe, and no reflection or standing modes are excited, making the use of particular equipment and an anechoic environment necessary. Alternatively, near field measurements can be done, provided that monopole approximation holds: possible solution are using a large plane baffle with a small hole, even if its finite dimensions will produce unwanted edge reflections, or enclosing the loudspeaker inside a spherical baffle. In both cases equation (3.2.15) has to be modified, as described by Jacobsen and in [7]. In the latter configuration it is possible to perform a good calibration also for shorter distances between source and probe, so letting the whole process to be possibly done even in normal environments. Direct sound in fact becomes leading near the source, or reflections can be detected and deleted applying appropriate windowing functions to the recorded signals. If it works for medium and high frequencies, low ones represents a problem in case of non-anechoic spaces: to solve this issue, Basten and de Bree proposed a two-step calibration [8]. In their work, for frequency higher than 1 kHz they used the already explained method based on admittance theoretical knowledge and a loudspeaker enclosed in a spherical baffle as source, while for lower ones they measured pressure inside the sphere: if the wavelength is much bigger than the diameter of the sphere, pressure inside the enclosure will be proportional to the membrane displacement. Taking its time derivative, a

relation between pressure *inside* the sphere p_{in} ad velocity of membrane u_n can be written:

$$u_n = -\frac{i\omega V_0}{\gamma A_0 p_{atm}} p_{in}$$

where V_0 is the volume of the enclosure, A_0 is the area of the moving surface, p_{atm} is the ambient pressure and γ is the adiabatic index. Air particle velocity $u_{theo}(r)$ can be expressed as a function of r, u_n and f, so velocity correction function can be directly obtained measuring p_{in} with a reference microphone and $u_{exp}(r)$: $S_u(\omega)$ is given by the ratio u_{theory}/u_{exp}.

Apart from calibration in a large anechoic room, the main disadvantage of the methods here presented is the change of configuration for high and low frequencies, which inevitably may introduce uncertainties and reduce the repeatability of the calibration process. Despite this, they provide fairly good results even in environments with reflections, so probes can be calibrated almost everywhere, being the only equipment needed the spherical sound source and a reference microphone

Standing wave field calibration

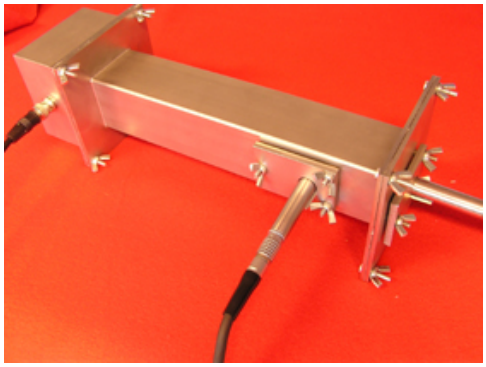

Standing wave tube is the first approach to calibration this kind of probes to have been developed [34] and it is still widely used. This method is based on the known relation between pressure and velocity in a standing plane wave field. In one dimension, limited field such as a wave guide, relation is given by:

$$Y(x) = \frac{i}{\rho_0 c} \tan\left(k\left(l - x\right)\right)$$

where k is the wave number, l the extension of the domain and x is the position in which pressure and velocity are calculated. This function however has the great disadvantage of not having neither a lower limit nor a higher one, so it is not properly suitable to determine a calibration curve for all frequencies. Solution of this problem was found considering another ratio between pressure and velocity, each one calculated at different points: $u(x)$

can in fact be related to pressure measured at the end of the wave guide, $p(l)$, and this "spatial propagated admittance" also can be analytically expressed as

$$\frac{u(x)}{p(l)} = \frac{i}{\rho_0 c} \sin\left(k\left(l - x\right)\right)$$

with the obvious advantage of having a limited function.

As just mentioned, this method is experimentally realized with Kundt's tube technique, usually adopted to determine absorbance coefficient of materials: at one end a loudspeaker excites the environment with a broad band signal, while at the other a reflective panel ensures that the field is almost entirely composed of standing plane wave. A small hole allows a reference microphone to be inserted in the reflective panel for $p(l)$ measurement. Results obtained can be used either to directly build an experimental correction curve or as the starting point of a fit process using analytical functions of the Microflown theoretical model, given by equations (3.1.3) and (3.1.4); usually this last option is preferable, since it leads to more robust results.

This method is very easy-to-do and, differently from free field procedure, does not depend on the particular environment because of the use of a wave guide; equipment is low cost and has reduced dimensions (70 cm is the length of the "long tube", while 30 cm is the "short tube" commercialized by Microflown Technologies itself). However, bandwidth is limited to about 4 kHz for geometric reasons (transverse dimensions of wave guide), since it has to be used for $^1/_2{}''$probes.

3.2.4 Calculation of the correction curve for progressive plane wave reference fields

The choice of the progressive plane wave field as a reference condition is based on acoustic simplicity, even if its practical implementation required a very special facility. As very well known, in this situation specific impedance is purely resistive and is represented by a real constant, independent from the position and equal to characteristic impedance air impedance z_0

$$Z^0(\omega) = \frac{P^0}{V^0} = z_0 = \rho_0 c \tag{3.2.16}$$

where ρ_0 is the unperturbed air density and c is the sound velocity. For this reference field correction function given in equation (3.2.13) is simply calculated as

$$\Gamma(\omega) = \frac{Z_m^0(\omega)}{\rho_0 c} \tag{3.2.17}$$

This function identifies any single p-u probe and has to be applied to successive measurements of acoustic impedance made with the same probe, in any

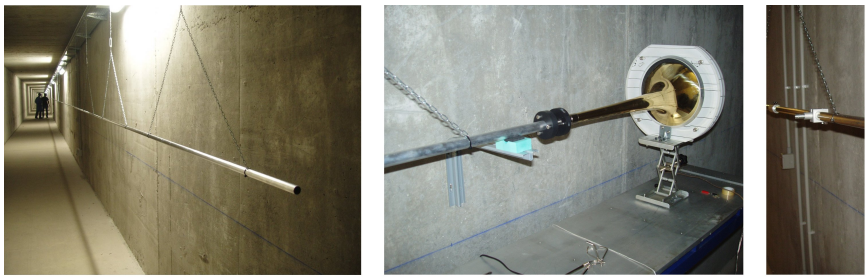

Figure 3.3.1: Progressive plane wave calibration apparatus: a) acoustic waveguide installed in the LARIX Lab of the University of Ferrara; b) sound source assembled with a bi-conical loudspeaker coupled to a trombone bell; c) probe mounting system for 1/4" microphones located at calibration point 15m far from the source.

other general field condition, in order to get the correct value of the acoustic operator $Z(\omega)$ given by Eq. 3.2.12.

3.3 Progressive plane wave calibration setup

The main idea behind the here exposed p-u probe calibration is to use an even simpler acoustic field than the ones given in previous methods: the progressive plane wave one. Using an idea of Wolfe for a reference in the measurement of flute impedance [35], a long, narrow one dimensional wave guide was built. In the following details will be given. This is a somehow conclusive point of a study which required several years and whose steps are given in [36, 37, 38, 39, 40].

3.3.1 Experimental implementation and acoustical characterization of the wave-guide facility

As seen from Figure 3.3.1 a), the LARIX laboratory consists in a 100 m long underground tunnel, which assures a weak dependence of the internal thermodynamic parameters from climatic changes over different period of the year. For example, an external variation of over 15 °Cof temperature over three months and about 30 %of relative humidity, quantities which air density, speed of sound and air impedance consequently depend on, led to a variation of about 0.9 °C (from 16.8 to 17.7 °C) and 10% humidity (from 67% to 76%).

The calibration reference field has been generated using a Tannoy® bi-conical loudspeaker, coupled to the wave guide through an impedance adapter (a modified tenor trombone, see Figure 3.3.1-b). This system is es-

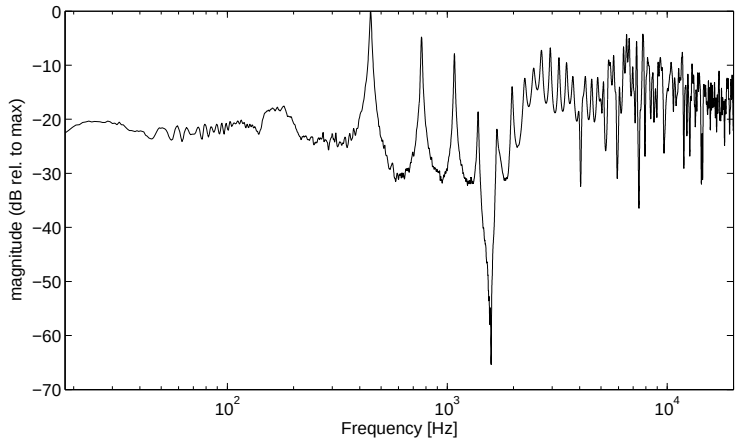

Figure 3.3.2: Transfer function magnitude (V/V) between pressure signal measured at different points and loudspeaker input signal from power amplifier. a) microphone is placed in front of the trombone;

sential to provide a good sound radiation into the wave guide in the whole frequency range from 20Hz to 20kHz, as it can be seen in Figure 3.3.2, where transfer function magnitude between pressure measured in front to the trombone end and Tannoy® loudspeaker input signal is reported. At the measure point a small hole with a customized mount (Fig. 3.3.1-c)) allows a measure of the acoustic fields both with the probe under test, in this work a Microflown PU match, and the reference microphone, quarter-inch B&K type 4939.

Transfer function magnitude with the microphone located along the wave guide at about 6.5 m and 17.5 m from the adapter end (source terminal), is shown in Figure 3.3.3. From the comparison of frequency responses reported in Figures 3.3.2 and 3.3.3, it seems that the whole wave guide system acts as a low pass filter, as expected for a progressive sound wave travelling in a guide.

The main issue now is to check whether the model field of progressive plane wave is reproduced with sufficient precision in the experimental apparatus. Two are the main constraints which has to be taken into account for a good approximation:

1. The wave field has to remain one-dimensional for a frequency range as wide as possible, theoretically for the whole audible bandwidth.

2. No stationary modes are to be induced, guaranteeing this way the progressivity of the reproduced field.

Both conditions are influenced by geometry of the wave guide, in particular its dimensions: wave front must be in fact constant for displacements ortho-

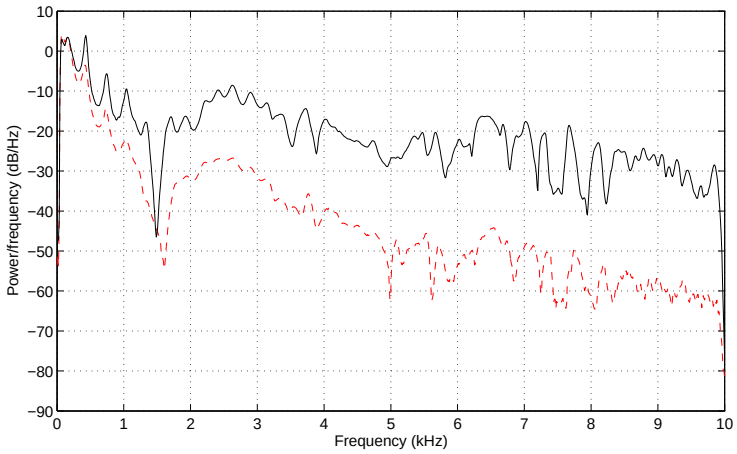

Figure 3.3.3: Transfer function, given in terms of power spectral density, measured inside the wave guide at about 6.5 m (black, solid curve) and17.5 m (red,dashed curve) from source. Scale is in dB rel to max.

gonal to the wave propagation. Provided that it is equivalent to state that no transverse modes have to be excited, it gives an upper limit for the minimum wavelength of the calibration field, equal roughly to twice the transverse dimension of the guide itself. Having chosen a circular section for the wave guide, from ([10], pp. 509-511) cutoff frequencies for transverse modes are given by formula

$$f_{mn} = \alpha_{mn}\frac{c}{2b}$$

where c is the speed of sound, b the radius of the duct and α_{mn} are the solutions of the boundary condition equation $J'(\pi\alpha) = 0$ for rigid walls; J represents a Bessel function of the first kind. First mode to be excited, $\alpha_{10} = 0.5861$, has a cutoff frequency, for a radius of 9mm, equal to

$$f_{10} = 0.5861\frac{c}{1.8\cdot 10^{-3}} \simeq 11\text{kHz}$$

which thus represents the sought upper limit for the excitation field.

Regarding the cut of possible reflections, the solution adopted was to build a wave guide so long that the field is attenuated via visco-thermal interaction with pipe walls before a perceivable reflection can be created. It was quite easy to experimentally demonstrate it, since the law of attenuation of a sound wave travelling in a duct is well-known, as described in literature [41, 42, 43]

$$P_{loss}\,[\text{Pa/m}] \simeq p_0 e^{-\alpha x};\ \alpha = \frac{(\gamma - 1 + \sigma)}{r\sqrt{\frac{\rho_0 c^2 C_p}{\pi\lambda}}}\sqrt{f} \tag{3.3.1}$$

where:

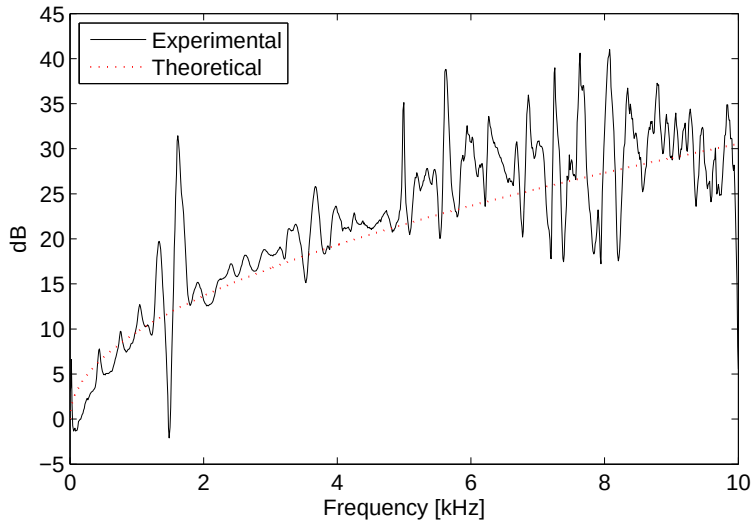

Figure 3.3.4: Comparison between experimental (difference of curves in figure 3.3.3) and theoretical (Eq. (3.3.1)) transfer functions between pressure at 6.5 m and 17.5 m from the source.

α is the attenuation coefficient;

γ is the adiabatic index;

r is the pipe radius;

$\sigma = \sqrt{\mu C_p/\lambda}$ is the square root of the Prandtl number;

μ is the viscosity coefficient;

λ is the thermal conductivity.

C_p is the specific heat at constant pressure

A length of 84 m, such as the guide built at LARIX, is therefore more than enough to guarantee no sound waves travelling back: for example, the attenuation coefficient can be estimated in about $0.88\,^{\mathrm{dB}}/_{\mathrm{m}}$ at 1 kHz for a pipe radius of 9 mm. As a test for the whole frequency range, experimental and theoretical transfer functions between two measurement points at 6.5 m and 17.5 m from the source were calculated, showing a good agreement with theoretical curve, as illustrated in figure 3.3.4.

The check of the field features require instead a more detailed study, in particular involving the use of p-u probes to consider spatial properties of acoustic specific impedance. The theoretical value of this quantity, for progressive plane wave field, is independent from position, real and equal to the characteristic air impedance z_0. Although, before the calibration, the "raw"

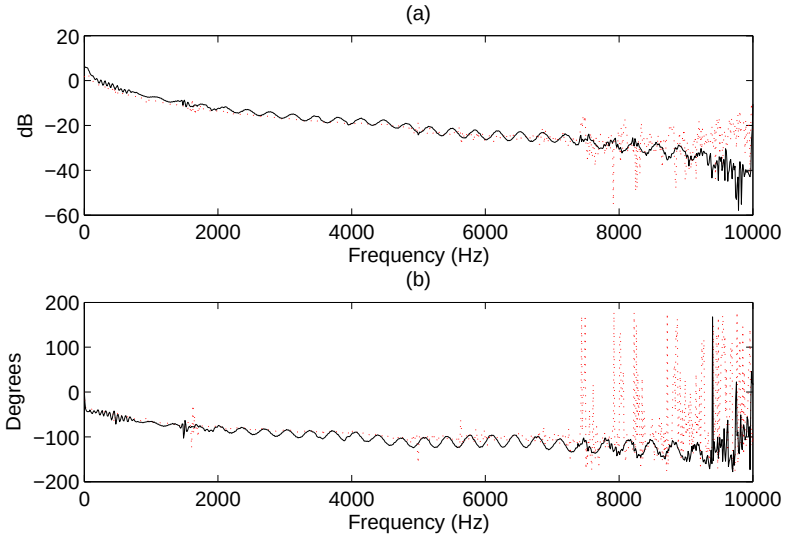

Figure 3.3.5: Amplitude (a) and phase (b) of the ratio between uncalibrated p and v signals. Black, solid lines refer to signals measured at a distance of 6.5 m from source; red dotted lines to a distance of 17.5 m.

ratio between pressure and velocity signals recorded by the given probe may be very different from the theoretical one, the invariance feature under spatial translations must be held: therefore, experimental specific impedance must not change if measurements are taken in different points, whatever the value it may assume. p and u were measured at the same points used for results in figure 3.3.3, then amplitude and phase relations of their ratio were compared. As figure 3.3.5 shows, the result of this test confirms an almost perfect agreement between theory and experiment. The jitter affecting impedance measurements at 6.5 m is caused by a reflection induced by probe itself, impossible to avoid but giving no critical effect upon the probe calibration, as it will be explained later

Another fundamental aspect for a good measure in general and an acceptable calibration procedure in particular is a sufficiently high signal to noise ratio. While in a more traditional environment for instrument calibration, such as an anechoic room or a short tube, it can be predicted that the floor noise remains quite low in the whole frequency range, a long wave guide requires a particular attention because unwanted noise at low frequencies could be trapped inside the wave guide and disturb the process. Although theory ensures that nothing like that would happen, an experimental check was conducted, recording the pressure and velocity levels with the calibration source on and off, for a time long enough to approximate the stationary condition.

Pressure and velocity has been measured at the calibration point, located

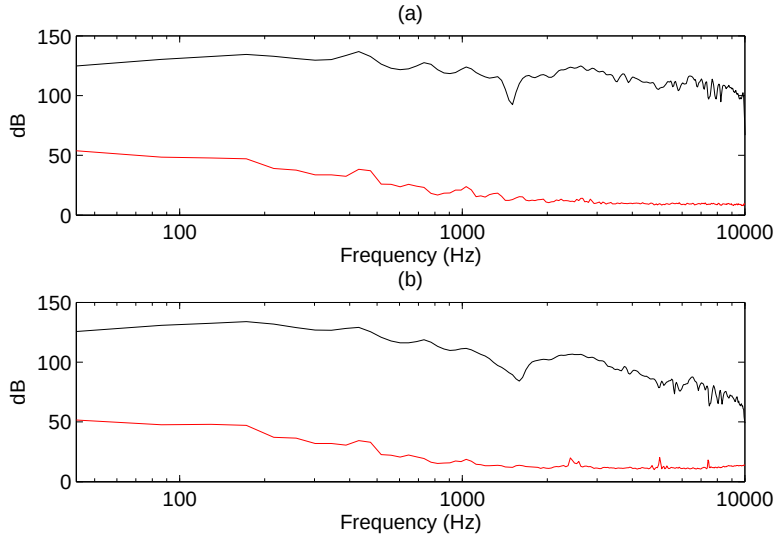

Figure 3.3.6: Signal-to-floor-noise ratio measured with the probe pressure (left) and velocity (right) transducers during a typical calibration session.

at about 7m far from the source terminal, in response to the typical sine sweep signal level used for calibration. Obtained results are reported in figure 3.3.6, where one can clearly see that calibration measurements has been always executed with a sufficiently high signal-to-noise ratio. It is also interesting to note that the systematic notch around 1.5kHz, caused by a loss of power of the source, ad it can be noticed from figure 3.3.2, has no significant influence on the calibration process.

It is worthwhile to consider here that, differently from other calibration methodologies known from literature, the present one allows a full bandwidth calibration of p-u probes to be executed with a single measuring session, in identical field conditions for the whole frequency band from 20 to 10000 Hz: a considerable advantage in terms of reliability and precision of measure, which somewhat repays the complexity of the facility, if compare with the spherical or the standing wave calibrators.

3.3.2 Time-domain characterization of the reference field

In order to determine whether the 84m long wave guide with the source at one terminal really behaves like a semi-infinite 1-D environment, two pressure impulse responses were measured in the reference field at 6.5 m and 17.5 m far from the source. Obtained impulse responses are reported in figure 3.3.7 (a) and (b), where it can be seen that the only reflections measured are caused by the probe itself when located at 6.5 m from the source. The path difference between direct and reflected impulse response turns out to be

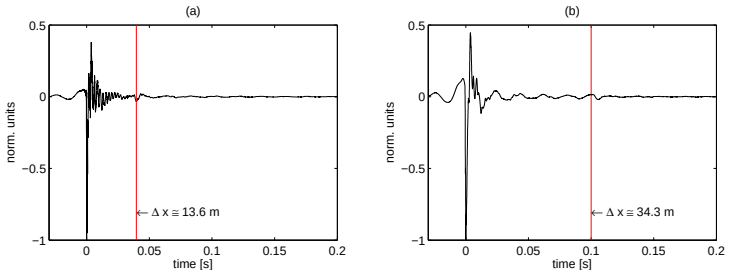

Figure 3.3.7: Pressure impulse responses measured at 6.5 m (a) and 17.5 m (b) from the source. The Δx arrow marks the reflections due to the probe itself.

about twice the distance between the probe and the loudspeaker: 13.5 m (see plot (a)). The reflections are almost no more detectable when the receiving point is moved to 17.5 m from the source (plot (b)). On the other hand, there is no measurable reflections from the far terminal. As a matter of fact, this terminal can be modeled as an image source located more than 150 m apart from both the measurement points so behaving – due to the wall losses – as an anechoic terminal. This is enough to safely state that the wave guide used for calibration fully assures the progressive character of the plane wave reference field, up to the cut-off frequency of $\approx$ 10 kHz . It is worth to report here that, also if detectable in time domain, the single auto-reflection from the 6.5 m mounted probe (see plot (a)) has no measurable effect on calibration results, since it can be deleted by the use of an appropriate windowing function. As said above, anyway, the 6.5 m probe location is preferable for its signal-to-noise ratio (see Fig. 3.3.6) than the 17.5 m one, and then, in spite of the reflections, it can be safely chosen as the standard probe position for the calibration measurements.

3.3.3 Determination of the calibration acoustic bandwidth: coherence

Before the relative calibration procedure is started, the determination of the frequency range where the intensimetric probe under test correctly works is necessary. In fact, measurements of the concatenated pressure and velocity waveforms at the same spatial position must agree in any general field with linear acoustic theory: in other words, signals measured p_m and v_m have to show a precise relation, regardless the calibration of the instrument. Linear acoustics states that, since pressure and particle velocity fields are both obtained by differentiation of the single velocity potential $\phi(\mathbf{x}, t)$ as:

$$p(\mathbf{x}, t) = -\rho_0 \frac{\partial \phi}{\partial t},\ v(\mathbf{x}, t) = \nabla \phi,$$

then the relation between the two observable fields p and v has to be linear and given by the Euler's equation and the mass conservation equation. A linearity check between the pressure and velocity sampled signals has then to be done, in order to determine the acoustic bandwidth of the sound intensity probe running under calibration conditions. As well known, this theoretical requirement can be checked on pressure and velocity signals by using a dual channel frequency analyzer by means of the coherence function $\gamma(\omega)$, which in our case may be rewritten as:

$$\gamma(\omega) = \sqrt{\frac{|S_{pv}(\omega)|^2}{S_{pp}(\omega)S_{vv}(\omega)}} \tag{3.3.2}$$

where $S_{pv}(\omega)$ is the cross-spectrum of pressure and velocity signals sampled at the same point and $S_{pp}(\omega), S_{vv}(\omega)$, are p and v auto-spectra. As long as this function is equal to 1, the linearity between pressure and velocity is assured, so the correct functioning of the probe is guaranteed. Thus, checking the condition $\gamma(\omega) = 1$ for any p-v probe under test using a 1-D calibration setup (i.e. within a 1-D reference field) allows to safely determine the frequency range where the obtained probe calibration filters are acoustically acceptable. Figure 3.3.8 shows the $[20, 11000]$ Hz coherence function of the probe under test, measured within the acoustic wave guide in calibration conditions. This result was obtained exciting the wave guide with broad band white noise. Although the excitation signal has an upper frequency much higher than 11 kHz, above this frequency the environment starts to behave as a 3-D one. Then, a linearity check would include all the component of acoustic velocity, which is out of interest for the aim of this measure. As it can be seen, the high frequency cut-off of the acoustic band-pass filter of the tested probe is well detectable at about 9 kHz, when the coherence function becomes definitely lower than 1. It is worthwhile to remark here that the sharp peaks of coherence loss found at about 1.5 kHz and 7.5 kHz have only a residual effect on calibration results as well assessed by the magnitude of the correction function $\Gamma(\omega)$ reported in Figure 3.4.3.

3.4 Determination of the experimental calibration filter and comparison with the nominal one

3.4.1 Full bandwidth comparison-calibration of the pressure transducer

All the here reported results refer to one of the Microflown® PU Match probes which is the part PT0702-04 of a system specially customized for hyper-intensimetric applications [17] (Microflown® kit #133, see Figure 3.4.1).

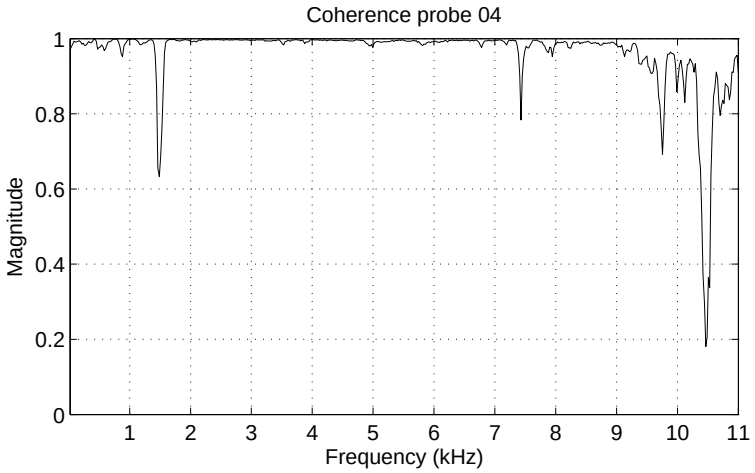

Figure 3.3.8: Coherence function $\gamma(f)$ of the probe under test, evaluated in calibration field conditions.

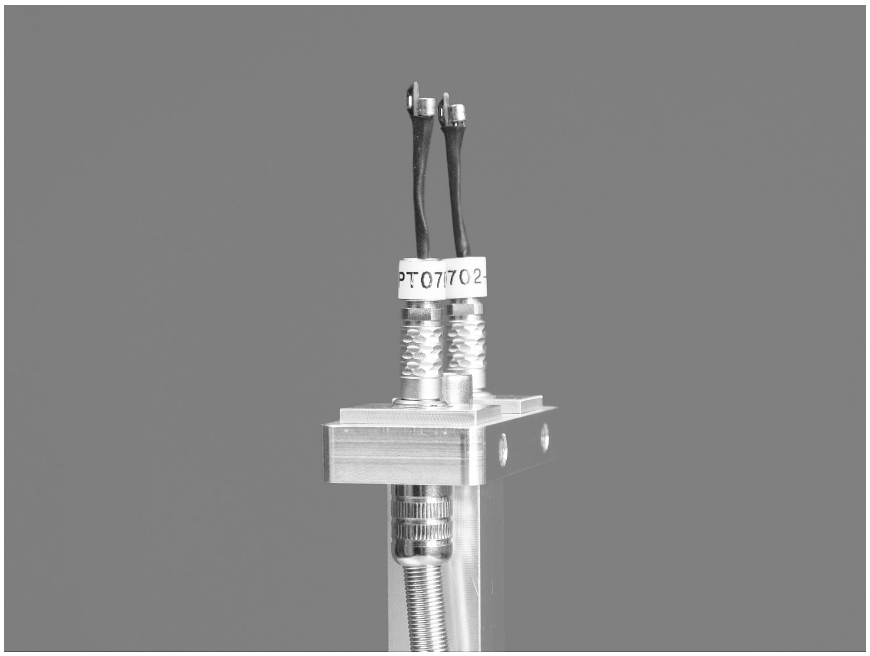

Figure 3.4.1: The hyper-intensimetric system: detail of the twin probes mount specially designed for the Microflown® kit #133 at the Acoustics Lab of Physics Department-Imamoter, Ferrara University.

The PT of the sound intensity probe under test is a $^1/_{10}''$ electrete microphone of cylindrical shape, having – as reported in the Calibration Report by the manufacturer [44] – a nominal sensitivity $S_p(1000\,\mathrm{Hz}) = 44\,^{\mathrm{mV}}/_{\mathrm{Pa}}$. Anyway, following the here proposed calibration procedure, PT sensitivity must be realigned at each frequency against the flat frequency response of a reference microphone. This frequency response, in turn, has to be determined using an FFT analyzer previously calibrated with a known source (usually a $94\,\mathrm{dB_{SPL}}$, 1 kHz pistonphone). In our case, a $^1/_4''$ B&K® type 4939 pressure microphone was used as reference microphone and its frequency response has been measured at the calibration point located 6.5 m from the source. The calibration reference field has been generated within the wave-guide using a broad-band signal (logarithmic sine sweep) and the comparison calibration between the B&K® pressure microphone and the Microflown® PT of the probe under test has been extended at once to the $[20, 10000\,]Hz$ frequency range. Since the analyzer was calibrated with a pure tone of 1 kHz, the sensitivity of PT was calculated comparing the power spectrum filtered in the third-octave band centered at the same frequency with the same result obtained with the reference microphone. This process lead to an experimental value of $S_p(1000\,\mathrm{Hz}) = 53\,^{\mathrm{mV}}/_{\mathrm{Pa}}$, about 21% higher than the nominal value given in the factory calibration report. Figure 3.4.2 shows a more general relation than the simple comparison between tonal frequency measurements: the difference in dB-SPL between the spectrum of the probe built-in PT and the B&K® type 4939 one. Clearly, the zero value at 1000 Hz marks the result of comparison calibration between the reference microphone and the probe PT when read over the same scale of a calibrated FFT analyzer. It is evident that the PT of the probe under test has a significant sensitivity loss for frequencies below 200Hz . Even if it does not affect the relative phase between the pressure and velocity signals, this regrettable feature of the PT transducer would have of course a destructive fallout over the relative calibration process. The full bandwidth comparison calibration of the PT transducer (i.e. the experimental determination of $S_p(\omega)$) is a necessary task in order to minimize the systematic error reported in Figure 3.4.2. The effect of $S_p(\omega)$ on the correction function $\Gamma(\omega)$ will be reported in 3.4.3.

3.4.2 Relative calibration of the velocity transducer

Relative calibration process consists mainly in determining the correction function $\Gamma(\omega)$, according to Eq. (3.2.17), but taking into account that acoustic pressure and velocity are both transduced over the same voltage scale, the relation has to be rewritten in the following form:

$$\Gamma(\omega) = \frac{\tilde{P}_m^0}{(\rho_0 \mathrm{c})\tilde{U}_m^0} \tag{3.4.1}$$

where now ρ_0c is only a dimensionless numerical factor. This expression

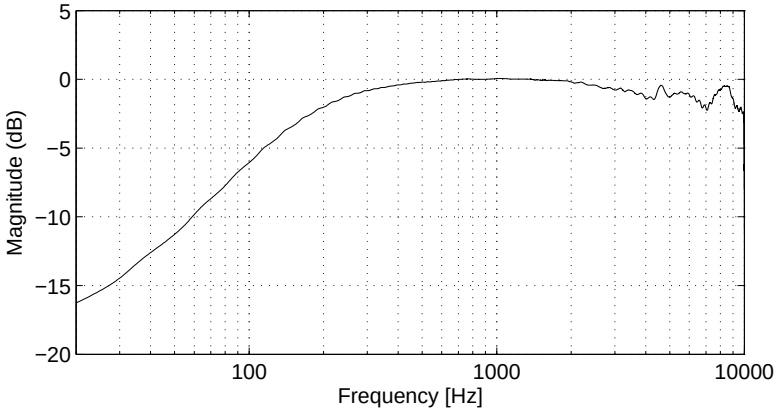

Figure 3.4.2: SPL difference between B&K microphone frequency flat response and that of the 1 kHz calibrated PT of the probe under test.

can be simply evaluated, from an experimental point of view, operating with FFT algorithm over the synchronized responses of PT and VT. Magnitude and phase of the function $\Gamma(\omega)$ for the probe n. PT0702-04 are reported in figure 3.4.3.

Once the correction function $\Gamma(\omega)$ has been determined with Eq. 3.4.1, according to Eq. 3.2.14 relative calibration process ends calculating the calibrated velocity signal as

$$U(\mathbf{x},\omega) = \frac{P(\mathbf{x},\omega)}{Z(\mathbf{x},\omega)}$$

where $Z(\omega) = \Gamma(\omega)Z_m(\omega)$ and $P(\omega) = S_p^{-1}(\omega)\tilde{P}_m(\omega)$ is the calibrated pressure signal. We are finally in the position of calculating the VT sensitivity $\mathrm{S}_u(\omega)\,{}^{\mathrm{V}}/_{\mathrm{ms}^{-1}}$ given in Eq. 3.2.7. This can be done by starting from the definition $S_u =: {}^{|\tilde{U}|}/_{|U|}$ and considering the dimensional relation $[|U|] = [{}^{|P|}/_{\rho_0 c}] = \left[\frac{|\tilde{P}|}{S_p \rho_0 c}\right]$, which converts the velocity sample equal to $2.4{\times}10^{-2}\,{}^{\mathrm{m}}/_{\mathrm{s}}$ to the same voltage scale of the pressure transducer. In fact

$$S_u = \frac{\left|\tilde{U}\right|}{|U|} = \left[\frac{\left|\tilde{\mathrm{U}}\right|}{\left|\tilde{\mathrm{P}}\right|}\frac{\mathrm{V}}{\mathrm{V}}\right]\left[\mathrm{S}_p\,\frac{\mathrm{V}}{\mathrm{Pa}}\right][\rho_0 \mathrm{c\ rayl}] = \frac{S_p\rho_0 c}{|\mathrm{Z}|} = \frac{\mathrm{S}_p}{|\Gamma|}\,\frac{\mathrm{V}}{\mathrm{ms}^{-1}}$$

just coincides with Eq. 3.2.7, once the dependence on frequency has been taken into account. Here |Z| indicates the magnitude of the acoustic admittance: when the pressure and velocity signals are measured on the same voltage scale, such as in this relation, it is clearly an adimensional quantity, and Eq. 3.4.1 was used in the last step. The value of VT sensitivity obtained at 250 Hz as a consequence of the calibration process is

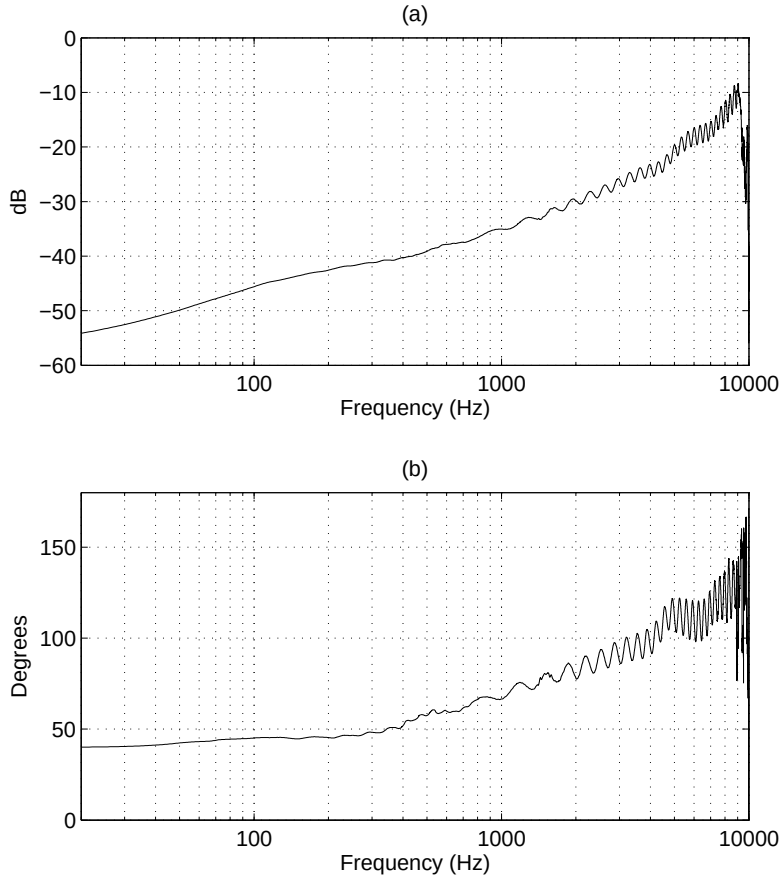

Figure 3.4.3: Fine band magnitude (a) and phase (b) of the correction function Γ evaluated from Eq.3.4.1. Moving average filter of about 6% of the data array length (200 samples over 32769) was applied to highlight the function trend.

$S_u(250\,\mathrm{Hz}) = |\Gamma(250\,{}^{\mathrm{Hz}}/)|^{-1}\mathrm{S}_p\,\mathrm{V}ms^{-1} = 19.4^{\mathrm{V}}/_{\mathrm{ms}^{-1}}$. This value turns out to be about 3% lower than the nominal one, which has been reported by the manufacturer as $LFS = 19.4^{\mathrm{V}}/_{\mathrm{ms}^{-1}}$ at 250 Hz in the factory calibration report.

3.4.3 Analytical model: comparison between nominal and experimentally fitted calibration filters

The velocity sensitivity curve for Microflown sensors is given by factory in terms of a parametric analytical function, which acts as a model of the probe. As explained in subsection 3.1.2, two different phenomena combine to take account of the velocity transducer sensitivity loss at high frequencies: the finite rate of the heat transport and the finite heat capacity of the wires. These effects, together with a low-frequency sensitivity decrease which has been experimentally observed but still not explained, have been related by the manufacturer to a nominal transfer function of the pressure element co-assembled into the p-u probe, obtaining the following magnitude and phase corrections for the velocity transducer:

$$\begin{aligned} U_{Mag-corr} &= \frac{1}{LFS}\sqrt{1+\left(\frac{F_1}{f}\right)^2}\sqrt{1+\left(\frac{f}{F_2}\right)^2}\sqrt{1+\left(\frac{f}{F_3}\right)^2} \\ U_{Phase-corr} &= -\arctan\left(\frac{C_1}{f}\right)+\arctan\left(\frac{f}{C_2}\right)+\arctan\left(\frac{f}{C_3}\right) \end{aligned} \quad (3.4.2)$$

Here $F_{i=1..3}$ and $C_{i=1..3}$ are the parameters (corner frequencies) characterizing respectively the magnitude and phase of the correction filters to be applied directly to the uncalibrated velocity signal in order to obtain the calibrated one; LFS (Low Frequency Sensitivity) is the nominal sensitivity of the Microflown VT ($LFS = S_u(f = 250\,\mathrm{Hz})$) for the probe under test). In the corrections of equations (3.4.2) the corner frequencies F_1 and C_1 are due to the amplitude and phase deviations of the PT from the reference microphone response at low frequencies (Fig. 3.4.2). $F_{i=2,3}$ and $C_{i=2,3}$ compensate instead the deviations typical of the VT transducer and their induced corrections can be removed by turning down the control switch of the probe signal conditioner provided by the manufacturer. This configuration is called "uncorrected" in the factory calibration report. The analog filter were clearly disabled for the calibration procedure, since the aim is to create a digital filter able to do this work much more precisely. From the above exposed remarks it follows that, in order to validate our calibration methodology and meanwhile to give a basis for a standardization of different p-u calibration processes, the magnitude correction of $U_{Mag-corr}$ in Eqs. 3.4.2 has to be compared with the experimental correction curve $\Gamma(\omega)/\mathrm{S}_p(\omega)$, where $S_p(\omega)$ is determined by the process described in 3.4.1 and $\Gamma(\omega)$ is reported in figure

3.4.3, while the comparison of $U_{Phase-corr}$ has to be done simply with the PT phase response. However, before starting the fit operation, preliminary exams showed that a residual gain was present in the experimental correction curve, perhaps caused by slightly different input gains of the MOTU I/O interface. To overcome this possible source of systematic error, a multiplying constant G was added to the model function of the magnitude and the experimental curve was first fitted by analytical curve, whose every parameter except G was fixed to its nominal value. In practice, the *level* of the model curve was adjusted in order to match the experimental one. The following step was the proper fit operation, where the six corner frequencies were calculated.

Experimentally, data required few pre-operation in order to get good results:

1. experimental $\Gamma(f)$ has a liner resolution in frequency, so to avoid an excessive weight of high frequencies over low ones a twelfth-octave filter was applied;

2. since algorithm is sensitive to local minima, different starting points (different values for $G_{default}$) were used, which all converged to a single value.

Result for G determination are reported in figure 3.4.4, while the final results of fit procedure are given in figure 3.4.5. (a) and (b), where analytical corrections from Eqs. (3.4.2) with $F_{i=1..3}$, $C_{i=1..3}$, LFS set to the nominal values and $G = 3.576$ as experimentally determined in our measurements; 2) dashed line: experimental corrections from $\Gamma(\omega)/S(\omega)$; 3) continuous line: analytical corrections best-fitted from experimental data using Eqs. (3.4.2) with $LFS = S_u(250\,\mathrm{Hz}) = 20.0\,\mathrm{V/ms^{-1}}$, $G = 3.576$ and the calculated parameters reported in Table 3.4.3.

As clearly seen in Figure 3.4.5(a), nominal and best-fitted amplitude filters have a very similar behaviour, diverging at most by 5 dB in magnitude at high frequencies. These results confirm the need of the low frequency correction to cancel out PT electro-acoustic shortage and the goodness of the Microflown® VT model for high frequencies but from the other hand claim for a more precise model of the PT transducer in the low frequencies range.

The effect of using $S_u(\omega) = \mathrm{S}_p\,(1000\,\mathrm{Hz})\,/|\Gamma(\omega)|^{\mathrm{V/ms^{-1}}}$ instead of $S_u(\omega) = \mathrm{S}_p(\omega)/|\Gamma(\omega)|^{\,\mathrm{V/ms^{-1}}}$ – i.e. of excluding the full bandwidth comparison calibration process of the PT from the relative calibration of VT versus PT – in order to obtain the VT sensitivity $S_u(\omega)$, whose inverse is shown in figure 3.4.6. It is evident here that the only way to remove the low frequency correction from the probe calibration filters should be that of improving the electroacoustical quality of the PT and optimizing accordingly the factory production process.

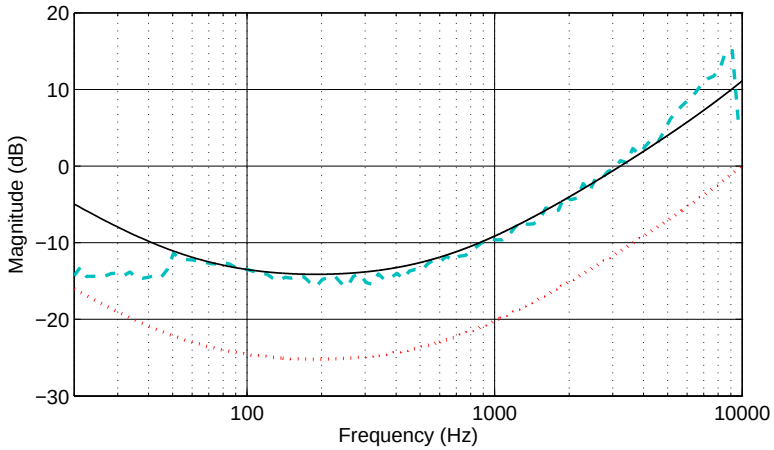

Figure 3.4.4: Gain empirical determination. Blue, dashed line: experimental curve; red, dotted line: model function without gain; black, solid line: model curve with $G = 3.576$

Table 3.1: Corner frequencies found by the fit algorithm, applied to experimental data, compared with the nominal ones.

Parameters	Nominal	Experimental
LFS (V/ms^{-1})	20	20.0
F_1 (Hz)	60	55.4
F_2 (Hz)	600	740
F_3 (Hz)	15000	4.01×10^3
C_1 (Hz)	60	41.4
C_2 (Hz)	550	621
C_3 (Hz)	20000	1.39×10^4

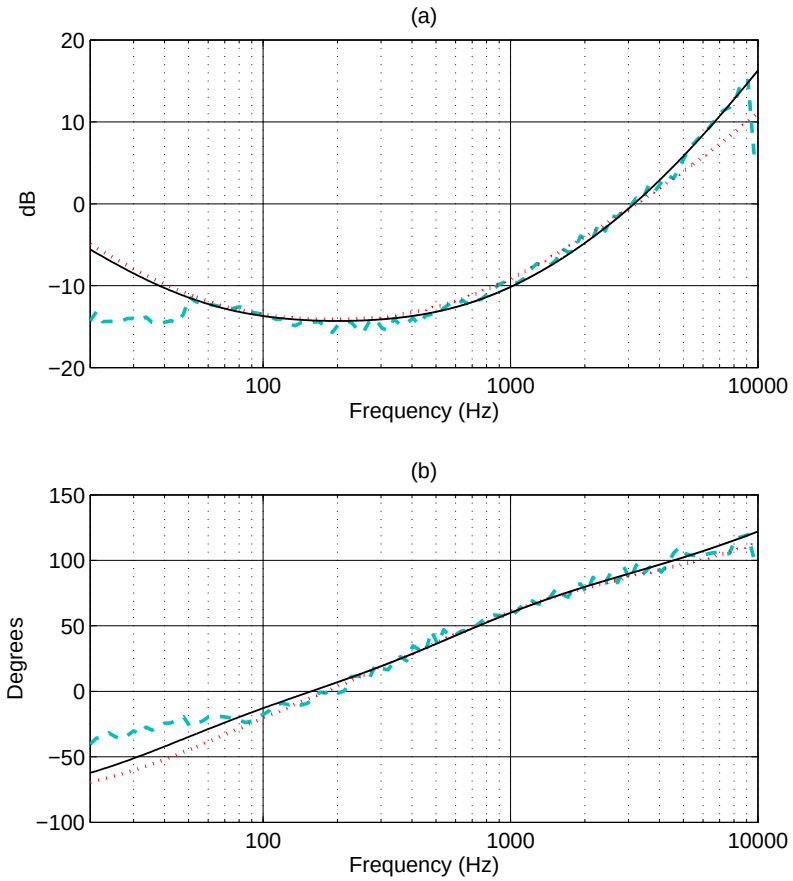

Figure 3.4.5: Amplitude (a) and phase (b) correction filters $S_u^{-1}(f)$. Blue dashed line: experimental filters; red dotted line: nominal filters; black solid line: optimized filters. N.B. excitation range is from 50 Hz to 10 kHz

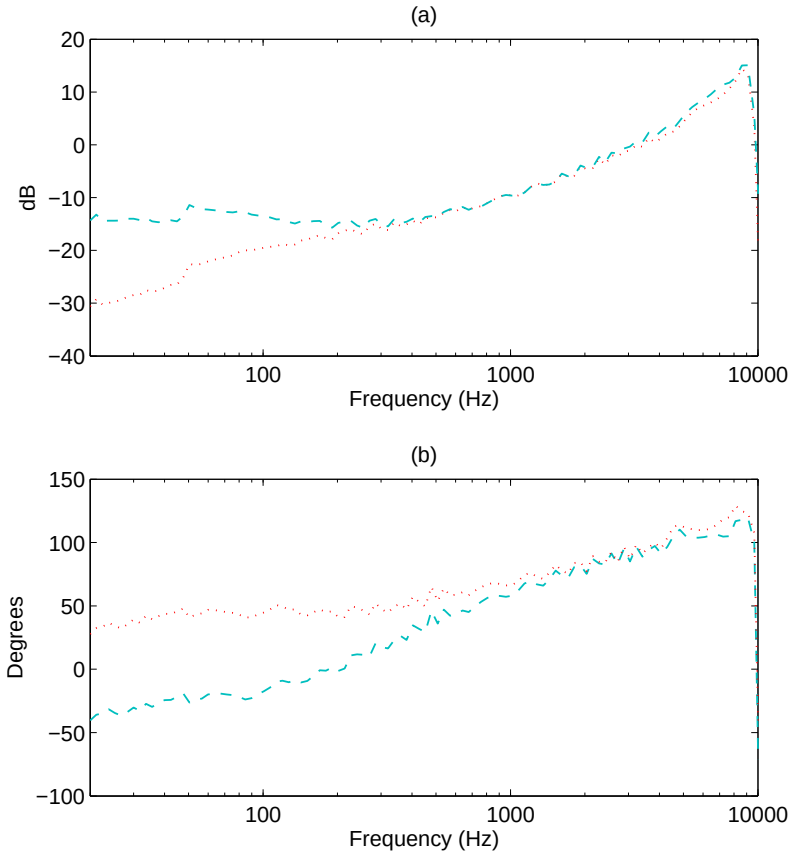

Figure 3.4.6: Comparison between experimental $S_v^{-1}(\omega)$ correction in magnitude (a) and phase (b) function with pressure correction for pressure transducer (blue, dashed) and without (red, dotted).

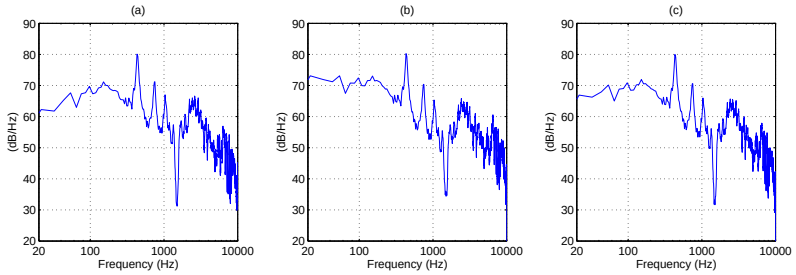

Figure 3.4.7: Pressure (a), Acoustic velocity (b) and Intensity (c) power spectral densities with calibrated probe. White noise was used as excitation signal.

Finally, sound pressure and acoustic velocity level[4] spectral densities, measured at the calibration point and calibrated with the best-fitted filters are reported, for the sake of completeness, in Figure 3.4.3 (a) and (b) respectively; (c) plot compares instead the sound intensity spectral density $L_I = 10\log(I/I_0)$, where $I_0 = 10^{-12}\,\mathrm{Wm}^{-2}$, obtained at each frequency with the best-fitted calibration. Here the average sound intensity I is a simple real scalar quantity defined for every single frequency ω as $I = PU\cos(\Delta\phi)$, as explained in section 1.3.

3.4.4 Calibration uncertainties

Calibration procedure was repeated many times in order to check repeatability of the process, over a period of several months. Moreover, experimental impedance $Z(\omega) = P(\omega)/U(\omega)$ was obtained using different methods: impulse responses from sine sweep technique and a direct record over about 15 s of white noise. Finally, opposite to what was stated above, calibration was also tried from experimental data obtained from the measurement point at 17.6 m from the source, obviously assuring that during the fitting process only range with sufficient SNR was taken into account. Resulting calibration function were extremely uniform, reflecting the robustness of the method here illustrated: biggest differences in magnitude were found to be less 0.4 dB for frequencies outside the range $[70, 6000]$ Hz, while inferior to 0.15 dB for frequencies inside it. Phase uncertainties showed on the other hand quite an opposite behaviour, with a maximum of variance around 500 Hz of 1.4 degrees, results in line with the ones in literature.

[4] expressed in dB rel $4.8 \times 10^{-8}\,\mathrm{ms}^{-1}$

Chapter 4

Application of sound energetics to power and conductance measurements

4.1 Sound power measurements

Among the great variety of possible applications of sound energetics, the measurement of sound power emitted from a source is surely among the most important and classical ones. It is an absolutely standard procedure, therefore it provides one of the best opportunities to test the behaviour of p-u probes and their newly defined calibration functions. This constitutes, in fact, the basic idea and the primary aim of the comparison test which will be illustrated in the following. A reference source B&K mod. 4204 was used to create a broad band noise and sound power was measured at the same time with both a standard p-p B&K half-inch probe and a Microflown PU Match one. Measurements were taken in two very different environments, a large reverberant shed of about $10^4\,\mathrm{m}^3$ at the Imamoter Institute of Italian National Research Council and the big anechoic chamber at the Engineering Department of Ferrara University, whose volume is approximately $800\,\mathrm{m}^3$, in order to test how instruments reacted to a considerable variation of field properties. The experimental procedure required some preliminary correction, as it will be explained, and results showed a good, though not perfect agreement between detected power levels.

4.1.1 Measurement procedure

For every radiative stationary phenomenon, power of an emitting source is equal to the energy flow, given by the integration of intensity, energy per unit of time and area, over a closed surface containing the source under

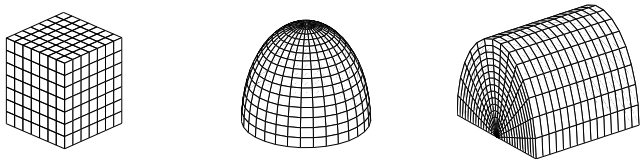

Figure 4.1.1: Most used surfaces for sound power measurements

investigation:

$$P_w = \int_S \mathbf{I} \cdot \hat{\mathbf{n}} \mathrm{d}S \tag{4.1.1}$$

where $\hat{\mathbf{n}}$ is the vector normal to the surface element $\mathrm{d}S$. Although in particular environments sound power can be esteemed from pressure signal alone, like in a free field or a totally reverberant one, this kind of procedure is much more robust, it can be performed nearly in every environment and is not affected by background noise or by presence of other sources.

Demonstration is quite straightforward: in stationary conditions, energy conservation principle states that variation of energy within a certain volume over time must be equal to its net flow over the whole surface enclosing the volume itself. Usually, several sound sources are present in the environment, both inside and outside the considered volume, and of course the component of intensity perpendicular to the surface element $I_n = \mathbf{I} \cdot \hat{\mathbf{n}}$ is the effect of all of them, but nevertheless it can be demonstated – under practical assumptions – that contributions of external sources to the total power of the monitored one can be neglected.

The choice of the shape of the surface is totally arbitrary, since nothing of what was written above depends on it, as long as the surface is closed: therefore, in sound power measurements very simple forms are typically used, easy to achieve and to manage, such as cubes, spheres or cylinders. In most of the cases, however, the source which has to be studied is either very hard to move from its location or firmly attached to the ground, making the definition of a surface totally enclosing it impossible in practise. In such a situation however, if the sound source lies on a rigid floor, simple considerations allow to provide a good measure of sound power even if surface is not closed: since materials such as concrete or similar ones are very hard and reflective from an acoustical point of view, then their approximation to a perfect reflecting surface, not absorbing any fraction of the sound energy emitted by the source is then very close to reality. It follows, that if no energy leaves the volume through ground surface integration over this part can be avoided, limiting this operation over the remaining faces. This is the main reason why international standards of power measurement [45] indicate cubes, half-spheres and half-cylinders as possible and preferable choices, as

given in figure 4.1.1.

In the experiment here described a cubic surface was chosen, mainly because it is the simplest shape to experimentally build and manage: versor $\hat{\mathbf{n}}$ has in fact only five different directions, one for each face excluded the one coincident with the ground, allowing thus to greatly simplify the positioning of the probes during intensity measurements, since not many changes of orientation are required. As equation (4.1.1) points out, only component of intensity orthogonal to the local element of surface contributes to determine overall sound power, and therefore an accurate determination of this direction makes possible the use of axial probes oriented parallel to versor $\hat{\mathbf{n}}$ instead of 3-D ones randomly positioned.

Experimental measurements require a discretization or an approximation of eq. (4.1.1), usually achieved in two different ways [45, 1].

1. Mean intensity estimation over part or the whole surface: sound power contribution of each face is given by $P_w^i = \bar{I}_n^i \cdot S^i$. In case of cubic surface, $\bar{I}_n^i$ is measured for each face sweeping the region with a constant motion in order to get with the same weight each spatial contribution. Total sound power is then given by

$$P_W = \sum_{i=0}^{5} \bar{I}_n^i S^i$$

.

2. Discretisation of surface is into subdomains. At the centre of each subdomain sound intensity is measured and, as in the other mothod total sound power is given by sum of all contributions:

$$P_W = \sum_{faces} \sum_{points} I_n^i \Delta S^i$$

. This procedure is usually more accurate and offer a better repeatability, thus was chosen for measurements here presented.

4.1.2 Experimental setup

To increase the variability of measurement conditions, two very different environments were chosen. The large shed of Ferrara Imamoter institute of National Research Council ($V \simeq 10^4\,\mathrm{m}^3$), containing various laboratories and experiments, provided a non-controllable acoustic situation: in fact, a lot of reflective and vibrating surfaces were distributed all around the environment, also in the nearby of the source and the measuring surface, as shown in figure 4.1.2; moreover, the background noise during the measurements was quite loud, say about 60-65 dB.

On the other hand, the big anechoic chamber at Ferrara University is a certified structure (Figs. 4.1.3-4.1.2), whose properties are available in

Figure 4.1.2: Noisy environment: an industrial shed (particular of the experimental setup)

literature [46]. In particular, results here presented were obtained in semi-anechoic configuration ($V \simeq 800\,\mathrm{m}^3$): in such situation, background noise is assured to be less than 20 dBA down to 50 Hz. An estimation of the background pressure noise with p-u probe pressure sensor confirmed it, as shown in figure 4.1.5.

Integration surface was defined as a 1.00 ± 0.01 m side cube and each face was divided into nine squares of side about 0.33 m each in both the environments. As a convention, each face was labelled with capital letters from A to E, where E represents the one parallel to the ground and the sixth, coincident to the floor, was omitted for the reasons explained above.

P-p probe and p-u probe were mounted together so that their acoustic centres were as close as possible (about 0.5 cm), as shown in figure 4.1.6; each record was 15 s long. P-p analysis chain, a B&K. half-inch p-p probe driven by B&K Pulse, provided pressure, intensity and power levels in third-octave bands from 125 Hz to 6300 Hz. P-u system involved a Microflown PU match probe with its signal conditioner, a MOTU 896 Hd I/O interface and Matlab routines for data analysis. Thanks to its adaptability, this latter system allowed a variety of different results, but, since the aim of the experiment was to compare the two instruments, same data of the first system were calculated. Before the beginning of each measurement session, calibration of p-p probe was validated with the help of a 250 Hz calibrator.

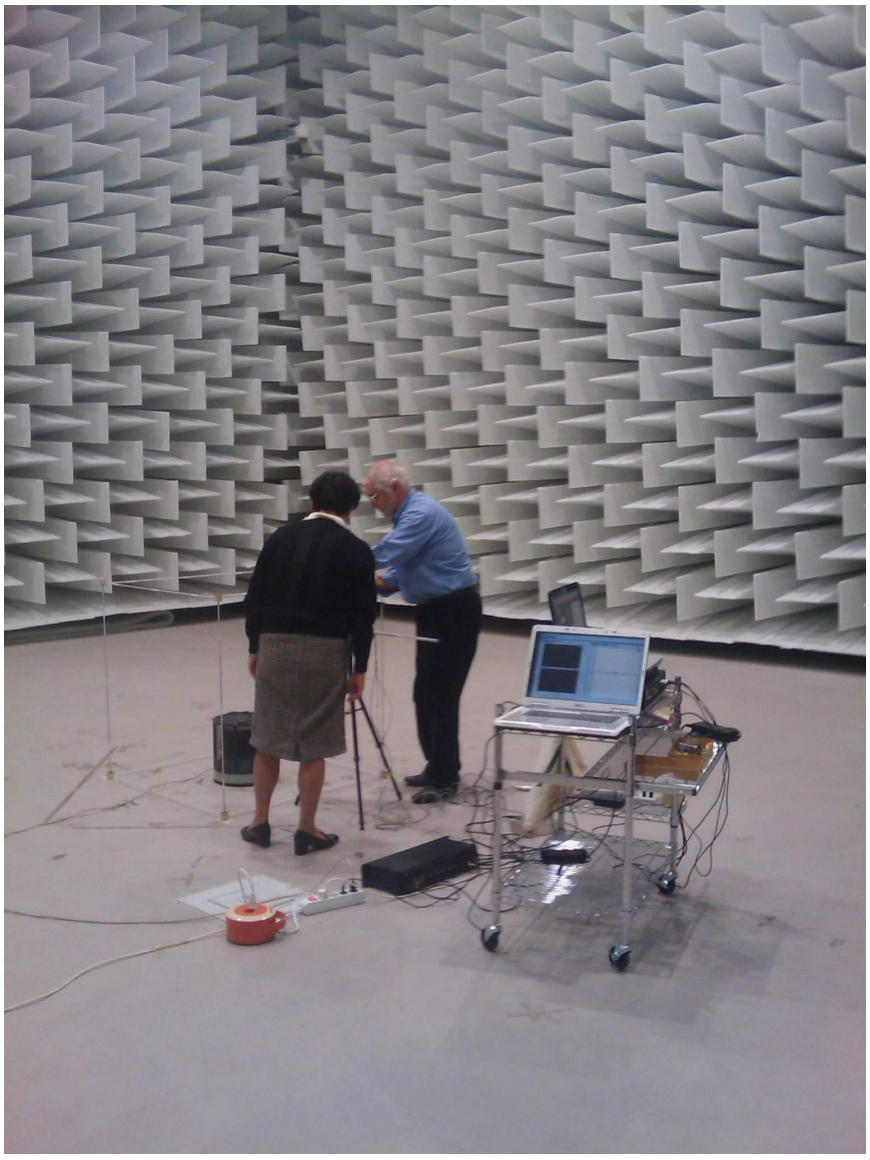

Figure 4.1.3: Anechoic room at Engineering Department, University of Ferrara.

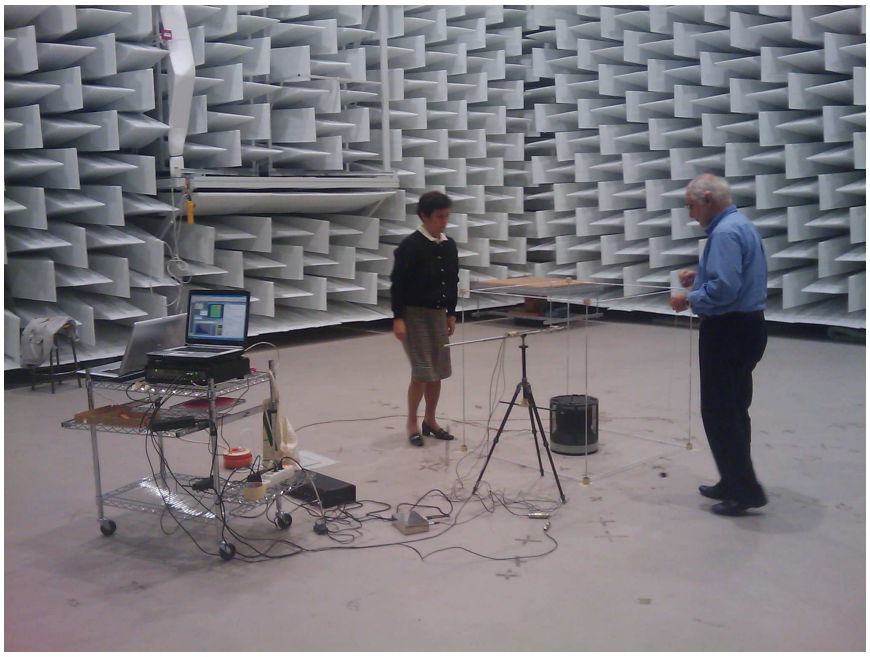

Figure 4.1.4: View of experimental apparatus.

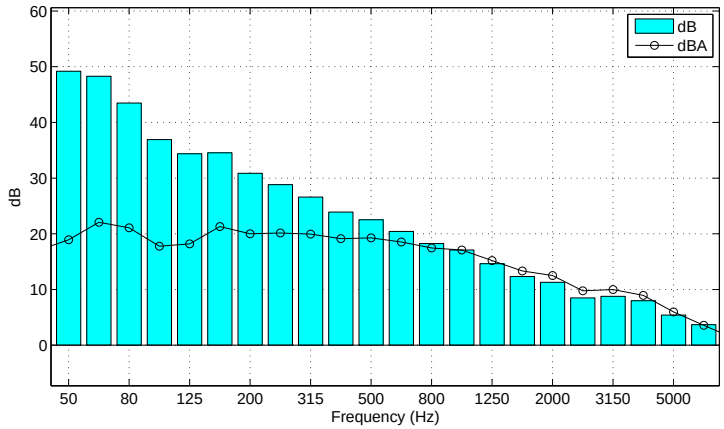

Figure 4.1.5: Background noise in anechoic chamber measured with p-u probe. Raw and A-weighted levels in third octave bands.

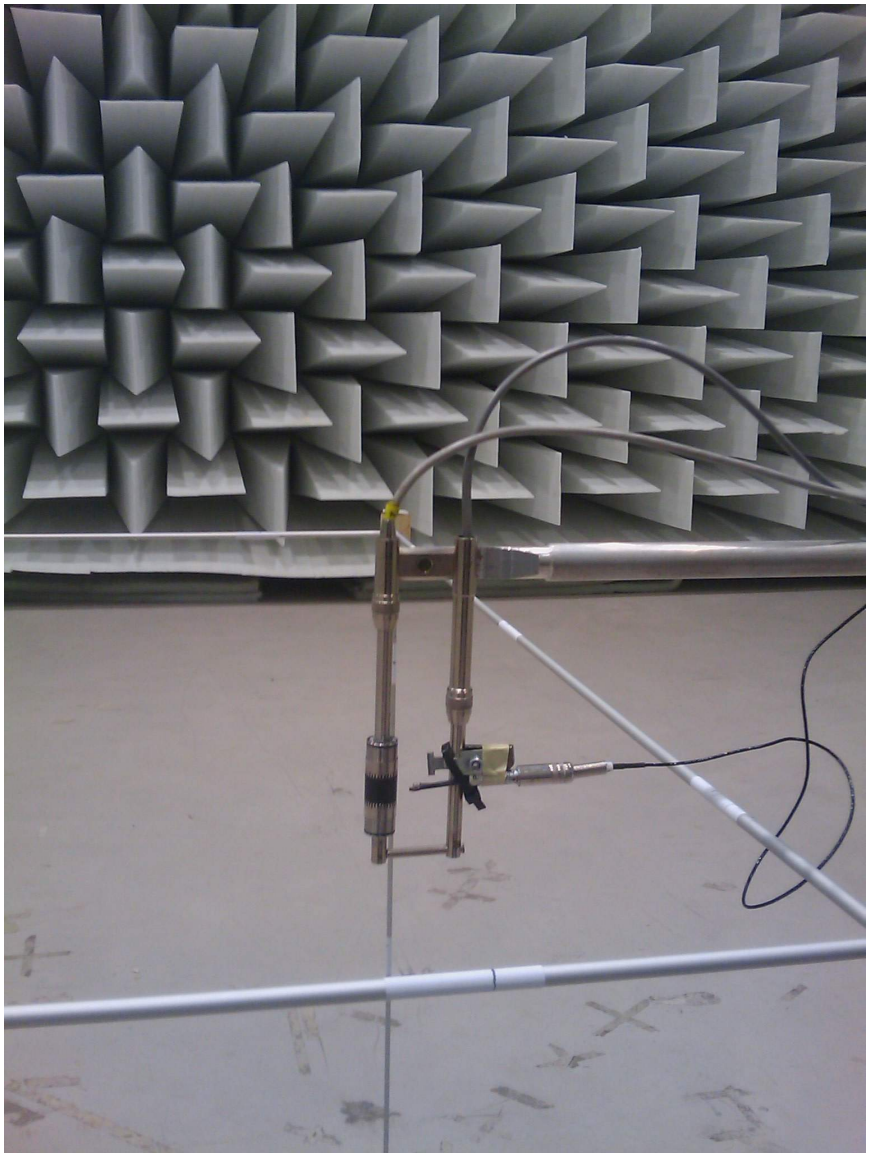

Figure 4.1.6: Detail of p-p and p-u probes.

4.1.3 Absolute calibration and pressure measurements

A preliminary but necessary step of the analysis of the experimental results is the comparison of the pressure levels measured with p-p and p-u probes: this step provides in fact the possibility to correct the sensitivity of p-u pressure sensor with respect of a more reliable and precise one, given by p-p probe itself. Among the measurement points defined on the surface, only the one at the centre of each face was considered, for a total of 5 in each environment, and values found were slightly different from the one obtained in the calibration environment (plane wave guide): since reference pressure microphone used in chapter 3 was never sent to the producing company to be re-calibrated, as was done for the p-p probe elements, this method was proved useful to obtain a sensitivity more in line with the other instrument: $S_p = 0.047\,\mathrm{V/Pa}$. Similarly, a new equalisation curve for pressure was calculated, by comparison with signal measured by p-p probe in the most controlled environment, i.e. the anechoic chamber, and then used for pressure sensor absolute calibration. The velocity sensor sensitivity and corner frequency (for magnitude only, since phase was left unvaried) were finally just scaled relatively to the newly calibrated pressure, as explained in section 3.4.2.

Once the p-u pressure sensor was calibrated and equalised with respect to the p-p one, a comparison between pressure levels could be performed: results for the different environments are given in tables 4.1 and 4.2, while level differences before and after pressure equalisation are reported in graphics 4.1.7. An obvious agreement for most measurement points in the anechoic chamber is found, as expected, since absolute calibration was carried out in that very environment, but it does not occur in the shed: p-u probe in fact gives an overall higher level of about 1 dB, which tends to increase of another dB over 3150 Hz. This fact suggests that pressure sensors of the two instruments react in a different way to a change of sound field conditions: if response of p-p probe for pressure measurements is reasonably assumed as a reference, this evidence leads to the conclusion that a more performing pressure sensor should be implemented in p-u probes, if precise measurements are required.

Another issue regarded results of measurements on the face parallel to the ground, E, which showed quite a different behaviour in the anechoic chamber with respect to the other measurement points: this is surely not caused by defects in calibration or sensitivity, because levels from other faces are more uniform, nor apparently from source itself or the particular choice of measurement points, because this deviation does not appear in the recordings taken in the Imamoter shed. No straightforward explanation was found, but hypothesis involved either a probable non-perfect mount or possible electrical problems, such as cable disposition or electric mass difference, a factor which the p-u probe used in this experiment was found very sensitive to. On the contrary, any acoustic cause can be discarded, at least in the low frequencies:

Table 4.1: Values of L_p measured with p-u (black) and p-p (red) probes inside the IMAMOTER shed

	A	B	C	D	E
Overall	**86.8 - 85.7**	**87.0 - 85.6**	**87.1 - 85.8**	**87.0 - 85.9**	**83.2 - 82.3**
125 Hz	71.2 - 70.0	72.1 - 71.0	72.6 - 71.5	72.7 - 71.8	63.1 - 62.3
160 Hz	71.5 - 70.5	72.0 - 70.9	72.2 - 71.3	72.0 - 70.9	64.1 - 63.2
200 Hz	72.6 - 71.0	72.1 - 71.1	72.6 - 71.6	72.0 - 71.1	65.1 - 64.1
250 Hz	71.8 - 71.0	71.7 - 70.7	72.0 - 70.9	72.1 - 71.5	67.1 - 68.5
315 Hz	71.8 - 70.8	71.7 - 70.7	71.6 - 70.6	71.7 - 70.9	69.4 - 68.5
400 Hz	70.3 - 69.2	70.4 - 69.1	70.8 - 69.8	70.7 - 69.7	67.4 - 66.3
500 Hz	69.6 - 68.8	69.6 - 68.4	69.7 - 68.6	69.9 - 69.0	67.8 - 66.9
630 Hz	70.9 - 70.2	70.7 - 69.6	71.3 - 70.2	71.1 - 70.2	71.1 - 70.3
800 Hz	74.9 - 74.1	74.9 - 73.9	75.1 - 74.0	74.9 - 74.0	74.3 - 73.6
1000 Hz	77.2 - 76.3	77.4 - 76.3	77.7 - 76.7	77.4 - 76.7	72.5 - 71.6
1250 Hz	78.1 - 77.2	78.3 - 77.1	78.1 - 77.2	78.1 - 77.1	76.5 - 75.7
1600 Hz	75.2 - 74.3	75.5 - 74.4	75.8 - 74.6	75.5 - 74.6	74.1 - 73.4
2000 Hz	77.3 - 76.3	77.4 - 76.2	77.4 - 76.1	77.3 - 76.3	71.6 - 70.6
2500 Hz	75.5 - 74.2	75.9 - 74.3	75.8 - 74.2	75.7 - 74.5	70.9 - 69.9
3150 Hz	74.7 - 73.3	75.2 - 73.4	75.1 - 73.3	75.0 - 73.6	68.0 - 66.4
4000Hz	74.9 - 73.2	75.3 - 73.1	75.4 - 73.2	75.2 - 73.6	68.1 - 66.4
5000 Hz	73.6 - 71.5	74.2 - 71.5	74.1 - 71.7	74.0 - 72.0	67.0 - 64.9
6300 Hz	71.5 - 69.3	72.0 - 69.2	71.6 - 69.2	71.6 - 69.4	64.1 - 61.7

it is true that, however near, the two sensors had been actually placed in two distinct spatial points, but this deviation is present and almost constant up to 2000 Hz: possible anisotropies in the acoustic field are more likely to occur at higher frequencies, but simple dimensional considerations make them totally negligible. At 6300 Hz, the higher frequency considered, the corresponding wavelength is 5.4 cm, ten times the distance between p-u probe and p-p probe, about 0.5 cm, so it cannot be excluded from having a role in the level difference.

4.1.4 Intensity maps

Before sound power was calculated, intensity component orthogonal to integration surface is examined to check at what measurement point and for which frequency band different probes showed distinct behaviours or if any systematic error is present, as for example pressure levels in the shed might suggest (Fig. 4.1.7). A comparison similar to the one given for pressure level shown in tables 4.1 and 4.2 pointed out an overall agreement of the results, except for certain measurement points at low frequencies. In most pathological cases, measured normal intensity components even have opposite sign.

Table 4.2: Values of L_p measured with p-u (black) and p-p (red) probes inside the Ferrara anechoic chamber

	A	B	C	D	E
Overall	**85.4 - 85.4**	**85.4 - 85.2**	**85.5 - 85.3**	**85.4 - 85.3**	**81.0 - 81.5**
125 Hz	71.1 - 71.1	71.5 - 71.5	71.2 - 71.2	71.1 - 71.1	61.2 - 62.1
160 Hz	70.5 - 70.5	70.8 - 70.7	71.0 - 70.7	70.3 - 70.4	61.6 - 62.4
200 Hz	70.9 - 70.9	71.2 - 71.0	71.2 - 71.0	70.8 - 70.7	62.4 - 63.0
250 Hz	70.8 - 70.8	70.6 - 70.5	70.9 - 70.7	70.6 - 70.6	64.2 - 64.7
315 Hz	70.2 - 70.2	70.0 - 69.8	70.4 - 70.4	70.3 - 70.4	67.2 - 67.5
400 Hz	68.9 - 68.9	69.0 - 68.8	69.5 - 69.2	68.9 - 68.8	64.8 - 65.2
500 Hz	68.3 - 68.3	68.3 - 68.0	68.6 - 68.3	68.3 - 68.2	65.6 - 66.0
630 Hz	69.7 - 69.8	69.6 - 69.5	69.9 - 69.6	69.7 - 69.7	68.6 - 69.1
800 Hz	73.8 - 73.8	73.6 - 73.3	73.9 - 73.5	73.8 - 73.7	72.4 - 73.1
1000 Hz	76.2 - 76.2	76.2 - 76.0	76.4 - 76.2	76.1 - 76.0	70.4 - 70.8
1250 Hz	76.7 - 76.7	76.5 - 76.3	76.6 - 76.4	76.5 - 76.4	74.5 - 75.1
1600 Hz	74.3 - 74.2	74.1 - 73.9	74.2 - 74.0	74.1 - 74.0	72.3 - 73.0
2000 Hz	76.2 - 76.2	76.0 - 75.8	76.2 - 75.9	76.2 - 76.1	69.1 - 69.5
2500 Hz	73.7 - 73.7	73.8 - 73.6	73.8 - 73.5	73.8 - 73.7	68.4 - 68.7
3150 Hz	72.8 - 72.8	72.8 - 72.6	72.9 - 72.7	72.9 - 72.9	64.5 - 64.5
4000Hz	72.9 - 72.9	73.0 - 72.7	73.1 - 72.9	73.1 - 73.1	65.2 - 65.3
5000 Hz	71.4 - 71.4	71.4 - 71.2	71.5 - 71.4	71.5 - 71.5	63.9 - 63.8
6300 Hz	69.2 - 69.2	69.0 - 68.7	69.0 - 68.9	69.0 - 69.0	60.2 - 60.0

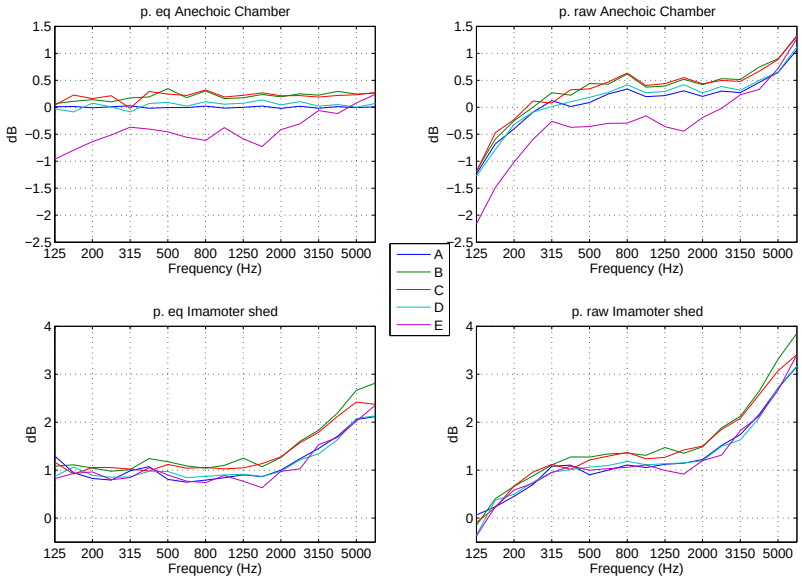

Figure 4.1.7: Differences between pressure levels measured at the centre of each face of the cubic surface with the p-u and p-p probes and effect of pressure equalisation. Left: p-u microphone equalised. Right: p-u, microphone not equalised. Top: Imamoter shed. Bottom: Anechoic chamber

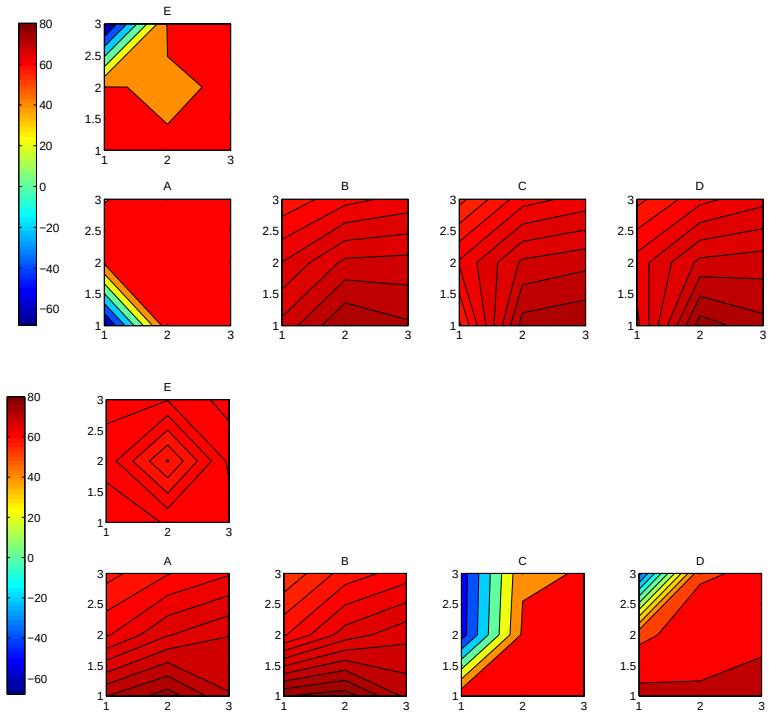

Figure 4.1.8: Intensity maps measured in the Imamoter shed with p-p (upper faces) and p-u (lower faces) probes; 125 Hz third-octave frequency band.

Because of the data volume, results are graphically rendered with intensity maps of cubic surface faces. Not all bands are here reported, but only those showing remarkable results, either good or bad.

In the reverberant environment, low frequency intensity maps show both outwards and inwards normal intensities, although placed at different points depending on the probe considered, as reported in figures 4.1.8. Then, while for p-u probes normal intensity is entirely directed outwards from 250 Hz up, this is not the case for p-p probe, which still at 630 Hz has an innwards intensity component measured in the face E (Fig. 4.1.9). From 1000 Hz, both instruments measure more similar levels (Fig. 4.1.10), even if the tendency of an overestimation of p-u probe over the p-p one at higher frequencies, noticed for pressure sensor, occurs here for intensity as well (Figs. 4.1.4).

In the anechoic chamber, measured results have almost the same features, yet more uniform, with quite different results over the bands from 125 to 250 Hz and more similar in the other ones. Intensity map are here reported for 125 Hz (Fig. 4.1.12), 1250 Hz (4.1.13) and 6300 Hz (Fig. 4.1.14) bands.

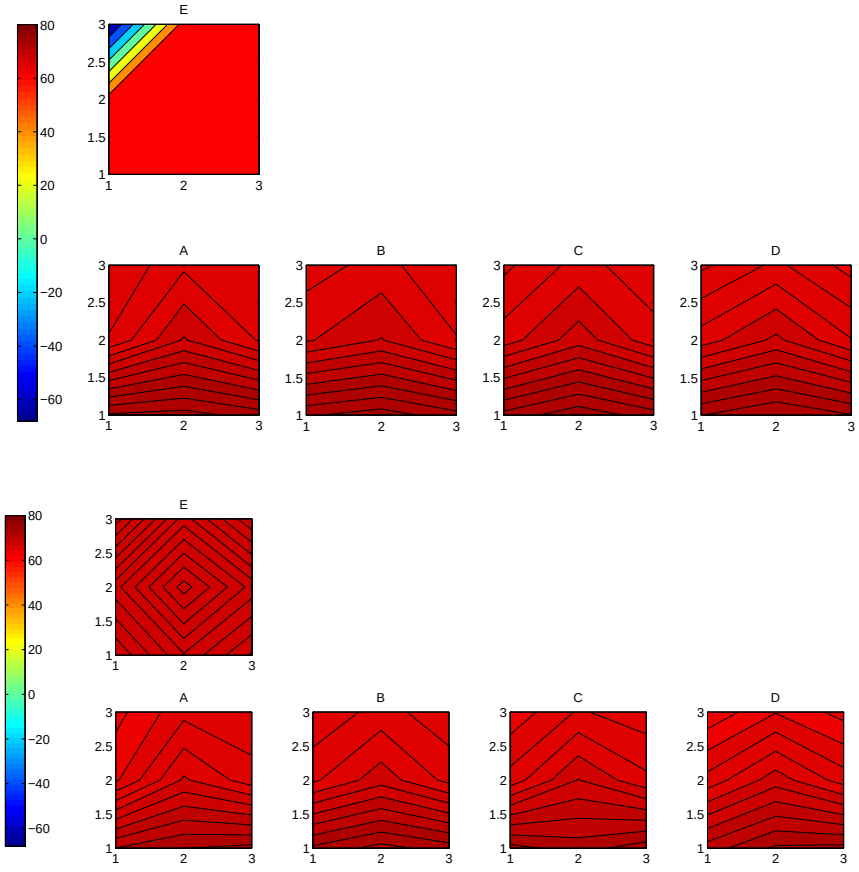

Figure 4.1.9: Intensity maps measured in the Imamoter shed with p-p (upper faces) and p-u (lower faces) probes; 630 Hz third-octave frequency band.

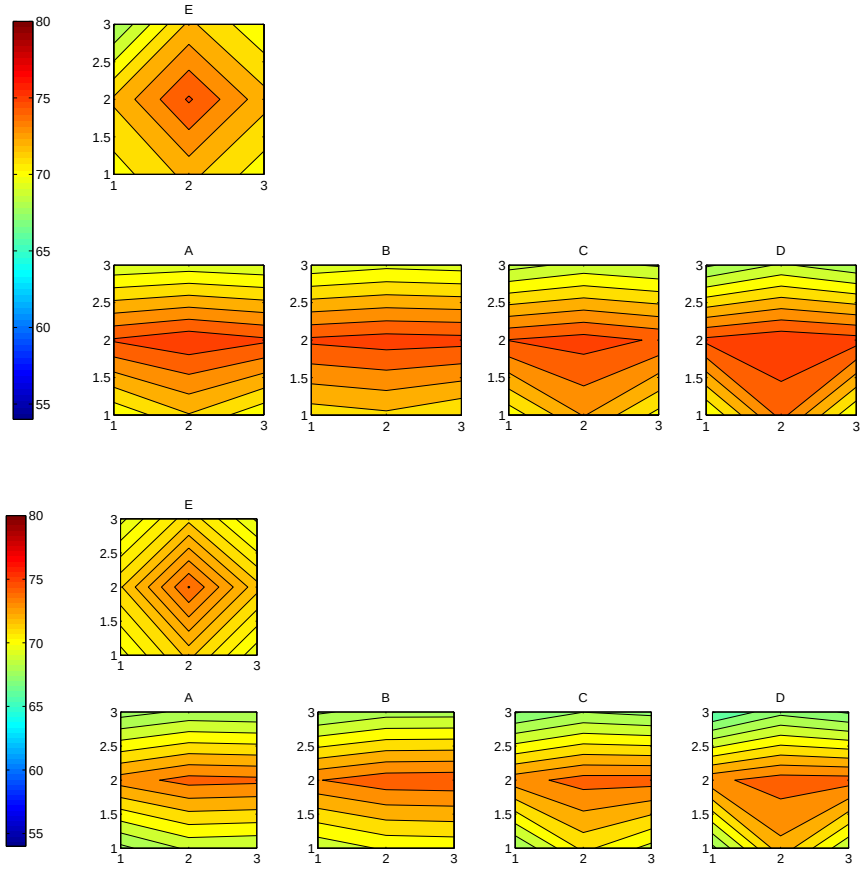

Figure 4.1.10: Intensity maps measured in the Imamoter shed with p-p (upper faces) and p-u (lower faces) probes; 1250 Hz third-octave frequency band.

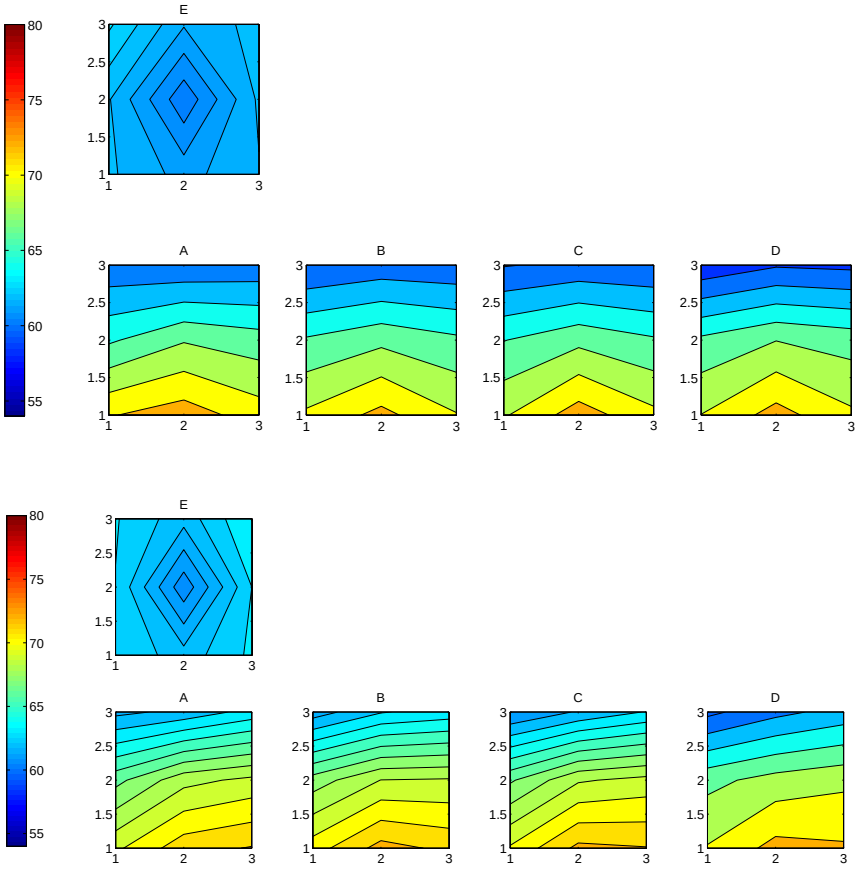

Figure 4.1.11: Intensity maps measured in the Imamoter shed with p-p (upper faces) and p-u (lower faces) probes; 6300 Hz third-octave frequency band.

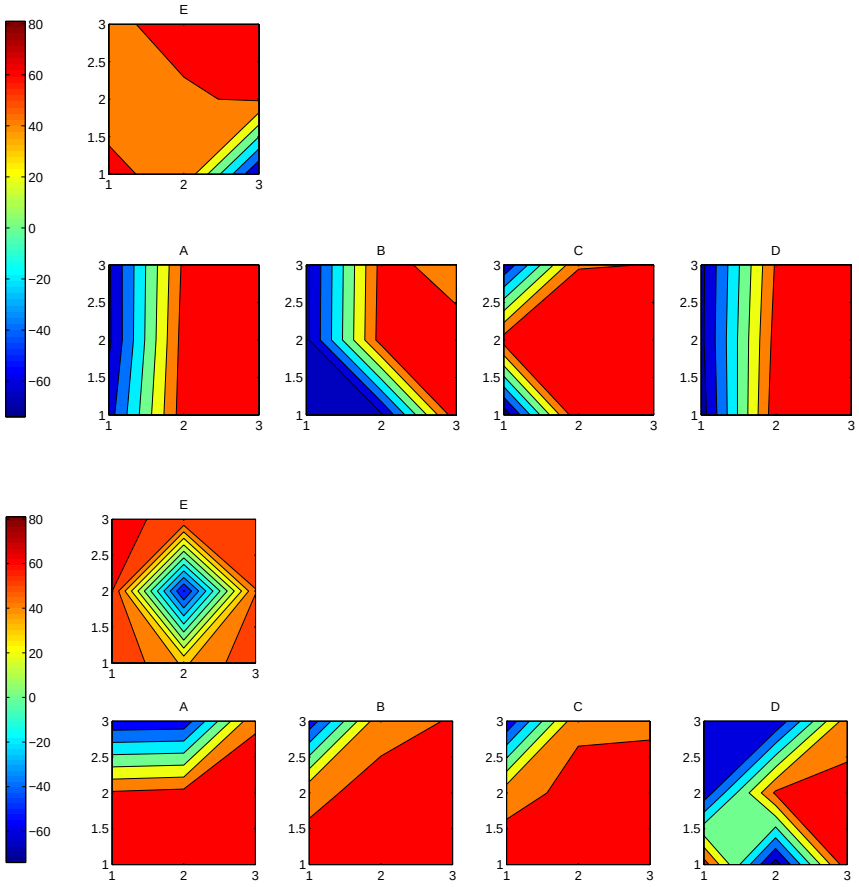

Figure 4.1.12: Intensity maps measured in the Imamoter shed with p-p (upper faces) and p-u (lower faces) probes; 125 Hz third-octave frequency band.

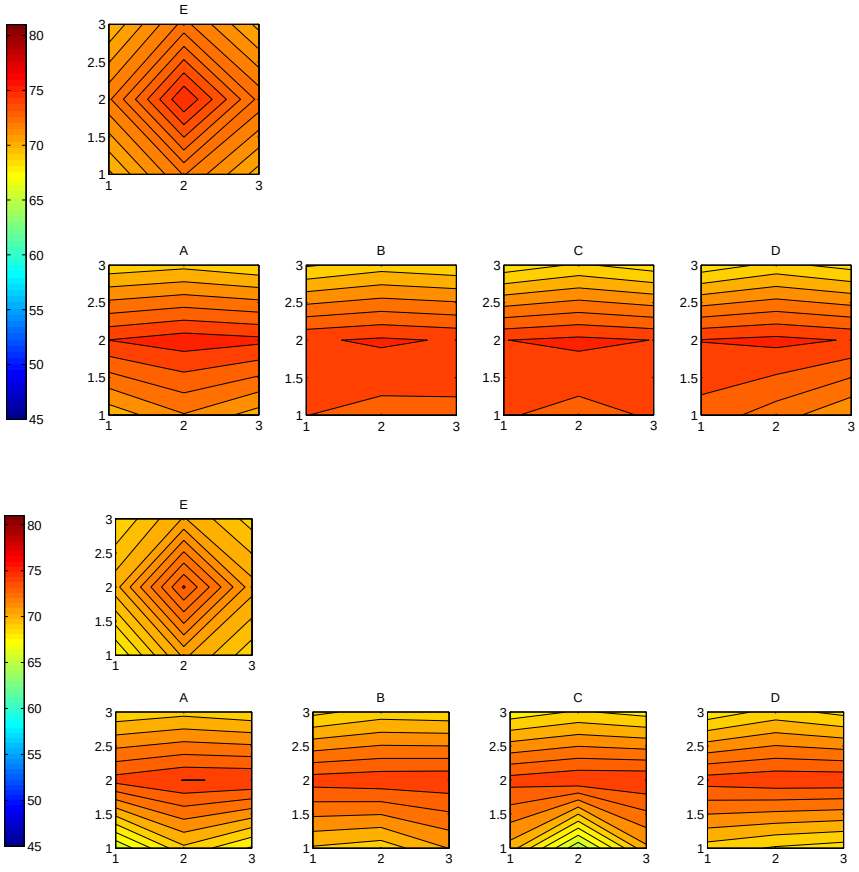

Figure 4.1.13: Intensity maps measured in the Imamoter shed with p-p (upper faces) and p-u (lower faces) probes; 1250 Hz third-octave frequency band.

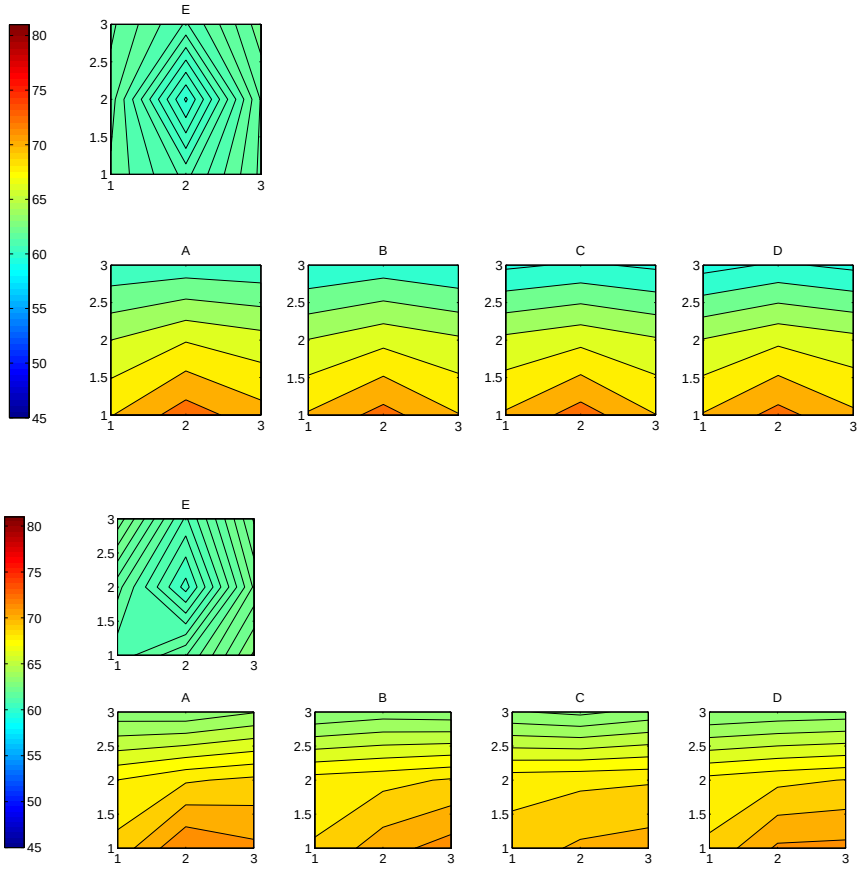

Figure 4.1.14: Intensity maps measured in the Imamoter shed with p-p (upper faces) and p-u (lower faces) probes; 6300 Hz third-octave frequency band.

4.1.5 Sound power measurements

Finally, total power emitted by source and its third octave band spectral components are obtained from intensity measurements and compared in both situations. As predicted by theory, results are almost independent from the environment for both p-p and p-u probes, a fact that can be interpreted as a confirmation of a correct experimental process. Total power levels are given in table 4.1.5 and show a good agreement, although in both cases p-u probe presents an underestimation of 1 dB, perhaps hint of a systematic error.

Table 4.3: Total sound power levels measured with the two probes in dB relative to 10^{-12} W

	Imamoter shed	Anechoic Chamber
L_W p-u	89.3	89.5
L_W p-p	90.3	90.4

From results in figure 4.1.15, reporting third octave band spectra, a fairly good agreement between what was obtained by the two instruments still can be seen, but the difference between measured levels tend to increase. In particular, both environments show a common behaviour: for p-u probe there seems to be an overestimation of about 2 dB at low frequencies and about 1 dB at high ones, an aspect already reported in literature [47], while for the middle ones quite the opposite happens, being levels from p-p probe from 1 to 2 dB higher. On the other hand, the 1dB level shift between anechoic chamber and big shed measured levels, found for pressure up to 2000 Hz, does not seem to affect sound power in any perceivable way, since in the two environments levels are almost the same in all the considered frequency range.

To check whether these differences were caused by the modified calibration filters, instead of the ones obtained by comparison with p-p probe, pressure equalization curve and sensitivities calculated in the original calibration environment, described in section 3.3, were applied to signals recorded in the anechoic chamber. Power levels for p-u probes were then recalculated: as figure 4.1.5 illustrates, it is clear that levels increase nearly in all the bands, which is good for the ones between 300 and 3000 Hz, but it is definitely not for the other ones. Moreover, from the plot it turns out that the biggest effect, quantitatively a rise around 1-2 dBs, occurs for those bands which already show a power level higher that the one given by p-p reference probe. This would lead to a maximum difference of over 3 dB for third octave band levels, too high to be accepted. Therefore, it can be concluded that, in order to compare the behaviour of two totally different instruments such as p-p and p-u probes, it is absolutely necessary a preliminary check and a possible calibration of p-u pressure sensor over p-p one (which can be interpreted as the mean between the two pressure microphones) has to be performed, if

one wants to avoid differences only due to an external, not always coincident reference level.

4.1.6 Determination of uncertainties

As found in the previous subsection, in both measuring environments sound power levels seem to show a systematic error of p-u probes estimated around 1 dB for the overall result. Different causes may concur to give this effect: calibration uncertainty gives an error of 0.5 dB for pressure signal and about 0.5 dB for velocity one, which together with the uncertainty for surface measurements give a confidence level in sound power measurements of 1.1 dB. The result is good for total levels in table 4.1.5, since sound power measured for p-p probe lies in the confidence interval in both cases implying that results are consistent, but it does not fully explain the 2 dB gap in power level of certain bands. Other comparisons between such instruments presented in literature showed that p-p and p-u uncertainties are due to substantially different principles and can be more or less important depending on various factors.

In particular, sound field itself plays an important role: in fact, in case of p-u probes even small phase errors may sometimes lead to critically wrong measurements, or on the contrary big uncertainties can be totally negligible, depending on the ratio between radiating and oscillating intensity. Basically, it can be synthesised as follows: a phase error between pressure and velocity ϕ_e propagates to intensity measurements in the following way:

$$\begin{aligned} I_m &= \Re\left(S_{p_m u_m}\right) = \Re\left(PUe^{-i\phi_e}\right) \\ &= \Re\left[\left(I + iQ\right)e^{i\phi_e}\right] \\ &= \Re\left[\left(I + iQ\right)\left(\cos\phi_e - i\sin\phi_e\right)\right] = I\cos\phi_e + Q\sin\phi_e \\ &\simeq I + Q\phi_e \end{aligned}$$

where I and Q are true active and reactive intensities, I_m is the measured active intensity and last expression is valid only for small ϕ_e. So, not only error ϕ_e but also "reactivity" of the sound field Q/I is a critical term to esteem uncertainty of intensity measurements – and consequently sound power measurements – for p-u probes. Other studies reported [47] that reactivity is an issue only either at lower frequencies, under 100 Hz, or if the measurements are taken very near the source, which is not the case. Nevertheless, reactivity estimation I_m/Q_m was calculates for both environments and results confirmed that field is mainly radiative, as shown in figure 4.1.17. Possible errors due to any residual phase mismatch between pressure and velocity transducers are then discarded.

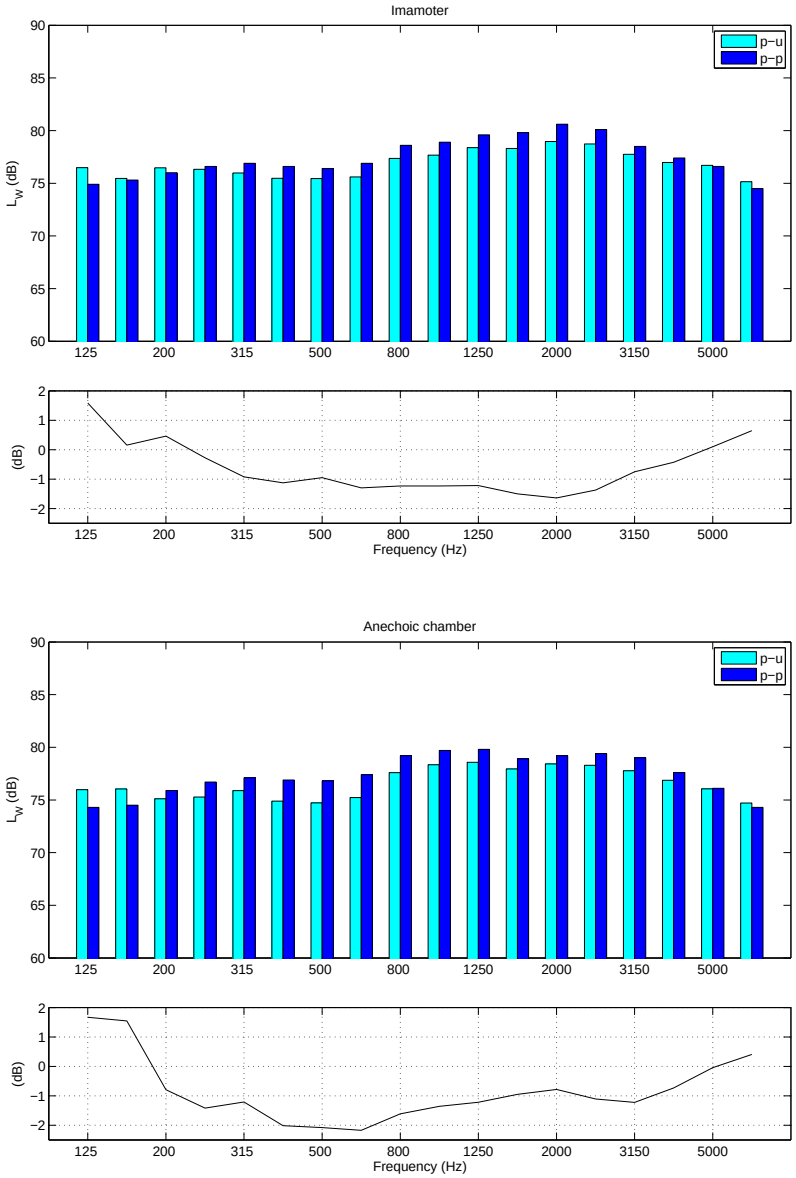

Figure 4.1.15: Power levels measured in third-octave bands with p-p and p-u probes in a reverberant industrial shed (Imamoter) and in the Ferrara Anechoic Chamber. Bar plots: power levels in dB relative to 10^{-12} W. Lower plots: difference between p-u and p-p detected levels.

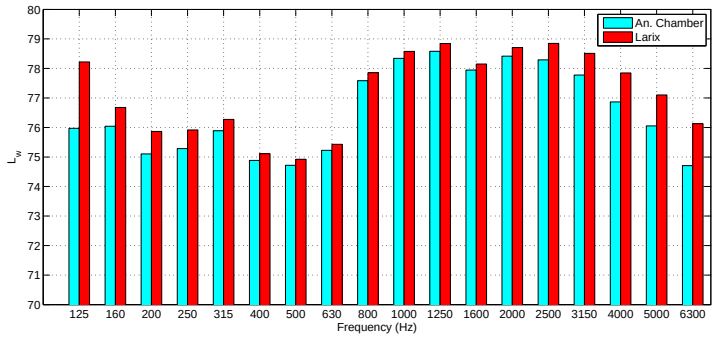

Figure 4.1.16: Power level detected by p-u probe: comparison between levels using different equalization curves for pressure sensor. Cyan: equalization calculated on anechoic chamber by comparison with p-p probe pressure level; red: equalization obtained in LARIX wave guide by comparison with a $1/4''$ B&K microphone type 4929.

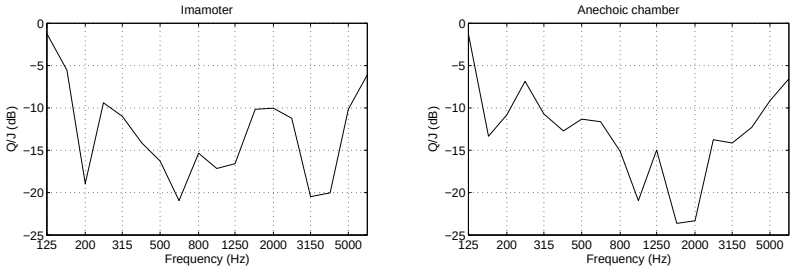

Figure 4.1.17: Ratio of reactive to active intensity in the large shed (left) and in the anechoic chamber (right)

4.2 Sound wave conductance measurements

As explained in section 1.3, acoustic conductance and acoustic susceptance are functions limited in the $[0, \rho_0 c]$ range which describe the average behaviour of energy. These quantities are very useful for a big variety of possible applications, the most of which still have to be studied. Just two cases will be here presented: the energetic analysis of sound within a tube and the measurement of energy absorbance of the human ear canal.

It was shown that sound wave conductance and parameter η, which describes the average velocity at which energy radiates along its trajectory, are closely related (see Eq. (1.3.18)), and similarly were susceptance B and indicator μ, defined by equation (1.3.20). Along with it, other quantities given by potential-kinetic energy equipartition index $|\bar{\sigma}|$ and power factor ξ will be studied in different one-dimensional environments, simulated by a wave guide ended with different terminations.

The second case study regards the measurement of sound conductance at the entrance of the external auditory meatus. Measurements of energetic properties of the human ear, in particular impedance of outer ear and ear canal, are critical to diagnose those pathologies of hearing related to mechanical deficiencies. At present, most widely used technique calculates ear impedance by measuring pressure level inside the ear canal in a very indirect way, using probes which couple several known volumes to the ear and some reference loads [48]. This has however a lot of drawbacks: measurements are quite complicate and time-consuming, at least compared to what it is here presented, quite a lot of post processing is involved and the method may become quite disturbing for subjects such as infants, since a thin tube has to be inserted in the ear canal. Procedure here proposed consists in the measurements of acoustic conductance and related quantities using an axial p-u probe. Test was taken for a dummy head first, then for human ear, whose preliminary results are here reported.

4.2.1 Study of spectral and spatial properties of a one dimensional field

Experimental apparatus and measurements

In order to simulate 1-D environments, a square section Plexiglas® tube was used as a wave guide, whose length is 4 m and transverse dimensions 0.28 m: from geometric considerations it is easy to estimate the upper limit of the frequency range, if transverse modes have to be avoided.

$$f_{max} \simeq \frac{c}{2L} \simeq 610\,\text{Hz}$$

Excitation was thus limited in the range$[85, 580]$ Hz: it was chosen so that lower bound allowed at least one wavelength inside the tube, while the upper

bound was within the cut-off frequency. Impulse responses were measured with a logarithmic sweep sine starting from a distance from the source of 90 cm up to 370 cm every 20 cm, for a total of 15 measurement points. The sound source was a Monacor Carpower subwoofer of diameter 25 cm, chosen so that diaphragm could match as well as possible the tube section (figure 4.2.1).

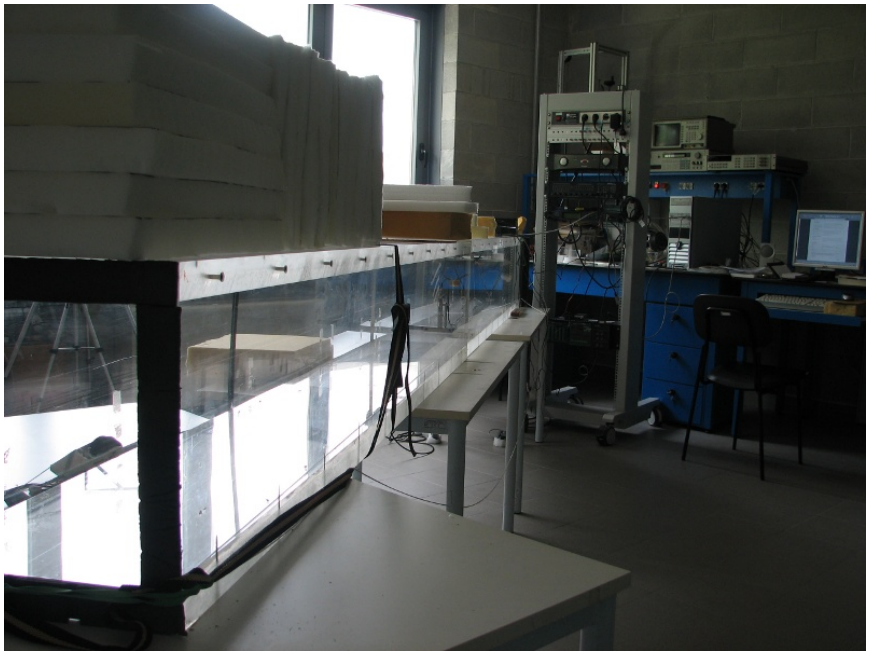

Figure 4.2.1: One dimensional wave guide

Three different environments were simulated, trying to achieve different levels of progressivity (i.e. acoustic conductance) by changing the properties of the free termination:

1. guide was closed by absorbant material (foam rubber);
2. guide was closed by reflective panel (plasterboard);
3. guide was left open.

For each environment, different measurements were done: a sweep which covered the whole frequency range, sweeps for each third octave band which fell within the range, a pure tone of frequency equal to the center of each band. Sweep duration was set to 5 s, a compromise solution which guaranteed enough energy to have impulse responses calculated with a sufficiently good signal to noise ratio in all the environments, and kept the time required for a whole complete session reasonable, usually about a day. Intensity probe was switched to different points with a mobile mount in the guide. In first set

Table 4.4: Third-octave band measurement criterion

Center Frequency (Hz)	Δx(cm)
100	80
125	60
160	40
200	40
250	20
315	20
400	20
500	20

of measurements the environment was excited with sine sweep over the whole considered band and for each third-octave band from 100 to 500 Hz: in order to contain measurements to the strictly needed ones, not all third bands responses were calculated for each position, but two every half-wavelength. Table 4.2.1 summarizes the criterion. In second set of measurements, excitation signal were instead pure tones at third-octave bands center frequencies within $[85, 580]$ Hz, given by first column of table4.2.1 as well.

Error in the probe position can be estimated in ± 1 cm, which corresponds about to $1/60^{th}$ of wavelength at the upper frequency limit: uncertainties of sound wave conductance and susceptance due to it can therefore be ignored.

Full band measurements and third octave ones were then compared in order to verify the robustness of the procedure. It was demonstrated in subsection 2.2 that

$$\eta(x) = \frac{2z_0 \left| \int_{f_0}^{f_1} \Re\left(G_{pu}(x,f)\right) \mathrm{d}f \right|}{\int_{f_0}^{f_1} \left[G_{pp}(x,f) + z_0^2 G_{uu}(x,f)\right] \mathrm{d}f}$$

where G_{pu}, G_{pp}, G_{uu} are one-sided pressure-velocity cross power spectral density and autopower spectral densities, z_0 specific air impedance and the expression was written for 1-D case. It was expected that value of η obtained by exciting the environment in a given band to be equal to the one obtained from a full band measure, performed in the same conditions, limiting however the integration range to that particular band. Confirmation of this statement is evident from figure 4.2.2, given for the 250 Hz frequency band.

Pulling this hypothesis to its limit, a possible interpretation could be given to what will be called $\check{\eta}(f,x)$, the ratio

$$\check{\eta}(f,x) = \frac{2z_0 \Re\left(G_{pu}(x,f)\right)}{G_{pp}(x,f) + z_0^2 G_{uu}(x,f)}.$$

as representing the components of normalized conductance η with respect to f, or in other words the value conductance would have had if a monochromatic field of that particular frequency had been used. However, although

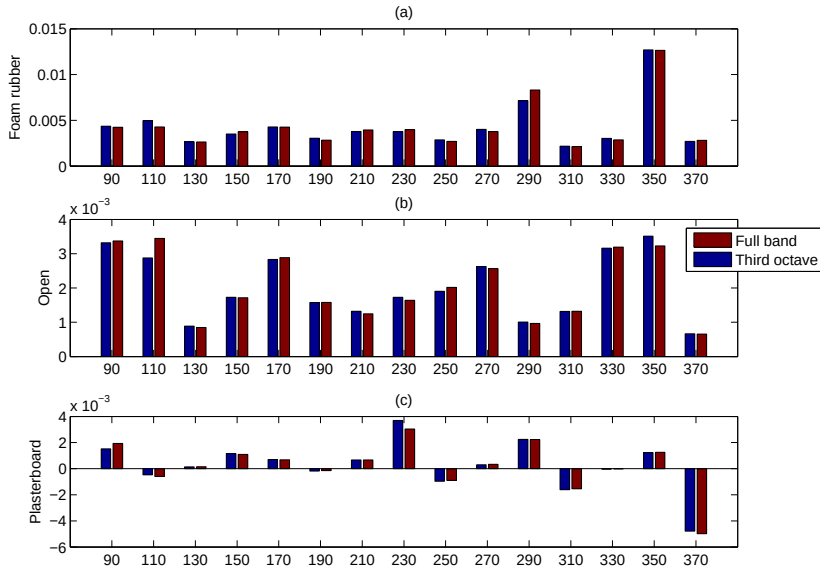

Figure 4.2.2: Comparison between values of η obtained exciting the environments in the 250 Hz frequency third octave band (blue bars) and the ones given by entire band excitation but integrated only in the same band.

still quite good, the agreement between broad band functions and experimental values obtained exciting the environments with pure tones do not coincide in every case, but on the contrary a few are very different (Fig. 4.2.3). What was thought above then seems to be affected by the integration bandwidth: the wider it is, the better results match. Actually $\check{\eta}(x, f)$ has a more subtle interpretation, representing every single frequency contribution to the total value $\eta(x)$, which, it is worth to stress, is the only parameter having a real physical meaning: negative components will give a negative contribution to the average value and vice versa.

Focusing then the attention on the point nearest to the end of the guide, the whole set of energetic parameters were calculated (normalised conductance and susceptance), both in "Cartesian" coordinates (η, μ) and in "polar" ones $(|\bar{\sigma}|, \xi = \cos\Delta\phi\ )$, along with relative frequency distributions, all of which are shown in figures 4.2.1 and 4.2.5 respectively.

Finally, spatial properties of normalized conductance were studied, using the definition of η-path integral given by equation (1.3.19) in its discretized approximation:

$$\mathring{\eta}(x_i) = \frac{\sum_{j=0}^{i} \eta(x_j)\Delta x}{x_i - x_0}$$

where Δx is in this case a constant (20 cm), x_0 is the first measurement point

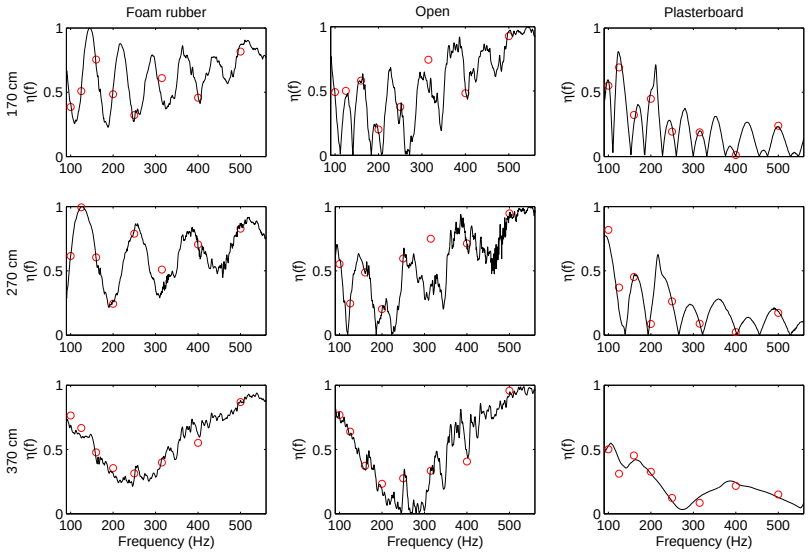

Figure 4.2.3: Comparison of $\check{\eta}(x, f)$ spectra (black lines) with respect to monochromatic results (red dots) for $x = 170, 270, 370\,\text{cm}$ (source position taken as origin). Plots show the relation with respect to frequency for different positions (rows) and different environments (columns).

(90 cm) and the line integral at the denominator is reduced to a simple difference thanks to straight energy trajectories. These results are shown in figure 4.2.6. Comparing how normalized conductance path integral $\mathring{\eta}$ approaches its mean value, some considerations about energetic properties of the different environments can be done. First one is almost trivial: conductance path integral is always much higher for absorbant termination than reflective or open ones, a consideration which would have been impossible to do if only local values near the terminations had been considered. Open termination conductance in fact, usually being of the magnitude of highly reflective environment, abruptly increases near the end of the tube up to values comparable with the ones obtained with foam rubber, a sign of local radiant behaviour. This trend is conserved also in the value of $\mathring{\eta}$, but it appears severely limited by the weight of all preceding values: what turns out from study of path integral is that, for example, energy mainly oscillates when the tube is open but tend to be radiated outside towards the end. Same considerations can be made for other two environments, although their behaviour is much more regular, a property which is reflected in a path integral mainly constant.

Veryinteresting is also the last point of function $\mathring{\eta}$, which represents the spatial *and* time average of normalized sound conductance: in the more radiative environment spatial average characteristic are well described by η

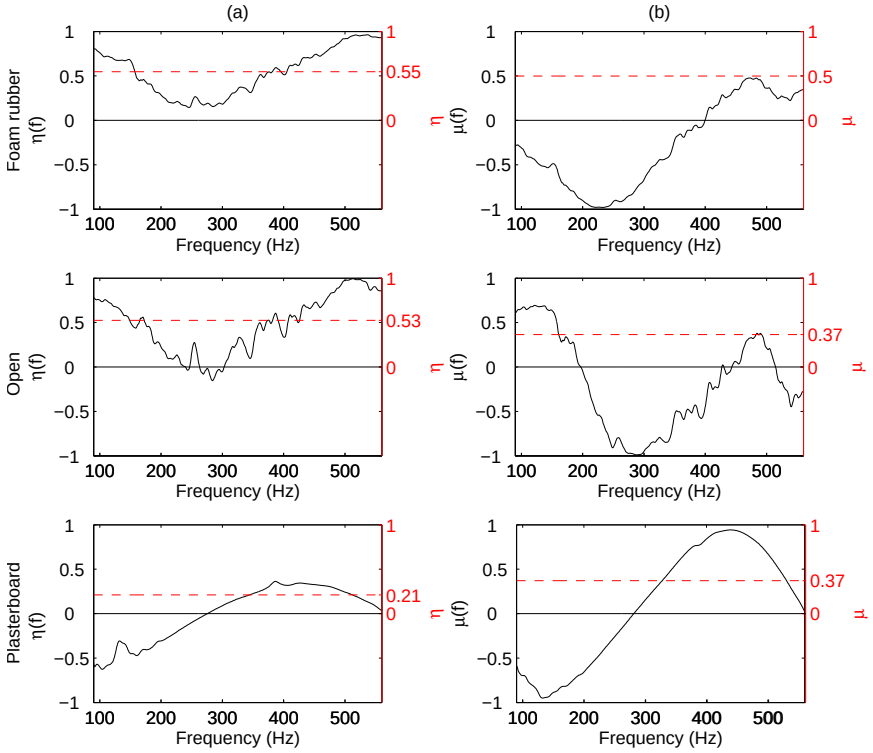

Figure 4.2.4: $\check{\eta}(f)$ (left column) and $\check{\mu}(f)$ (right column) along with their time average values for the measurement point nearest to guide end (370 cm) for different terminations. Overall level are in evidence.

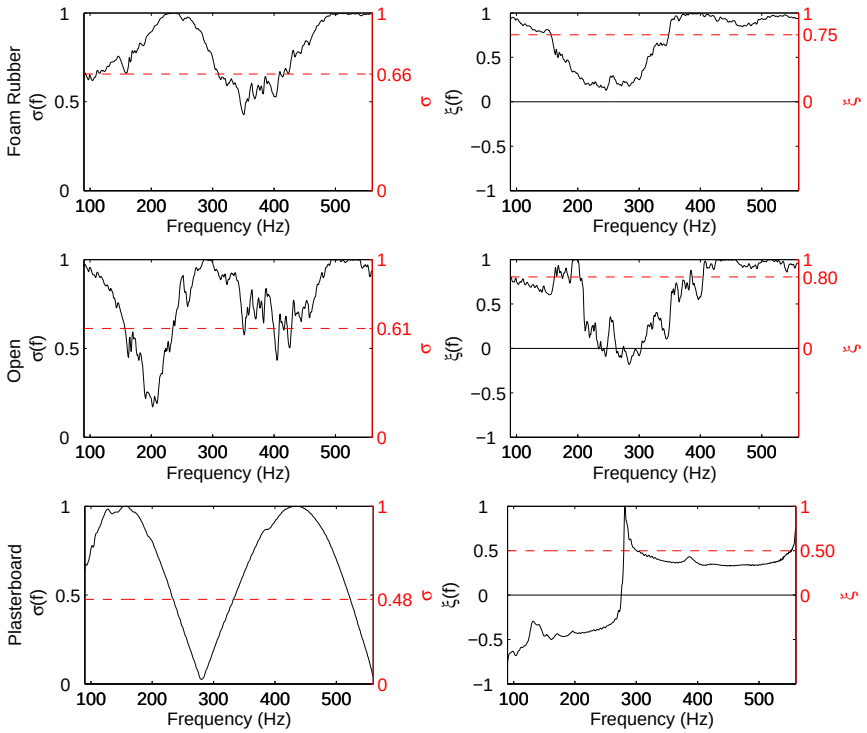

Figure 4.2.5: $\check{\sigma}(f)$ and $\check{\xi}(f)$ functions for the measurement point nearest to guide end (370 cm) for different terminations. Overall level are in evidence.

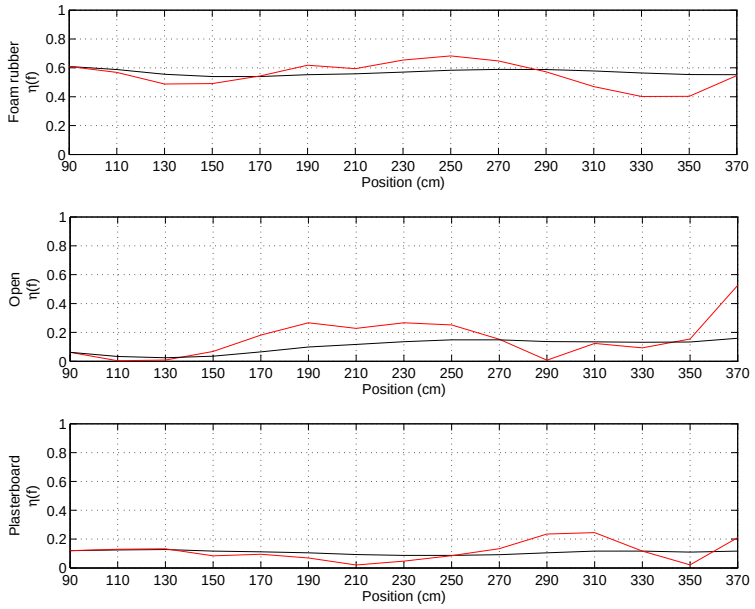

Figure 4.2.6: Comparison between values of $\eta(x_i)$ and path-integral ones $\mathring{\eta}(x_i)$. Starting point x_0 is here 90 cm.

calculated in the last point, as it coincides with $\mathring{\eta}$, while this is not the case for the other two environment. This seems to confirm again the more uniform behaviour of propagated sound energy of radiative environments rather than reverberant ones also in a simple case such as a 1-D field.

4.2.2 Sound wave conductance at the entrance of human ear canal

The pilot study of ear canal acoustic conductance involved three subjects, of different age and hearing conditions: a 28 year old male and a 56 year old male, both of normal hearing, and a 77 year old male with bilateral otosclerosis. They underwent to sound conductance measurements, performed by exciting the room where the experiment took place with a broad band signal and recording pressure and velocity on-axis component at the beginning of external auditory meatus with a p-u probe. The test was repeated several times for both ears of each subject.

During the measure, people were sat on a stool at a distance of about 1 m from the source, a couple of good performing desktop loudspeakers (Bose Companion 2.0) which assured a good excitation over the whole bandwidth studied, with the studied ear facing directly the source (ipsilateral measurement). Using a sine sweep stimulus in the range [20, 9000] Hz, sound probe working bandwidth (see subsection 3.3.3), pressure and velocity impulse responses at right and left ear canal entrances of each person were measured using the Microflown PU match probe calibrated with the method illustrated in chapter 3 and placed at the entrance of the ear canal, as shown in figure 4.2.7. Obtained results for the conductance $\check{\eta}(f)$, defined in expression (2.2.3), are reported in figure 4.2.8 and compared with the overall (stationary time-averaged) value calculated as equation (2.2.3) states. Although a single set of measurements is here reported, it is necessary to stress that procedure was repeated several times for each subject, leading to almost identical results. Normalized conductance for both ears show how pathological behaviour of last subject's ears appear absolutely evident in conductance plots: in particular, peak around 3000 Hz partially (left) or almost completely (right) vanishes.

A peak of conductance around 3000 Hz is consistent with literature results and it is usually interpreted as the resonance of ear volume in the canal, which acts as a resonator: what turns out is that field is mainly radiative around that frequency, which means that a bigger fraction of energy propagates along the trajectory which goes in the canal. This fact is in line with the human hearing sensitivity curves, which usually have a maximum about at this frequency.

An experimental check of what stated above was tried: doing an analog measurement with an artificial dummy head having an ear canal roughly of the same volume magnitude of an average human one and a latex membrane

Figure 4.2.7: p-u probe placed for ear conductance measurements (left); detail of the p-u probe (right).

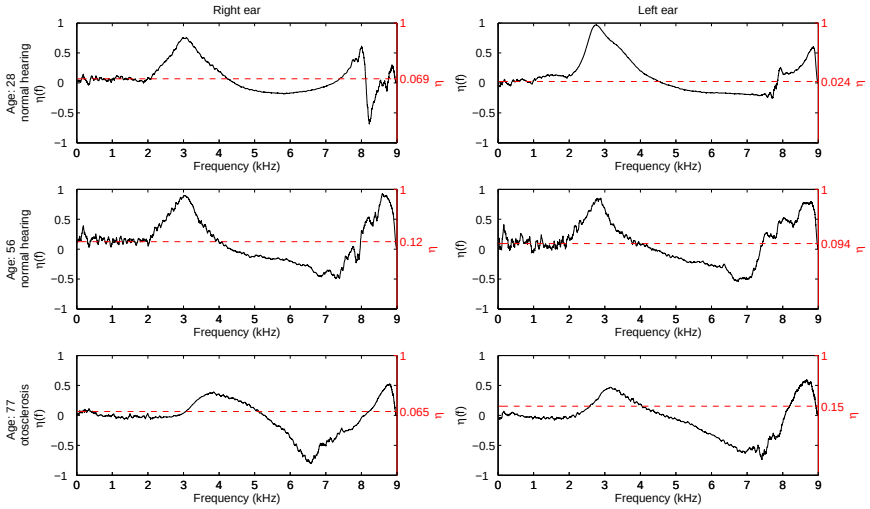

Figure 4.2.8: $\check{\eta}(f)$ function and conductance η comparison with repsect to age and hearing condition.

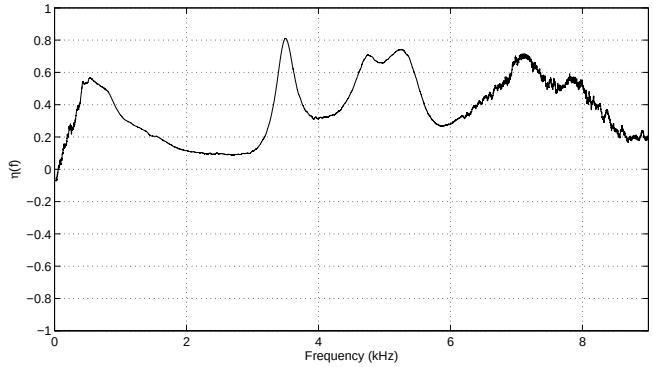

Figure 4.2.9: $\check{\eta}(f)$ measured for a dummy head

in place of the eardrum. Conductance actually showed peak at almost the same frequency as the human subjects' ones (Fig. 4.2.9), even if obvious differences occur in the overall frequency spectrum. This was taken as a confirmation of the hypothesis.

Same measure was then carried out involving more subjects, to test reliability of the experimental apparatus and a first estimation of variability of this parameter, depending for example on the way the probe was placed near the meatus: in particular, four students of age around 20, none of whose suffering of any hearing pathology, agreed to take a preliminary test. At a distance of about 3 m from the source, they sat so that the monitored ear directly faced the source. Although the signal suffered a poor ratio, results showed a significant agreement with the studied subjects, as shown in figure 4.2.10: to make the curves more understandable, conductance spectra were cleaned with a moving average filter. Conductance peak was quite uniform in most of subjects.

In order to verify to what extent the position of sound source with respect of the monitored ear affected the measure of ear conductance, the target was rotated in the room and signals were recorded for different angles. Graphics in figure 4.2.11 show conductance obtained for a subject, placed so that monitored ear was on axis with the source itself, then rotated respectively $90°, 180°, 270°$. It is clear that very little influence comes from the direction of sound, at least up to 5 kHz, apart for a more disturbed curve due to to a worse signal to noise ratio. For higher frequency instead, as expected, directionality becomes important and conductance shows a net decrease for measurements made for orientations different from on-axis configuration, mainly due to a poor incoming energy in this range.

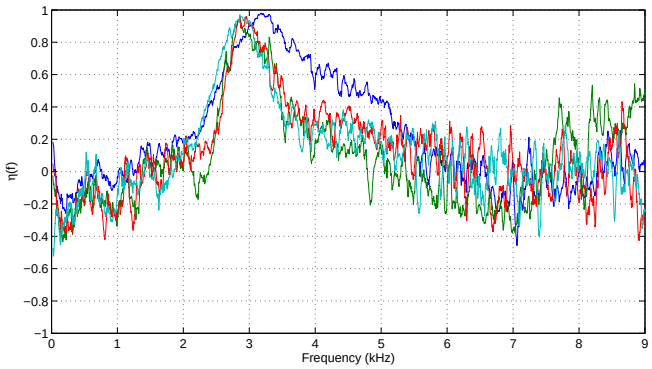

Figure 4.2.10: Conductance spectra $\check{\eta}(f)$ for four different subjects (age ~ 20, no pathologies).

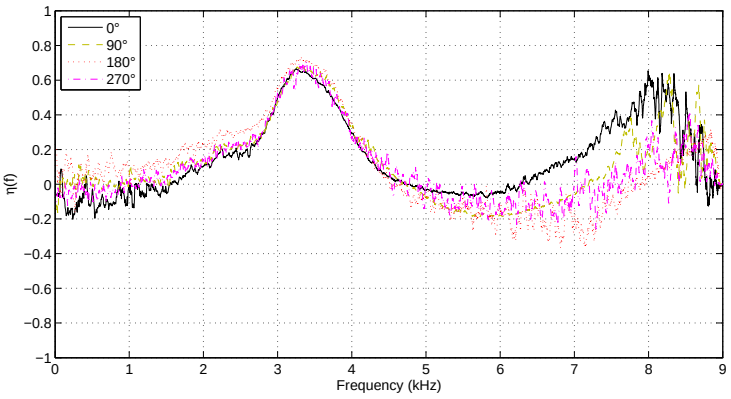

Figure 4.2.11: Dependence of $\check{\eta}(f)$ from angle between sound source and ear canal. All measurements are from a single subject

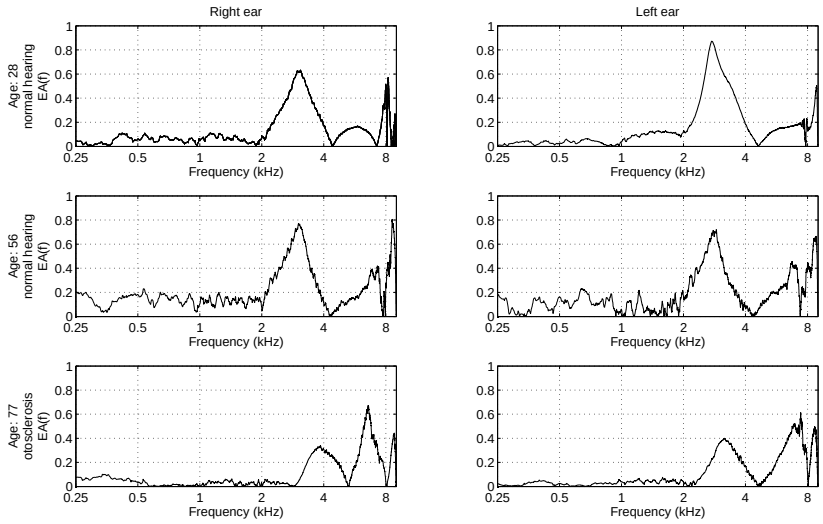

Figure 4.2.12: Frequency distributions of energy absorbances EA(f) measured at the ear-canal entrances of the three people under test.

Sound energy absorbance

A useful indicator which allows an almost direct comparison with similar results in literature is called *energy absorbance*, in agreement with Keefe [49] and can be defined as:

$$EA(f) = 1 - ER(f) =: 1 - \sqrt{\frac{1 - \check{\eta}(f)}{1 + \check{\eta}(f)}} \tag{4.2.1}$$

$EA(f)$ represents, for any given frequency f, the fraction of incident energy in the ear canal that is not reflected at the tympanum membrane. This statement can be easily proved for simplified 1-D monochromatic plane wave field models of the ear-canal acoustics, where ER is just related to the amplitude of the reflected wave (see Appendix (A)). For this reason plots of $EA(f)$ reported for the three tested cases in figure 4.2.12, left column, can be safely compared with the statistical pattern of the energy absorbance shown in literature with completely different methods [49, 50]. Again, a great difference occurs between normal hearing subjects and the the one suffering otosclerosis, in particular around 2-4 kHz. The definition of $EA(f)$, as given by equation 4.2.1, is the proper extension of the ear canal energy absorption concept to general sound fields of whatsoever geometry and spectral composition.

Conclusions

The main research topic presented in this work regarded the study, both theoretical and experimental, of a new method for anemometric p-u probes calibration. The obtained results have been here detailed and organized in a complete presentation, enriched with the essential characterization of the calibration facility, which is an original outcome of the thesis work. Moreover, the calibration precision and uncertainties analysis of experimental results has been performed and consistently compared with the ones reported in literature.

The approach here exposed has some advantages if compared to the other p-u calibration mothods, such as the great simplicity of the post-processing elaboration and a good stability. Another important feature of the here presented methodology is the possibility to achieve fine calibration curves for the whole working bandwidth of p-u probes up to 10 kHz with a single measurement. On the other side, of course, the progressive plane wave methodology here adopted, is not indicated for a quick check of p-u probes before doing some measurements. The calibration facility is in fact far from portable, but represents a good accommodation between quality and spent resources: if good precision is needed the wave guide facility is much more affordable than a big anechoic chamber, otherwise necessary for fine calibration.

This research can be, and will be, improved: being the final aim a standardisation of p-u probe calibration systems. The next step could be in fact the direct experimental comparison of the method here proposed with the ones based on different reference fields, carried out for several probes and by different laboratories (round robin test). The author opinion is that this way represents the only possibility for this kind of instruments to be proved reliable enough to be used in the common practise of sound intensimetry. Safe calibration will also lead to a considerable improvement in applied and experimental acoustic research in general, and especially in the advancement of Sound Energetics.

Another important consideration regards the micro dimensions of new silicon-based acoustic p-u sensors. The single-chip assembling of these probes make them extremely versatile, allowing advanced measurements in situations otherwise impossible or extremely difficult to manage. The energetic characterization of acoustic field at the entrance of ear canal represents a

clear example: very few studies were found in literature regarding this topic, and none using this kind of acoustic sensors. Results here presented, although still at the preliminary stage due to the few number of tested persons, lead to very encouraging results. Again, comparison with already consolidated techniques is required to find out which one is better, or at least in which case each one is preferable. This kind of study in the audiometric field may also represent a good benchmark for the p-u probe design itself.

Finally affordable and reliable p-u based acoustic instrumentation will allow a precise experimental determination of the new acoustical quantities introduced in this work, such as sound energy conductance and susceptance, as well as the generalized concept of apparent sound intensity, mutuated from AC-circuit formalism and here generalized for all kinds of acoustic fields.

Appendix A

Relation between sound conductance and Energy Reflectance (ER): monochromatic case

Approach and results here reported are taken from Acoustics lecture notes of prof. G. Schiffrer of Department of Physics at the University of Ferrara [51].

The simplest case to study reflection phenomenon is given by monochromatic plane wave: an analytic expression can be in fact obtained quite easily, a relation which can be extended to general fields under some constraints.

Velocity potential for this field is known and given by the superposition of two waves, one of which travelling in positive direction, i.e. on the same verse of chosen spatial axis, the other one in the opposite way. Explicit relation is given by

$$\phi(x,t) = Ac\left[e^{i(kx-\omega t)} + Re^{i(kx+\omega t+\vartheta)}\right] \tag{A.1}$$

where A is the displacement amplitude, $k = \omega/c$ is the wave number, R is the scaling factor of reflected wave and ϑ is its (constant) phase shift. Differentiating equation(A.1) one obtains values of instantaneous pressure and velocity (Eqs. (1.1.10)):

$$\begin{aligned} p(x,t) &= \Re\left(Az_0\,(i\omega)\left[e^{i(kx-\omega t)} - Re^{i(kx+\omega t+\vartheta)}\right]\right) \\ u(x,t) &= \Re\left(A\,(i\omega)\left[e^{i(kx-\omega t)} + Re^{i(kx+\omega t+\vartheta)}\right]\right) \end{aligned}$$

Their mean quantities are given by integration over a time period $T = 2\pi/\omega$, which gives

$$\begin{aligned}
\left\langle p^2 \right\rangle (x) &= (Az_0\omega)^2 \frac{1}{T}\int_0^T \left[-\sin(kx-\omega t) + R\sin(kx+\omega t+\vartheta)\right]^2 \mathrm{d}t = \\
&= (Az_0\omega)^2 \left[\underbrace{\frac{1}{T}\int_0^T \sin^2(kx-\omega t)\,\mathrm{d}t}_{=\frac{1}{2}} + R^2 \underbrace{\frac{1}{T}\int_0^T \sin^2(kx+\omega t+\vartheta)\,\mathrm{d}t}_{=\frac{1}{2}} \right. \\
&\qquad \left. -2R\underbrace{\frac{1}{T}\int_0^T \sin(kx-\omega t)\sin(kx+\omega t+\vartheta)\,\mathrm{d}t}_{=\frac{1}{2}\cos(2kx-\vartheta)} \right] = \\
&= (Az_0\omega)^2 \left(\frac{1+R^2}{2} - R\cos(2kx-\vartheta) \right) \qquad \text{(A.2)}
\end{aligned}$$

for squared pressure. Same calculations lead to mean square value of velocity, here omitted

$$\left\langle u^2 \right\rangle (x) = (A\omega)^2 \left(\frac{1+R^2}{2} + R\cos(2kx-\vartheta) \right) \qquad \text{(A.3)}$$

These terms are proportional to kinetic and potential energy densities: final step is the calculation of $I = \langle pu \rangle$:

$$\begin{aligned}
\langle pu \rangle &= (A\omega)^2 z_0 \left[\underbrace{\frac{1}{T}\int_0^T \sin^2(kx-\omega t)\,\mathrm{d}t}_{=\frac{1}{2}} - R^2 \underbrace{\frac{1}{T}\int_0^T \sin^2(kx+\omega t+\vartheta)\,\mathrm{d}t}_{=\frac{1}{2}} \right] = \\
&= \frac{1}{2}(A\omega)^2 z_0 \left(1-R^2\right) \qquad \text{(A.4)}
\end{aligned}$$

Recalling finally that $\rho_0 c$-normalized conductance η is given by I/W (Eq. (1.3.15)), its explicit expression can be obtained from relations (A.2),(A.3),(A.4):

$$\begin{aligned}
\eta &= \frac{\frac{1}{2}(A\omega)^2 z_0 \left(1-R^2\right)}{\frac{c}{2}\left(\frac{\langle p^2\rangle}{\rho_0 c^2} + \rho_0 \langle u^2\rangle\right)} = \\
&= \frac{\frac{1}{2}(A\omega)^2 z_0 \left(1-R^2\right)}{\frac{c}{2}\frac{1}{2}(A\omega)^2 \rho_0 (1+R^2)} = \\
&= \frac{1-R^2}{1+R^2}
\end{aligned}$$

Last step consists in inverting the relation so that reflection coefficient in term of normalized conductance is obtained:

$$R = \sqrt{\frac{1-\eta}{1+\eta}}$$

Bibliography

[1] F. J. Fahy, *Sound Intensity*, 2nd ed. London: E & FN Spon, 1995.

[2] D. B. Nutter, T. W. Leishman, S. D. Sommerfeldt, and J. D. Blotter, "Measurement of sound power and absorption in reverberation chambers using energy density," *Journal of the Acoustic Society of America*, vol. 121, no. 5, pp. 2700–2710, 2007.

[3] D. Stanzial, "On the intensimetric analysis and monitoring of flue organ pipes," in *Proceedings of Forum Acusticum*, Budapest Hungary, 29th August-2nd September 2005, pp. 641–646.

[4] N. Prodi and D. Stanzial, "A novel intensimetric technique for monitoring the radiative properties of sound fields," *Journal of the Audio Engineering Society*, vol. 47, no. 5, pp. 363–372, May 1999.

[5] J. W. Parkins, S. D. Sommerfeldt, and J. Tichy, "Narrowband and broadband active control in an enclosure using the acoustic energy density," *Journal of the Acoustic Society of America*, vol. 108, no. 1, pp. 192–203, 2000.

[6] D. Stanzial, G. Sacchi, and G. Schiffrer, "Active playback of acoustic quadraphonic sound events," in *Proceedings of Meetings on Acoustics*, vol. 4, 2008.

[7] F. Jacobsen and V. Jaud, "A note on the calibration of pressure-velocity sound intensity probes," *Journal of the Acoustic Society of America*, vol. 120, pp. 830–837, 2006.

[8] T. Basten and H.-E. de Bree, "A full bandwidth calibration procedure for acoustic probes containing a pressure and particle velocity sensor„" *Journal of the Acoustic Society of America*, vol. 127, pp. 264–270, 2010.

[9] D. Stanzial, D. Bonsi, and G. Schiffrer, "Four-dimensional treatment of linear acoustic fields and radiation pressure," *Acta Acustica united with Acustica*, vol. 89, pp. 213–224, 2003.

[10] P. M. Morse and K. U. Ingard, *Theoretical Acoustics*. Princeton University Press, 1 1987.

[11] L. Landau and E. Lifshitz, *Fisica Teorica.* Roma: Editori Riuniti University press, 2009, vol. 1 - Meccanica.

[12] K. Beissner, "The acoustic radiation force in lossless fluids in eulerian and lagrangian coordinates," *Journal of Acoustic Society of America*, vol. 103, pp. 2321–2332, 1998.

[13] G. Schiffrer and D. Stanzial, "Energetic properties of acoustic fields," *Journal of Acoustic Society of America*, vol. 96, pp. 3645–3653, 1994.

[14] D. H. Towne, *Wave phenomena.* New York: Dover Publications, 1988.

[15] D. Stanzial, N. Prodi, and G. Schiffrer, "Reactive acoustic intensity for general fields and energy polarization," *Journal of Acoustic Society of America*, vol. 99, pp. 1868–1876, 1996.

[16] D. Stanzial, "From guidonian hand to sound energy compass," in *Proceedings of Forum Acusticum*, Budapest, Hungary, August-September 2005, pp. 331–334.

[17] D. Stanzial and G. Schiffrer, "On the connection between energy velocity, reverberation time and angular momentum," *Journal of Sound and Vibration*, vol. 329, pp. 931–943, 2010.

[18] D. Bonsi, "Theoretical and experimental study of energetic properties of confined sound fields," Ph.D. dissertation, University of Ferrara: Department of Physics, 1997/98.

[19] J. Bendat and A. Piersol, *Random data Analysis and measurement procedure.* John Wiley & Sons, inc., 2000.

[20] S. W. Smith, *The scientist and engineer's guide to digital signal processing.* San Diego, CA, USA: California Technical Publishing, 1997.

[21] G. L. D'Spain, W. S. Hodgkiss, and G. L. Edmons, "Energetics of the deep ocean's infrasonic sound field," *Journal of the Acoustic Society of America*, vol. 83, no. 3, pp. 1134–1158, 1991.

[22] J. C. Valiï¿œre, P. Herzog, V. Valeau, and G. Tournois, "Acoustic velocity measurements in the air by means of laser doppler velocimetry: dynamic and frequency range limitations and signal processing improvements," *Journal of Sound and Vibration*, vol. 229, no. 3, pp. 607 – 626, 2000.

[23] H.-E. de Bree, P. Leussink, T. Korthorst, H. Jansen, T. Lammerink, and M. Elwenspoek, "The microflown; a novel device measuring acoustical flows," *Sensors and Actuators: A, Physical*, vol. SNA054/1-3, pp. 552–557, 1996.

[24] G. Rasmussen and M. Brock, "Acoustic intensity measurement probe," in *Proceedings of Recent Developments in Acoustic Intensity Measurement*, Senlis, France, 1981, pp. 81–88.

[25] F. Jacobsen, V. Cutanda, and P. M. Juhl, "A numerical and experimental investigation of the performance of sound intensity probes at high frequencies," *Journal of Acoustic Society of America*, vol. 103, pp. 953–961, 1998.

[26] H.-E. de Bree, Lammerink, Elwenspoek, and Fluitman, "Use of a fluid flow measuring device as a microphone and system comprising such a microphone," Netherland Patent NL95/00 220, 1995.

[27] H.-E. de Bree, *The microflown E-book*, 2007.

[28] V. Svetovoy and I.A.Winter, "Model of the μ-flown microphone," *Sensors & Actuators*, vol. 86, pp. 171–181, 2000.

[29] L. Sena, *Units of physical quantities and their dimensions*, 2nd ed. Moscow: MIR, 1973.

[30] E. Perucca, *Fisica generale e sperimentale.* Torino: UTET, 1949, vol. Vol. I.

[31] A. Zemanian, *Distribution theory and transform analysis*, 2nd ed. Dover, 1987, vol. Chapt. 10 "Passive systems".

[32] L. L. Beranek, *Acoustical Measurements*, revised ed., A. S. of America, Ed. AIP, 1988.

[33] R. Raangs, T. Schlicke, and R. Barham, "Calibration of a micromachined particle velocity microphone in a standing wave tube using a lda photon-correlation technique," *Measurement Science and Technology*, vol. 16, no. 5, pp. 1099–1108, 2005.

[34] D. Stanzial and D. Bonsi, "Calibration of the p-v microflown r probe and some considerations on the physical nature of sound impedance," in *Proceedings of Euronoise*, no. 149, May 2003.

[35] J. Wolfe, J. Smith, J. Tann, and N. Fletcher, "Acoustic impedance of classical and modern flutes," *Journal of Sound and Vibration*, vol. 243, pp. 127–144, 2001.

[36] D. Stanzial, G. Sacchi, and G. Schiffrer, "Calibration of pressure-velocity probes using a progressive plane wave reference field and comparison wih nominal calibration filters," *Journal of Acoustic Society of America*, vol. (submitted), 2010.

[37] G. Sacchi and D. Stanzial, "A new method for axial p-v probe calibration„" in *Proceedings of ICSV 16*, Krakow, Poland, July 2009, p. paper n. 765, icsv16.

[38] D. Stanzial, D. Bonsi, and G. Sacchi, "Method for relative p-v probe calibration (italian, invited)," in *Proceedings of Seminar: Instruments and methods for acoustic and vibration measurements*, Ancona, Italy, September 2008.

[39] D. Stanzial and G. Sacchi, "Taratura assoulta di sonde intensimetriche p-v (italian)," in *Proceedings of 36Â° Congress of Italian Acoustic Association*, Torino, Italy, June 2009.

[40] D. Stanzial, D. Bonsi, G. Cengarle, and G. Sacchi, "Procedimento ed apparecchiatura per la calibrazione di sonde intensimetriche p-v (italian)," in *Proceedings of 35Â° Congress of Italian Acoustic Association*, Milan, Italy, June 2008.

[41] E. Meyer, E. Neumann, and J. t. J. M. Taylor, *Physical and applied acoustics : an introduction.* Academic press, 1972.

[42] H.-E. de Bree, "Add-on microflown for a high-end pressure-gradient microphone," in *Audio Engineering Society Convention 109*, 9 2000.

[43] N. H. Fletcher and T. D. Rossing, *The physics of musical instruments*, 2nd ed. New York: Springer, 1998.

[44] H.-E. de Bree, "calibration report of microflown kit no.133," Microflown Technologies, Tech. Rep., 2007.

[45] *Determination of sound power levels of noise sources using sound intensity*, EN ISO Std. 9614, Rev. 2, August 1996.

[46] N. Prodi, F. Pompoli, R. Pompoli, P. Fausti, P. Bonfiglio, A. Farnetani, and U. Fabbri, "Caratterizzazione acustica della nuova camera anecoica dell'universitï¿œ di ferrara (italian)," in *Proceedings of 35Â° Congress of Italian Acoustic Association*, 2008.

[47] F. Jacobsen and H.-E. de Bree, "A comparison of two different sound intensity measurement principles," *Journal of Acoustic Society of America*, vol. 118, no. 3, pp. 1510–1517, 2005.

[48] S. E. Voss and J. B. Allen, "Measurement of acoustic impedance and reflectance in human ear canal," *Journal of Acoustic Society of America*, vol. 95, no. 1, pp. 372–384, 1994.

[49] Y.-W. Liu, C. A. Sanford, J. C. Ellison, D. F. Fitzpatrick, M. P. Gorga, and D. H. Keefe, "Wideband absorbance tympanometry using pressure

sweeps: System development and results on adults with normal hearing," *Journal of the Acoustic Society of America*, vol. 124, no. 6, pp. 3708–3719, 2008.

[50] R. H. Withnell, P. Parent, P. S. Jeng, and J. B. Allen, "Using wideband reflectance to measure the impedance of the middle ear," *Hearing Journal*, vol. 62, no. 10, pp. 36–41, October 2009.

[51] G. Schiffrer, "Lezioni di acustica (2)," 1998.